Theses and Dissertations

Summer 2017

Development of methodology to support estimation of snow drifting with application to snow fence design

Heng-Wei Tsai
University of Iowa

Recommended Citation

Tsai, Heng-Wei. "Development of methodology to support estimation of snow drifting with application to snow fence design." MS (Master of Science) thesis, University of Iowa, 2017.
https://doi.org/10.17077/etd.mvy65k8l.

DEVELOPMENT OF METHODOLOGY TO SUPPORT ESTIMATION OF SNOW

DRIFTING WITH APPLICATION TO SNOW FENCE DESIGN

by

Heng-Wei Tsai

A thesis submitted in partial fulfillment
of the requirements for the Master of Science
degree in Civil and Environmental Engineering in the
Graduate College of
The University of Iowa

August 2017

Thesis Supervisors: Adjunct Professor Marian Muste
Professor George Constantinescu

Graduate College
The University of Iowa
Iowa City, Iowa

CERTIFICATE OF APPROVAL

_____

MASTER'S THESIS

_____

This is to certify that the Master's thesis of

Heng-Wei Tsai

has been approved by the Examining Committee for the thesis requirement
for the Master of Science degree in Civil and Environmental Engineering
at the August 2017 graduation.

Thesis Committee: _____
                     Marian Muste, Thesis Supervisor

                     _____
                     George Constantinescu, Thesis Supervisor

                     _____
                     William E. Eichinger

                     _____
                     Corey Markfort

To my family, friends and my Mother Pei-Ni Chen

ACKNOWLEDGEMENTS

ABSTRACT

Drifting and blowing snow is an extremely problematic and perilous aspect of roadway travel in four-season areas subject to intense snowfalls and winds during the winter season. Snow drift happens when an adequate amount of loose snow is available on the ground and the wind velocity magnitude and temperature surpass the critical values. In order to prevent the snow from reaching the road, which leads to decreased visibility and increased accidents, snow fences are designed and deployed on the road. Their orientation is based on the dominant wind direction.

In this present study, the objective for exploration is to prove and test a set of new technologies that efficiently support the design and evaluation of snow fence performance by taking advantage of the new non-intrusive measurement technologies (image-based method). Several preliminary experimental set-ups were designed and implemented onsite to develop the measurement protocol to use for snowfall and snowdrift quantification. The current measurement protocols are outmoded, higher cost, and display measurement uncertainty. The majority of the current measurement required installing intrusive instruments, therefore, it poses a significant risk for the safety of personnel. Multiple non-intrusive measuring techniques are introduced and comprised in the present research with the discussion of each individual measurement's fundamentals physics (see Chapter 3), and the application purposes for tracking both snowfall and snowdrift velocity were developed and described in Chapter 4. Chapter 5 and 6 describe the actual measurement outcomes observed from various snow events in order to test these image-based approaches compared with the physical measurement to validate the methodology used to estimate the snow velocity and map the snow deposition.

PUBLIC ABSTRACT

Drifting and blowing snow is an extremely problematic and dangerous aspect of roadway travel in four-season areas subject to intense snowfalls and winds during the winter season. It will not only cause concern for maintenance and repair of roadways, but also affect the safety and efficiency of transportation. Snow drift happens when an adequate amount of loose snow is available on the ground and the wind velocity magnitude and temperature surpass the critical values. In order to prevent the snow from reaching the road, leading to decreased visibility and me numerous accidents, snow fences are designed and deployed on the road oriented based on the dominant wind direction.

In this present study, the goal is to apply the new non-intrusive measurement technologies, image-based method, to prove and efficiently support the design and evaluation of snow fence performance. Multiple preliminary experimental set-ups were designed and implemented on-site to develop the measurement protocol to quantify snowfall and snowdrift measurements. Studies showed that with conventional ways of obtaining snowfall and snowdrift measurements, researchers are required to stay out in wintery conditions for a long time. With an image-based technique, less exposure to outdoor conditions is needed. This method will not only reduce the safety risk, but also increase the efficiency of the result gathering.

Multiple non-intrusive measuring techniques are introduced in this research with the discussion of each individual measurement's fundamentals physics, measuring protocols and the experimental results.

TABLE OF CONTENTS

LIST OF TABLES

LIST OF FIGURES

CHAPTER 1 INTRODUCTION

1.1 Research background

Drifting and blowing snow is an extremely problematic and dangerous aspect of roadway travel in four-season areas subject to intense snowfalls and winds during the winter season. Snow drift occurs when a sufficient quantity of loose snow is present on the ground and the wind velocity magnitude and temperature exceed critical values. In the present context, the main concern is caused by blowing and drifting snow up to 5 m from the road surface. Snow blowing across the road and accumulating (or drifting) on the roadway reduces drivers' visibility and safety (Figure 1.1a) and, ultimately, increases accidents during the winter season (Figure 1.1b). The U.S. Midwest, and especially Northern Iowa are often exposed to strong winds and large quantities of snow. Blowing and drifting snow are also the main cause for ice cover formation on roads and can reduce the effective road width (Figure 1.1c). Several studies (Andrey & Olley, 1990) concluded that the combined effect of the snowfall-induced hazards can lead to an increase of traffic accidents by 100% or more compared with normal weather conditions. Most of the studies, however, found more moderate (but statistically still significant) increases in number of traffic accidents during adverse weather conditions (Andreescu & Frost, 1998).

a)   b)   c)

Figure 1.1 Effects of the snow blowing on Iowa roads: a) reduced visibility; b) accidents, c) reduction of the effective road width (photos: Tsai, 2015, I-35 Hwy, Iowa).

The unquestionable detrimental impacts of the snowfall and snow drift on highway traffic are mitigated with a plethora of methods and activities implemented before, during and after the snow storms. Reducing the impacts of drifting snow on highway operations can be mainly accomplished through two approaches (Perchanok, 1998): a) controlling how the snow moves across the road and b) preventing the snow from reaching the road. To control the snow movement over the road, the road design should include provisions to facilitate accumulation of snow in the ditches and to prevent the snow to move or accumulate on the road. Alternatively, the road cross-section should be streamlined to maintain a smooth wind flow across the driving surface so that drifting snow incoming from adjacent areas continues to move over the road without stopping. Designing roads such that snow drifts never accumulate on the roadways is not always possible, especially when the local topography is prone to snow accumulation and/or the right-of-ways are narrow.

Most often, the preferred approach to reduce the impact of snow drifting on highways is to prevent the snow from reaching the road. The present study focuses on some of these measures and activities. Preventive actions are included both in the road design stage as well as after road construction through road maintenance activities. Development of an effective snow-retention solution is preferred to maintenance activities, as the latter can become a large component of winter maintenance costs for states or local agencies. Removing snow mechanically from roadways is costly due to equipment expenses and salaries of the snow removal crews. Moreover, snow removal results in lower usage of the roads between the time the snow deposits and the time the snow is removed (e.g., Tabler, 1991, and 2003; Iowa DOT, 2005; Sañudo-Fontaned et al., 2011). According

to Perchanok (1998), blowing and drifting snow (as opposed to falling snow and frost) are responsible for about 30% of the plowing, salting and sanding activities used to maintain the roadway operational.

The most often-used blowing-snow prevention measure has been, and continues to be, the deployment of snow fences; they can either be constructed at the site or set in the form of living fences (e.g., shrubs, trees, or local grasses) planted along the road. For constructed snow fences, the typical materials used to build the fence include wood, metal rails, plastic nets, polymer rails and woven fabric. Fence materials are attached to supporting structures (e.g., posts) made of steel or wood or to truss-type, custom-designed frames set in the ground. Living fences are increasingly used as alternatives to constructed snow fences as they are beneficial not only for protecting the road against snow drifting and accumulation (see Nixon et al., 2003) but also for providing important ecological and esthetical benefits.

Constructed snow fences are generally installed perpendicular to the prevailing wind direction in the vicinity of the roadways, as illustrated in Figure 2a. Drifting snow particles approaching the fence tend to deposit on the downwind side of the snow fence, where the velocity magnitude is smaller than the velocity on the upwind side. By slowing down the speed of the snow particles and promoting snow deposition downwind of the fence, installing snow fences can result in a dramatic decrease of problems related to snow blowing and drifting, as illustrated in Figures 2b and 2c. The snow-fence efficiency differs depending on their position and orientation with respect to the road as well as on snow fence construction details such as height, orientation, porosity, and bottom gap (Keshav et al., 2015). Constantinescu & Muste (2015) found that the snow fence

efficiency is mainly a function of the fence porosity and the size of the bottom gap. Fences can be fit with additional hydrodynamic features (e.g., adjustable blades and variable opening geometry) to improve their operational efficiency (Kaneko et al., 2012). However, the simple snow fence designs continue to be widely used, as they are easy to install and do not require adjustments. Moreover, they have proven to be highly economical when compared to alternative snow mitigation techniques and practices (Keshav et al., 2015).

a)

b)
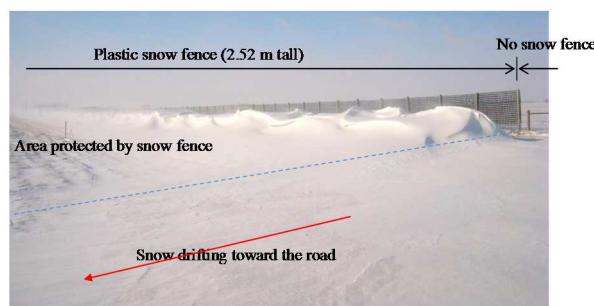
c)

Figure 1.2 Effect of snow fence presence (photo: Tsai, 2014, I-20, Iowa): a) comparison between road area with and without snow fence protection (photo: Tsai, 2014, I-20, Iowa); b) similar comparison after another storm event at the same site as in Figure 1a (Keshav et al., 2015); c) snow accumulation at fence (photo: Tsai, 2014, I-20, Iowa)

Several states (e.g., Minnesota, Utah) have established a clear link between the deployment of snow fences in critical areas of highways and a significant decrease (by about 50%) in the number of serious accidents which result in human injuries. This was accompanied by a major cut in the winter maintenance costs (see Figure 3). A more recent study conducted in Wyoming, a state that deals with an extremely high amount of winter weather related crashes, shows that up to 25% of the crashes that take place on Interstate 80 have occurred in areas without snow fences, whereas a mere 11% of crashes occur in areas protected by fences (Peel et al., 2017). The cost of snow fences and their installation is 1-2 orders of magnitude lower than that of mechanical snow removal. Tabler (2005) states that mechanical snow removal typically cost about $3 per 2,205 lb. For comparison, a snow fence 4 ft. tall can retain 4.2 tons of snow/ ft.
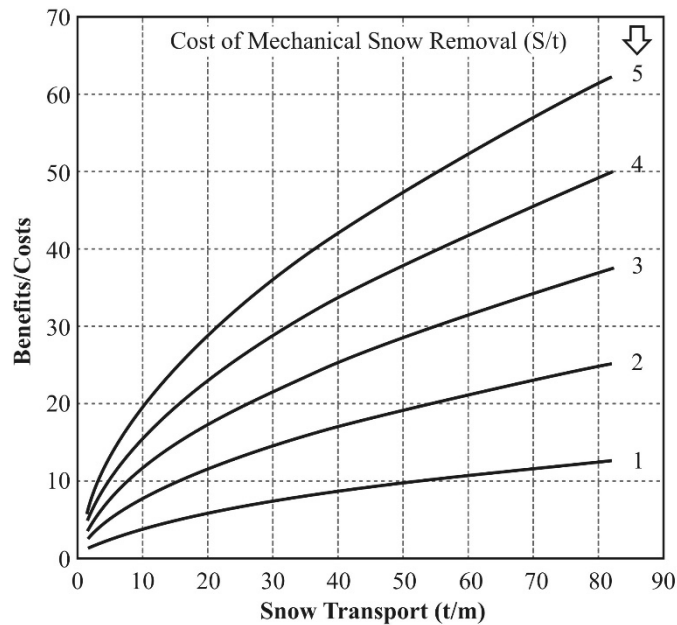
Figure 1.3 Benefit-to-cost ratios for permanent snow fences in relations to seasonal snow transport and costs for mechanical snow removal (Tabler, 2005)

5

The design of snow fences is based on a set of local or regional weather conditions estimated over long-term and by taking into consideration the topography of the site. In general, the design of snow fences for prevention of snowdrift entails the following steps (Kaneko et al., 2012):

1) Site characterization (i.e., collection of meteorological and snowdrift information on past snow storms) and selection of a road route based on local topological conditions

2) Site survey and analysis (i.e., collection of additional topographic and meteorological information, quantification of the snow drift features for the selected route)

3) Establishment of the orientation, geometry and specifications for the snow fence structural characteristics (i.e., overall geometry, materials and hydrodynamic aspects)

4) Evaluation of the snow fence performance (i.e., survey of all aspects of the operational performance from retention efficiency to maintenance costs)

The design activities described above require technical expertise from various road operation domains (i.e., planning, meteorology, structural design, and maintenance). Consequently, the responsibilities and flow of information for snowdrift control design become complex and require a given scale of the business process to be available for the mitigation agency (typically, at the state level). Irrespective of the agency scale, designing snow fences requires sound engineering judgment on two main aspects: a) evaluating the potential for snow blowing and drifting at the construction site (Step 2 in the design process) and b) providing specifications regarding the snow-fence orientation

6

and construction details commensurate with the estimation obtained through activity a)

above (Step 3 in the design process). The layout and dimensions of the fence are

determined using formulae related to the annual quantities of drifting snow expected at

the site, the road alignment, the surrounding terrain features and the desired efficiency.

The design equations can be simple analytical formulae, graphical solutions based on

empirical and semi-empirical equations, and (increasingly) more complex numerical

models (Liang, 2010 and Naaim, 1998). The methodology implemented in the snow

fence design is reviewed in Chapter 2.

1.2 Research goals and motivation

The overall goal of the proposed research is to prove and test a set of new

technologies that efficiently support the design and evaluation of snow fence performance

by taking advantage of new non-intrusive measurement technologies. Specifically, the

present research contributes with elements necessary in Steps 1, 2 and 3 of the design

process outlined above by prototyping new or emerging measurement techniques for:

a) quantifying the snowfall and snowdrift required in Steps 1 and 2 of the design

   process, and

b) supporting the evaluation conducted in Step 3 of the design process.

The current measurement protocols used for snowfall and snowdrift quantification

and evaluation of the design efficiency are outdated, costly, and of unknown (presumably

quite low) accuracy. Most of the current instrumentation pitfalls are related to the fact

that the measurements are acquired with intrusive instruments. Data acquisition

performed with these type of instruments also requires extended exposure to adverse,

frigid, and windy conditions that pose a significant risk for the personnel safety and health.

To be able to efficiently design the snow fence, one has to obtain detailed information on the records of snowfall, temperature, length of the snow season and local data on the intensity and direction of the wind. This information is needed to estimate the storage capacity of the snow fence (failure to design for the correct snow capacity required in a certain region is a common mistake), their extent (e.g., the fence should be about 20 fence heights longer on each side of the region that one wants to protect), direction (in general, fences should be placed perpendicular to the dominant winter wind direction) and position with respect to the road (e.g., fences positioned too close to the road can result in increased snow drifts on the roadways) and to design for their height. The information on wind and temperature is well covered by the meteorological observations at the national scale (i.e., NOAA's Local Climatological Data provides summary data for about 1,600 U.S. locations) complemented by other federal and state wind data repositories (e.g., National Renewable Energy Laboratory - www.nrel.gov/gis/data_wind.html and Iowa Energy Center - http://www.iowaenergycenter.org). Similarly, data on rainfall (including snow) is available from national and local observations (e.g., National Centers for Environmental Information - - and Community Collaborative Rain, Hail & Snow Network – www.cocorahs.org- respectively). The above data are readily processed to enable access to annual and seasonal summaries of the observed data for practically any location on the map in the U.S.

While the data for rain, temperature and wind are well established, snowfall data are acquired at 90% of the stations using intrusive methods, such as direct tape measurements of snow deposited on (white) boards over a certain time span (NOAA, 2013). Most precipitation gages operated by the U.S. National Weather Service are situated in exposed locations (such as airports), and not all are equipped with wind shields; therefore they underestimate the actual precipitation when wind is blowing. At windy sites, where the gage is not equipped with a wind shield, the true precipitation can be as much as twice that collected by the gage. When using precipitation data, it is wise to visit the weather stations involved to determine whether some allowance should be made for gage-catch error (Tabler et al. 1990).

There are few research-grade snowfall measurement stations that are designed to eliminate the effect of wind on the snowfall estimation (personal communication with J. Angel, Illinois State Climatologist). Moreover, even if the duration of the measurements is relatively short (10 minutes), a certain degree of compactness of the accumulated snow layer affects the accuracy of the snowfall quantification. For the particular application case of snow fence design, the use of correct raw snowfall data is critical, as this quantity is used for estimation of the Snow Relocation Coefficient (SRC), a critical input for the snow fence design (Tabler, 1994). The measurement method proposed in this research is non-intrusive (image based), portable (can be easily deployed at the snow fence site), and direct (does not involve the board). Snowfall density and wind-resolved fluxes are readily available from the processing of the collected images of the snowflakes moving within a control area as described in Chapter 3.

Obtaining quantitative information on the snow drift is even more challenging, as currently this parameter is rarely directly measured. Snow drift is a complex type of particulate transport. To form, snow drift requires several conditions to be met. Specifically, when the horizontal wind velocity is above a given threshold (i.e., about 5 m/s), there are two other factors that decide the severity of the snow drift: a) the snow pack characteristics (e.g., snow pack surface tension, snow pack temperature, snow depth, snow age, and others) and b) the characteristics of the roadway (i.e., local topography and land cover) surrounding the fence location within the snow fetch distance (Osborne et al., 2012). When all the conditions are met, the physical process, collectively labeled as snow drifting, is quite involved because it results from several near-bed interactions as described in Chapter 2. Given the complexity of the in-situ measurement of the snow drift, several empirical and semi-empirical relationships have been developed to quantify drifting snow based on independent process parameters (e.g., Tabler, 1991; Pomeroy and Gray, 1995; Baker and Williams, 1990; Perchanok, et al., 1993). The empirical relationships are typically site-dependent; therefore their accuracy might be low when applied to other geo-climatologic areas. The measurement method proposed in this research is non-intrusive, applicable to the site of snow-fence construction and proof-tested for other similar bed-transport processes (Muste et al., 2016). Details on the measurement method is provided in Chapter 3.

Given the current limitations in the estimation of such critical design elements such as snow fall and snow drift, the assessment of the post-construction efficiency of snow fences is critical. The assessment is critical not only because the design is typically assuming a one-storm event at the fence site but also because multiple thermal processes

are acting on the snow trapped at fences during and between successive storms which are not accounted for in the design. Moreover, the variability of weather conditions from storm to storm is not a parameter considered in the standard snow fence design procedure. Based on the above considerations, one can conclude that the quantification of snow accumulation at the fence site is the ultimate qualifier that determines the performance of the snow fence design. Direct observations of the post construction snow fence provide useful feedback for continuously improving the design guidelines. Conventional methods for quantification of snow accumulation are tedious, expensive, and, given the harsh winter weather environment, risky at times. The present research further refines the use of close-range photogrammetry developed through previous work (Keshav et al., 2015) for providing a general methodology for non-intrusive remote estimation of the snow deposit volume using automated data acquisition protocols.

<u>1.3 Contributions and layout of the thesis</u>

Given the limitations of the current measurement technologies as applied to snow transport measurement and the gaps in our analytical capabilities to describe them, the research reported in this study is based on a purely experimental approach for obtaining direct measurements of critical process variables. The main contribution of the present research stems from the assemblage of a set of measurement techniques that uniquely leverage advancements made in other areas of research. This set of techniques and methodologies is applied in the present study to a problem that benefits a socioeconomic activity that is critical for the functionality of any community located in areas with winter seasons. To the knowledge of the author, the application of the Particle Tracking Velocimetry and Large-Scale Image Velocimetry coupled with Photogrammetry is a first

attempt to directly quantify through direct measurements, rather than inferring, critical weather parameters such as snow fall and snow drift. Not only are the tested techniques of superior accuracy, but they are also efficient in data acquisition, portable, and safe to operate by reducing the exposure of the individual performing the measurements to an adverse, often harsh, environment. These technologies rely on image-based techniques that are easy to be used and widely available as off-the-shelf products making the access and transfer of technology faster. The raw information provided by the instruments are processed with customized or commercial software that offers opportunities to extract additional information following the measurement process. Collectively, the set of instruments, measurement protocols and processing procedures developed through this research creates a reliable measurement infrastructure for advancing the research in snow fence engineering and possible other aspects of winter road maintenance and safety. The development of the measurement techniques described in this research are also relevant to the broader area of hydrometeorology.

The thesis is organized as follows. Chapter 1 outlines the context of the research and the motivation for developing the proposed measurement methodologies. Chapter 2 reviews the theoretical background of snow transport in the lower region of the atmospheric boundary layer and conceptualizes the transport modes relevant to snow fence design. The chapter also reviews the current semi-empirical approaches to estimate snow drifting and the design software available for transportation design units. Chapter 3 reviews the fundamentals and essential elements of the measurements techniques utilized in the present research (Image Velocimetry, Large-scale Particle Image Velocimetry and photogrammetry) and extends the application areas of this techniques such that they can

be used to perform measurements of critical snow related variables, i.e.,. Also described

is the ancillary software used in conjunction with processing of the final results of the

measurement protocols. Chapter 4 describes the protocols developed for documentation

of snowfall, snow drift and snow deposit mapping. Given that the experimental sites

used to develop the various protocols were different, they are described and placed in the

wider context of the investigated subject. Chapter 5 presents the actual implementation of

the developed protocols as applied to event-based monitoring at various locations

exposed to snow drift. Chapter 6 present the main conclusions and discusses further lines

of research stemming from the research performed as part of this study.

CHAPTER 2 BACKGROUND ON RELEVANT PHYSICAL PROCESSES AND VARIABLES

This chapter reviews some important aspects of physical processes related to air and snow transport at sites where important snow precipitation occurs during the winter. Of particular interest is to describe how snow transport occurs over the ground and how this transport is affected by the presence of a snow fence. Given that the main role of snow fences is to diminish the adverse effects of snow drifting, the focus is on snow transport via drifting. Also some of the main variables used in snow-fence design are introduced (e.g., snow relocation coefficient) and their significance is discussed.

2.1 Snow transport via drifting

When small snow particulate is transported from the layer of snow on the ground by the wind, this is called snowdrift. The wind entrained the surface snow particle when the velocity is large and/or turbulence in the airflow over the surface layer. The threshold for entrainment of particles is a function of snow surface properties and flow conditions. Generally, wind velocity larger than 5 m/s is needed to entrain the particles from the top snow layer into the airflow. (Kobayashi, 1978; Pomeroy, 1989). Snowdrift can stop when one or more of these conditions occurs: (1) the wind velocity decays below the threshold value required for particles to move either via saltation or in suspension, (2) the temperature is large enough to produce the melting of the snow particulates part of the snowdrift, or (3) the particles become so sticky that they will remain attached when they interact with the top of the snow layer.

Both snowfall flux and wind velocity affect the amount of snow particles carried over the fixed layer of snow that is deposited on the ground surface. The three main modes of movement of the loose snow particles forming a snowdrift are rolling, saltation

and suspended transport. The total snowdrift flux is the sum of the fluxes associated with each mode of movement. Since the majority of the snowdrift transport occurs in a layer of less than 2 m thickness (Weather Online), the total flux is calculated by integrating from the top of the snow layer to about 5 m above it. For a certain mean wind velocity, the largest volumetric flux of snow within the snowdrift (0 m<z<5 m) is proportional to the mean velocity at power α, where α is close to 4 based on regression analysis of field measurements (Kathlein, 2009).

When wind speed is low enough, particles rolled along the ground forming slowly migrating snow dunes in a mechanism called creep. The size of the snow dunes ranges form few millimeters to several centimeters in height. When wind speed increases, the creeping snow particles began to bounces or jumps on the top layer of snow reaching the height of few millimeter to a few centimeters. The particles move downwind several centimeter falling to the ground where they free new snow particles when impacting the surface crust. When wind velocity is large, particles are entrained in the suspension layer which has negligible interaction with the top surface. This flow over the top layer of deposited snow is two-phase flow of air and solid snow particles. A two-phase coupling occurs between the transporting air phase and the snow granular particles. It was stated in Kathlein (2009) that in general, the maximum height of the saltation layer is a few tens of centimeters and the average jump height of saltation is less than 1 m. In fact, the height of the saltation layer is proportional to the square of the bed friction velocity for a good approximation.

The energy extracted by the snow particles when it is entrained by the wind affects flow characteristics such that flow without the presence of the snow particles under similar conditions is somewhat different. For example, a phenomenon called saltation-induced friction where particles via saltation collide causes a decrease in flow strength when compare to the equivalent one-phase flow (Dyer, 1986; Schmidt, 1986; Bintaja, 2001). The majority of the energy provided to the snow particles in suspension come from the turbulent eddies present in the top of the snow layer (Adams and Weatherly, 1981; Bintanja, 2001). Buoyancy effects can also be an important factor on the snowdrift (Bintanja, 2001). As wind speed increase, the effects of saltation is less prevalent because most of the particle inside the snowdrift move in suspension. The wind speed of 12 m/s are needed for the suspension mechanism to dominate. The remaining transport is done by saltation which is usually only 10% of the total snowdrift flux (Katlein, 2009). 90% of these particles lifted by the turbulent eddies do not reach a height of more than 2 m from the top layer. (Katlein, 2009).

Snowflakes take on different forms in characteristics while falling to the ground (e.g., dendritic flakes, icy pellets). As they fall, the crystals become more rounded in shape and the density is the function of the crystal characteristics. A detailed analysis of the difference types of snow are outside of the scope of this study but McClung and Schaerer (1993) contain a comprehensive description of the three different types of snow classification systems and their characteristics for reference. The first and simplest system is based on the degree of riming. The system is split into three categories to differentiate between compactness levels, age of the snow (fresh new snows and old), and graupel type snow crystals whose branches have been filled in by riming. The second

system adopted by the International Commission on Snow and Ice is comprised of eight categories where temperature ranges are associated with only some of these categories. Lastly, the third system includes approximately 80 categories. Typically after several hours, snowflakes deposited on the top of the snow layer become interlocked forming the bonded crust. Drifting may occur if the wind is strong enough to entrain snow particles from the crust. The snowflake characteristics determine the stress necessary to entrain snow particles from the top of the snow layer and the flow of these particles inside the suspension/saltation layer. As the snow particles move with the snowdrift, abrasion and particle-particle interactions cause particle rounding and the size reduction. Equilibrium conditions of snow layer particle entrainment generally needs 150 to 300 m above a certain surface (Takeuchi, 1980). Nonlinear snow flux at the stop snow layer occurs along the wind direction until about 250 m when it reaches equilibrium.

Moreover, energy is extracted from the mean wind flow by the snow particles. With increasing distance from the top layer of snow, snow particle density decreases and the airflow becomes somewhat stably stratified. It was shown in (Bintanja 2001) that stratification effects on snowdrifts close to the top of the snow layer becomes more important. For instances, observation was found that the turbulent kinetic energy of the flow is reduced by up to 40% due to dissipation form the presence of snow particles compared to the same flow with no snow particles. Kobayashi (1978) also found that shear-induced turbulence production is larger in the case the flow carries snow particles.

Under the assumption of sufficiently large particles or weak flow, the dissipation term from density drifting effects (Elgobashi and Abou Arab, 1983) is proportional to the velocity difference between the particle and the carrying (air) flow at that location and

with the mean vertical (z) gradient of the particle volume concentration, C. If the velocity

difference is approximated in the order of terminal fall velocity and Stokes law is

assumed (strictly applies to snowflake diameters less than 400 μm), then the extra

dissipation term referred to as the particle-induced buoyancy destruction component is

defined as (Bintanja, 2001):

$$B_p = - ((\rho_p / (\rho_f - 1) / \rho_p)) \, g * K * dC / dz \tag{2.1}$$

where ρ_p is the density of the suspended particles (e.g., snowflakes), ρ_f is the density of

the medium fluid (e.g., air), g is the gravitational acceleration and K is the turbulent

diffusivity. In theory, a contribution unrelated to density stratification effects is included

in the dissipation term, (dC/dz not equal to zero). In practice, when estimating the total

extra dissipation, this term is difficult to quantify and in most cases is neglected. Bintanja

(2001) stated for snowflakes moving in suspension that the particle-induced buoyancy

destruction term dominate the total extra dissipation.

The following discussion of increasing bed roughness in flow with snow particles

via saltation is based on analysis by Bintanja (2001). The study introduced an empirical

relation which accounts for the actual roughness length (z'_0), incorporating effects

induced by snowdrift. Actual roughness length is due only to friction at the top of the

snow layer when snow moving particles are not present via saltation and is always larger

than the standard roughness length, z_0. Using the friction velocity (u_*), the relation is

defined as:

$$z'_0 = 0.0029 u_*^{2.48} \tag{2.2}$$

Eqn. (2.2) was plotted in Figure 2.1 with experimental data used to generate the

best statistical fit. The increase of z'_0 with u_* is caused by more snow particles being

entrained from the top of the snow layer with increasing wind velocity, resulting in an increase of u_*. Since the standard roughness length (z_0) was 0.0001 m, the effective roughness length used in log-law wind velocity profiles over the top of the snow layer is about one order of magnitude larger compared to the corresponding case with no snowdrift for friction velocity values close to 0.6 m/s. Furthermore, it was shown by Bintanja (2001) that the mean fall velocity of the snow particles increases with friction velocity and therefore with the mean wind velocity (e.g., the mean fall velocity increases by more than 50% for an increases of friction velocity from 0.3-0.5 m/s). Since stronger flow can entrain larger snow particle from the top of the snow layer, the presence of larger particles with larger fall velocity generate more turbulence while interacting with the carrying flow.
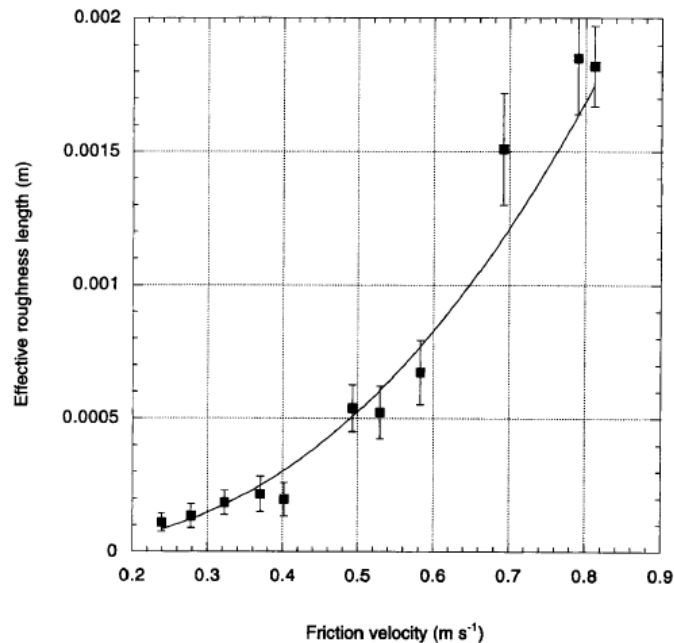
Figure 2.1 Dependence of the effective (or apparent) roughness length, as determined from the wind speed profile, on friction velocity. Reproduced from Bintanja (2001)

As previously discussed, a somewhat stably stratified flow inside the saltation/suspension layer is created by the differential concentration of the snow

particles entrained from the top of the snow layer. The heavier snow particles extract

turbulent kinetic energy from the carrying flow which allows them to remain above on

the top of the snow layer. As a result, the mean vertical wind velocity profiles are

different from those observed in a flow with no particulates. For such cases, a modified

wind vertical profile, U(z), was proposed by Bintanja (2001) of the form:

$$U(z)=(u_*/k)(\ln(z/z_0')+Az/L_{tot}) \tag{2.3}$$

where k is the von Karman constant, A is the empirical equal to 5, and L_{tot} is the

Obukhov length that accounts for particle buoyancy effects. Figure 2.2 introduced the

variation of z/L_{tot} with the friction velocity, determined experimentally by Bintanja

(2001). Figure 2.2 includes separate lines for the length scales associated with thermal

effects (z/L_θ) and buoyancy effects (z/L_η), showing that particle buoyancy effects are

critical especially under the high wind values.
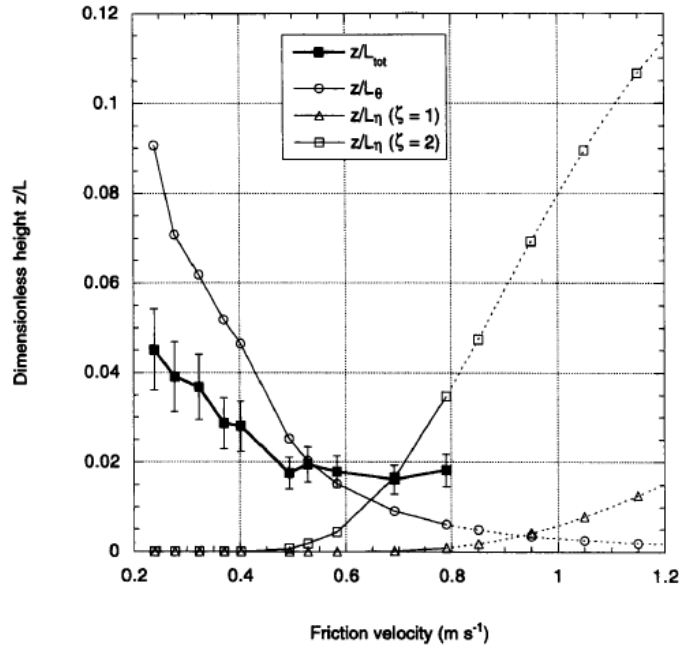
Figure 2.2 Dependence of stability parameter z/Ltot on friction velocity at z=2 m from
the top of the snow layer based on log-linear fitting of measured wind velocity profiles

The mean velocity is linearly related to bed friction velocity for single-phase flow. It was stated in Bintanja (2001) that non-linear dependency of the friction velocity on mean wind speed and particle buoyancy is related to snow particles transported via saltation or suspension in the snowdrift affecting the wind velocity profiles. This is particularly important for high wind speed where buoyancy effects become non-negligible. The experimental data confirmed that friction velocity increases faster for entrained flow larger than 10 m/s compared to the equivalent flow without snow particles. Stable stratification decreases turbulent fluctuations which increases the bed friction velocity values for the same mean wind velocity. Additionally, saltation effects were shown to increase the bed friction velocity particularly during moderate wind conditions. The increase in bed friction velocity causes the wind velocity profiles gradient to increase near the top of the snow layer. A different effect caused by the presence of snow particles above the top of the snow layer results in an increases of turbulent kinetic energy production. For wind speed over 12 m/s, the particle buoyancy effects increase the turbulence production by more than 100% (Bintanja, 2001). When compared to the case without snow particles, saltation is the main contributor for the increase of turbulence production while stable stratification tends to decrease the turbulence production.

2.2 Physical factors affecting snow drifting

In large open areas snow drifting cannot be avoided, but in various locations it can be reduced using snow fences. The fences purpose are to collect the snow in between its location and the road, it also can be used to blow snow away (blowing snow fence). The strength of the snow drift depends on the wind fetch, and as previously discussed, the

21

roughness of the top layer of deposited snow. A larger wind fetch indicates that the particles are directed over a large surface. The total flux of the snow increases with the fetch until equilibrium occurs, (a distance along the wind direction larger than 250 m) and then becomes constant and independent. Tabler (1994) and Pomeroy and Gray (1990) provided the empirical relationships relating the total flux of snow to the fetch distance and the roughness of the top of the snow layer.

The geometry of the surface can affect deposition and where erosion occurs, it also shows how severe the erosion or deposition can be at that specific location. The existence of a barrier (e.g., snow fence) can modify the snows erosion/deposition process. As mentioned by Schaerer (1972), "the critical task in planning protection against snow drifting is to predict the direction of drift producing winds". The wind should be measured locally because of the obstruction, which has to be taken into account.

As discussed by Schaerer (1972), the combination of natural objects (hills, valleys, vegetation) and man-made objects (fences, structures) can significantly modify the deposition and erosion patterns. The area of interest for this study are highways that need to be protected from the effects of snow drifting. For instance, smallest snowdrifts occur at the top of hills, assuming the hill is not situated in the wake of another large terrain obstructions. On the other hand, largest snow deposition is observed on the areas of lee ward side of the hills. For secluded objects (fences, buildings, trees) the upwind causes the wind to slow and allows the snow to be deposited on the downward side of the obstruction. The idea is that the distance between the obstruction and the highway should be small, so that the snow does not deposit on the road. Tabler (1994) provides the

approximate procedure on how to determine the distance over which snow deposits downstream of an obstruction.

Vegetation that either has no snow or is covered by a thin layer of snow increases the roughness of the snow layer. When the snow is melting or there are high wind speeds, the snow layer decreases and the vegetation projects itself over the top of the snow layer. Which causes an increase of roughness the can affect the wind velocity were snow particles can be entrained. The snow fence is placed in the dominate wind direction at that location. During the winter season the wind direction is not stable and adverse effects can be produced when the wind changes direction. The analysis of the physical features of the terrain can be used to predict and control snow drifting onto the highways.

2.3 Snow transport modes relevant to snow fence design

Different snow events have different snow transport modes. Three various transport modes are introduced and discussed below. At any site part of the snow movement can be described as snow falling. Most of the snow-flake movement can be described as snow falling under very low wind conditions such that the snowflakes move, in the mean, along the vertical direction. Snow drifting is formally defined as being the snow moving fairly parallel to the ground surface in between this surface and a height of six feet above the ground. The horizontal movement of snow transported above this height is typically called snow blowing.

Figure 2.3 indicates that under negligible wind where most of the snow movement can be assimilated with snow falling, the deposition of snow at a site where a snow fence is present is basically the same with or without the fence present. In both cases, snow

particles fall straight down to the ground. This is a first mode of snow transport than can be observed at a site where a snow fence is present.
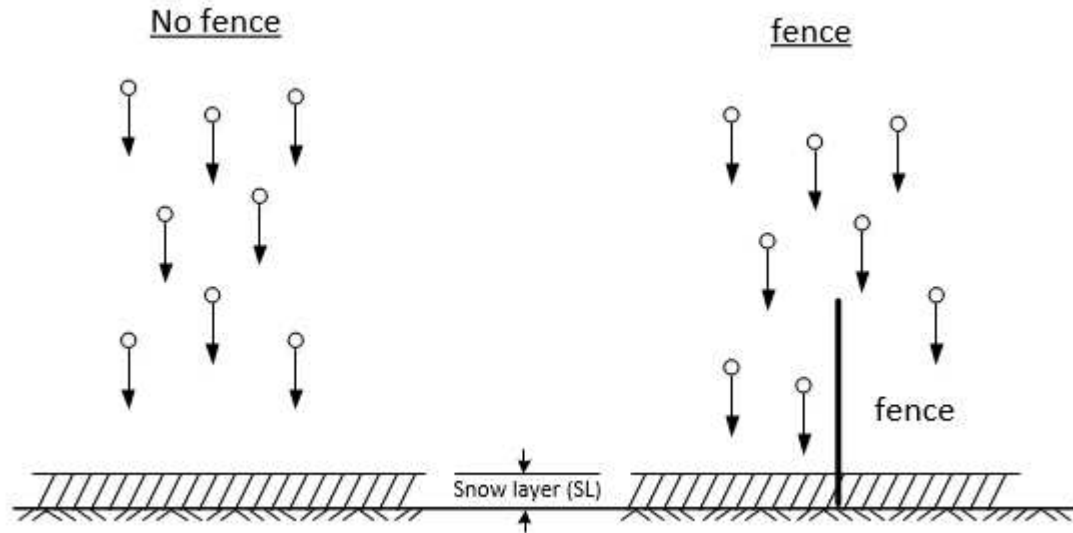
Figure 2.3 Sketch showing the movement of snowflakes at a site with no snow fence (left) and at a site where a snow fence is present (right) for the case when the first snow transport mode (snow falling under negligible lateral wind) is dominant

The second transport mode observed during a snow event at a site containing a snow fence occurs when the wind component parallel to the ground is not negligible but the wind velocity does not exceed the threshold value, called drift velocity, at which snowflakes deposited on the ground are entrained into the boundary layer developing over the snow-covered ground, move via saltation and are eventually relocated further downstream along the horizontal wind component direction (snow drifting is not active). Several studies (e.g., Kobayashi, 1978; Pomeroy and Gray, 1990; Schaerer, 1972) have proven that the threshold value for the wind velocity to produce snow drifting is close to 5 m/s or about 10 miles/h. When this transport mode is dominant, the snowflakes do not follow close to vertical trajectories. Figure 2.4 illustrates in a graphical way the second

transport mode, where V is the mean horizontal wind velocity; V_D is the drift velocity. Another relevant velocity is the snow drift velocity, V_{SD}, which is the actual velocity of the moving layer of (high-concentration) snow close to the bed. For this mode of transport, V is smaller than V_D and $V_{SD}=0$. At sites not equipped with a fence, snow particles will approach the ground with a non-zero angle relative to the vertical direction. If a snow fence is present at the site, due to the blockage induced by the fence, snow deposition in the vicinity of the fence will be affected by the presence of the fence.
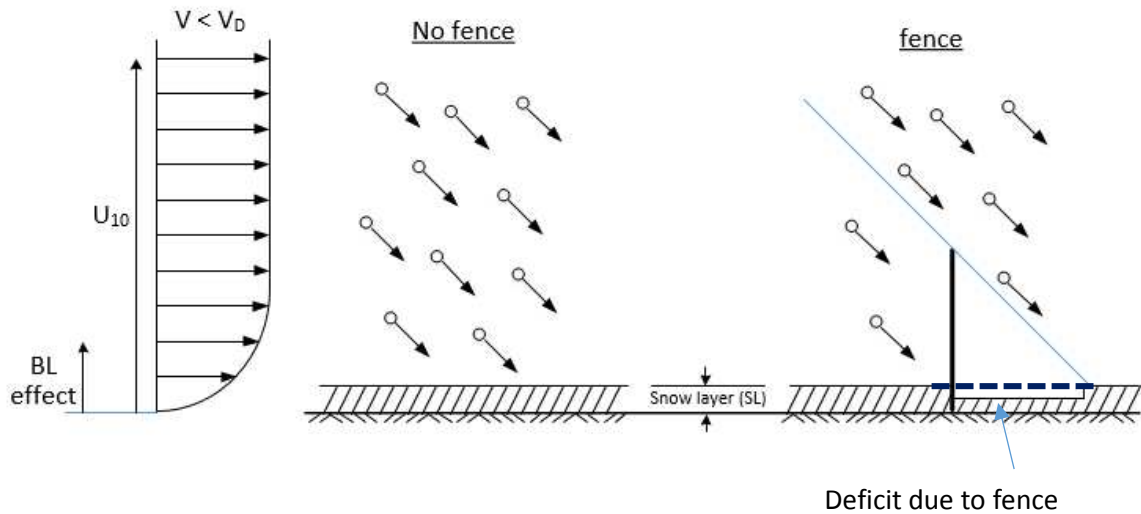
Figure 2.4 Sketch showing the movement of snowflakes at a site with no snow fence (left) and at a site where a snow fence is present (right) for the case when the second snow transport mode (lateral wind is present but its velocity is not sufficiently large to induce significant snow drift in the vicinity of the ground surface) is dominant

The third snow transport mode occurs when the wind velocity component parallel to the ground exceeds the threshold value (V>V_D). This mode of transport is dominated by snow drifting, which is the focus of the present study. Three different possible situations are presented in Figure 2.5 corresponding to the case when no snow fence is present at the site, the case when a snow fence is present at the site during the snow event

(snowfall is non negligible) and the case when a snow fence is present at the site after a snow event that generated a snow layer over the ground from which snow can be entrained and carried by the wind via drifting. If in the case when snowfall and wind are strong and no snow fence is present that the snow particles will pile up and generate larger deposition. However, if a snow fence of performant design is deployed at the site, one expects the snow fence will significantly reduce snow accumulation on the downwind side of fence by trapping snow particles. Also associated with drifting is the snow drift velocity, V_{SD}. Note that once snow accumulated on the ground, this mode of transport can be obtained even outside snow falling events when a strong wind is present at the site.
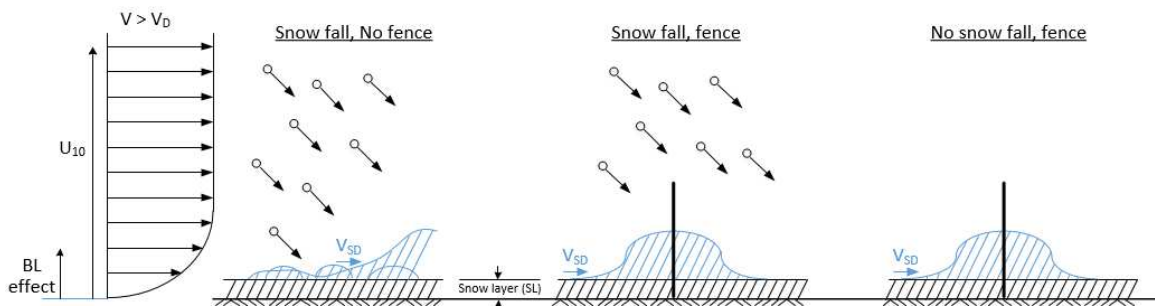
Figure 2.5 Sketch showing the movement of snowflakes at a site with no snow fence (left) and at a site where a snow fence is present (right) for the case when the third transport mode (wind parallel to the ground surface is present and its velocity is sufficiently large to induce snow drifting in the vicinity of the ground surface) is dominant.

In summary, several types of snow transport modes can be present at a site where snow precipitation occurs. For the snow drift to be significant, the wind velocity should exceed a threshold value. Snow drift can occur even in the absence of significant snow falling.

2.4. Estimation of snow transport and snow relocation coefficient

Multiple factors should be assessed in order to correctly design for the snow fence deployed at the site while evaluating snowdrift directly at the site where snow gathering on the road. The particular interest is to estimate the mean annual snow transport at the site and the retained snow capacity trapped at the fence. In spite of the several approaches proposed in the literature, the leading research conducted from Tabler (1994, 2003) which is the standard procedure utilized by majority of the State Department of Transportations (DOT) in the United States to design snow fences. This literature demonstrate several empirical formulas which determined based on in-situ experiments conducted in Wyoming. The major obscure is to observe what extent formulas calibrated for Wyoming can be used to obtain the accurate predictions in other regions where larger snow precipitation occurs during the winter season. Moreover, these empirical formulas are derived from the mean annual estimates of the relevant fluxes and thus they are not site particular. As mentioned in the previous subsection, the geometrical characteristics of the site can greatly impact the flux of drifted snow. Similar to other researchers, Tabler considered that most of the snow transport occurs from the top of the fixed layer of snow and go up to 5 m.

The mean annual snow transport (Kg/m) is calculated by following equation:

$$Q_t = 500 * T * S_{rwe}(1 - 0.14^{F/T}) \tag{2.4}$$

where S_{rwe} is the mean monthly relocated snowfall water equivalent causing from the wind (meters); F is the fetch length (meters) and T is the maximum transport distance (meters). Several factors (including relative humidity, air temperature, and wind speed) impacting the maximum transport distance (T) can considerably varies from storm to

other storms, however, the seasonal averages appear to be relatively stable. Tabler (2003) estimated the mean average T to be 3000 m (10000ft.) when estimated under Wyoming conditions. In order to determine the fetch length (F), aerial photographs were used after the direction of the mean dominant wind is observed. The definition of the fetch is the distance between the location to be protected and the nearest location on the upwind side from where snow particles are entrained toward that location from the top of the snow layer. If under the circumstances that the fetch cannot be clearly estimated from the photographs, it can be assumed that the second term of the equation 2.4 is equal to zero. Beside the mean annual snow transport (Q_t), the other important factor influences with the snow flux is the evaporation loss (Q_e) in Kg/m of width across the wind. The evaporation loss is calculated by Tabler (2003) to be:

$$Q_e=1000*S_{rwe}F-500*T*S_{rwe}(1-0.14^{F/T}) \quad\quad\quad (2.5)$$

The general schematic showed all the contribution of the snow fluxes of snow occurred at a site where a snow fence is present are provided in Figure 2.6.
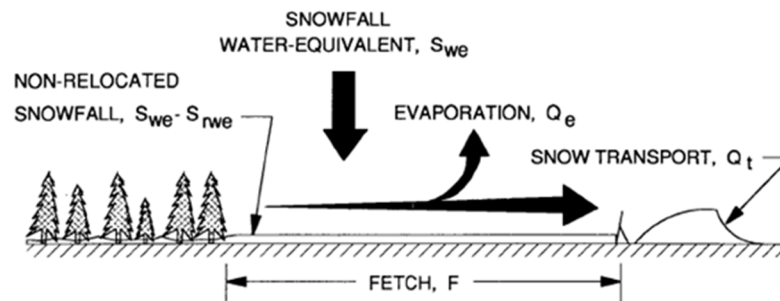
Figure 2.6 Diagram of snow transport in the vicinity of a snow fence. Reproduced from Tabler (1994)

Tabler's (1994) estimated the S_{rwe} based on the total mass flux of horizontal snow transport carried by the wind over a distance of 5 m from the top of the snow transport layer (Q_{0-5}) and U_{10} is the wind velocity in meter/second measured 10 meters up from the

28

bed. This discharge has the units of kg/s per meter of width across the wind and is estimated as:

$$Q_{0-5} = \frac{U_{10}^{3.8}}{233847}$$ (2.5)

Additionally, the S_{rwe} is obtained from

$$S_{rwe} = \frac{Q_{0-5}}{500\ T}$$ (2.6)

As noted by Tabler (1994), S_{rwe} is the part of the snowfall relocated by the wind and excludes snow retained by vegetation and topographic features, or snow that hardens or melts in place. Equations 2.5 and 2.6 were derived from a regression equation relating mass flux to wind speed and height above the surface (Mellor and Fellers, 1986). These two equations show that the rate of snow transport is strongly affected from the wind speed. For instance, by increasing a factor of wind speed will have the results in close to 15 times increment of the snow transport. This reduction of snow transport rate causing by the local reduction of wind condition because of the presence of an obstruction is the main effect on which the design of snow fences relies.

The overall amount of winter snow precipitation also expressed as a water-equivalent snow depth is observed at the nearby reporting meteorological stations for the records of monthly snow precipitation. Generally, this water-equivalent values obtained from the meteorological measurements has to be calibrated especially for the effect of wind blowing even though the gauging station collecting the snow precipitation were shielded. Tabler et al., 2003 suggested that the snow precipitation should be estimated

based on measurements of peak snowpack water-equivalent following the procedures applied from the US National Resources Conservation Service.

The reasonable estimation of S_{we} presented in Tabler is calculated by using the snowfall depth / 10 (meters), where the average snowfall depth is estimated by the nearby reporting station (as close as possible to the site). The non-relocated snowfall is then estimated as S_{we}-S_{rwe} (see in Figure 2.6).

Finally, once S_{rwe} and S_{we} are estimated, the snow relocation coefficient (SRC) can be calculated by using:

$$\theta = \frac{S_{rwe}}{S_{we}} \tag{2.7}$$

which the SRC represents that the fraction of the snowfall water equivalent relocated by the affection of the wind movement. In general, the values of θ are less than 0.7 (Tabler, 2003) and for the SRC calculated in the northeastern part of the United States is ranging from θ=0.2-0.3. SRC is the key factor when designing for the snow fence thus this variable is very important to be determined accurately. The current software used to design for the snow fences used in Wyoming Department of Transportation (WYDOT Snow Drift Profiler) are strongly dependent on the input value of the snow relocation coefficient. With the better estimation of the SRC, it will not only improve the predictions of the snow volume retained and deposited on the fence, it also reduce the risk of overtopping the snow fence. However, this SRC value contains a large uncertainty. Iowa DOT uses the conservative SRC value of 0.5 for the design parameter because of lacking of the studies specifically related to the state of Iowa, and there are no simple approaches to get a more precise estimation at a given site. However, the intuition

and engineering experience suggest that the input SRC for Iowa should be much smaller (approximately ¼ of this value for State of Iowa).

The other two input variables for the snow fence design software used in IDOT are the snow-water equivalent and the fetch distance. Regarding of one parameter can estimate the better result for mean estimation of the variable specifically for Iowa, however, since the condition varied from site to site, the input parameters need to be adjusted dependent on the local site-specific condition. For instance, the site contain the high vegetation condition would have different relocated snow compared with a site with similar meteorological conditions but with a bare flat ground surface.

In the following chapters, a set of experimental procedures and techniques will be outlined in order to directly measure the snow relocation coefficient at any given site. The proposed procedure will eliminate the values which is hard to obtain (e.g., the fetch distance). Large scale particle image velocimetry (LSPIV) technique will be used to quantify the average snow drift velocity close to the top of the snow layer (horizontal movement) at the site whereas particle tracking velocimetry (PTV) technique is applied to directly measure the snowfall precipitation of the vertical snow particle fall velocity.

CHAPTER 3 MEASUREMENT TECHNIQUES AND INSTRUMENTS USED FOR IN-SITU SNOW DRIFT ESTIMATION

3.1 Introduction

Conventional methods for estimation of snow drifting are still in development and most of them rely on direct measurements acquired in situ. The targeted variables for estimation of the snow drift and snow deposit extent are wind characteristics (magnitude, orientation, and their spatial variation over short and long time intervals), wind-fetch length, snow deposition geometry (extent, shape, orientation), and rates of snow transport in the vertical direction. Investigations on drifting snow are typically made up to 5 m from the ground level. For example, the leading study conducted by Tabler (1994) is based on an extensive dataset assembled from various studies carried out with diverse experimental methodologies (Figure 3.1). Most of the measurements are acquired with ground-based intrusive instruments including snow traps (Budd, 1966; Tabler, 1971), however, Tabler, 1990 demonstrated the intrusive measurement error can go up to 15%.
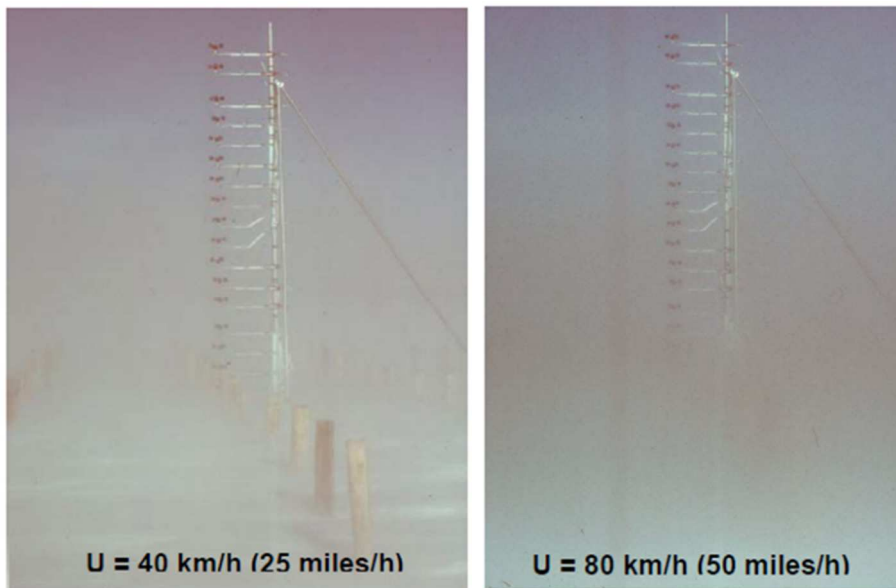
Figure 3.1 Direct measurement for wind speed of 25 and 50 mph from arrays of anemometers (30-cm apart) to obtain the vertical wind distributions (Tabler, 1994)

Major pitfalls of measuring in particulate flows with intrusive instrument regardless of the working fluid (i.e., water or air) are the probe-particle interaction and hence the difficulty to sample the flow such that to obtain a representative measurement. Moreover, direct measurements of snow falling, blowing, and drifting with intrusive approaches requires long-term exposure in wintery conditions that sometimes limits the extent and quality of the experimental data. From this perspective, non-intrusive methods such as those proposed in this study are making a great leap in improving the accuracy and efficiency of the results. Measurement of snow particle transport with image-based methods is one of the best candidate for this purpose. Not only that the image-based techniques can be remotely controlled avoiding extended exposure to outdoor conditions but their lack of interference with the natural movement of the particles increase the accuracy of the results and provide simultaneously information regarding sizing, density and velocity-derived quantities over a range of scales, up to the size of the imaged area. In this study, measurements of snowfall and drift are acquired in natural environment subjected to various weather conditions using image-based methods. These methods are discussed next.

3.2 Image-based techniques

3.2.1 Image velocimetry

Image-based methods for tracking particles stem from the visualization techniques that have been continuously developed over time. Their original purpose of the technique was to visualize flow patterns in free-surface flows. Later one, the technique has been completed with means to quantify velocities of individual or group of particles carried by the flow. Particle Image Velocimetry (PIV) and Particle Tracking

Velocimetry (PTV) are the most representative techniques from this family of velocimeters (Adrian, 2005). Whereas PTV technique tracks individual particles, PIV is used to track groups of particles moving within the flow. The measurement principle of the image-based techniques is based on the simple speed-distance-time equation, provided below:

$$Speed = \frac{Distance}{Time}$$ (3.1)

The estimation of the distance traveled in time by the particles is obtained by tracking individual or groups of particles with statistical inference tools (i.e., spatial auto-correlation or cross correlation) applied to successive images taken at short time intervals. The end result of image-velocimetry based measurements are two-component velocity vectors estimated at discrete points across a 2-dimensional slice of the flow field.

The image velocimetry process entails of four major elements: seeding, illumination, recording, and image processing. A generic schematic of the image-based velocimetry setup is provided in Figure 3.2. Before starting the measurements, the working fluid in the experimental facility is "seeded" with small reflective particles that are assumed to follow accurately the structures in the flow. Next, the flow area to be investigated is illuminated with a thin sheet of light produced by continuous or pulsed lasers. Images are subsequently recorded from an angle perpendicular to the light sheet plane using specialized or conventional (off-the-self) cameras. There are several combinations of camera and illumination sequencing used to obtain sharp particle images and small displacement of the particle from an image to another (Westerweel et al., 2013).
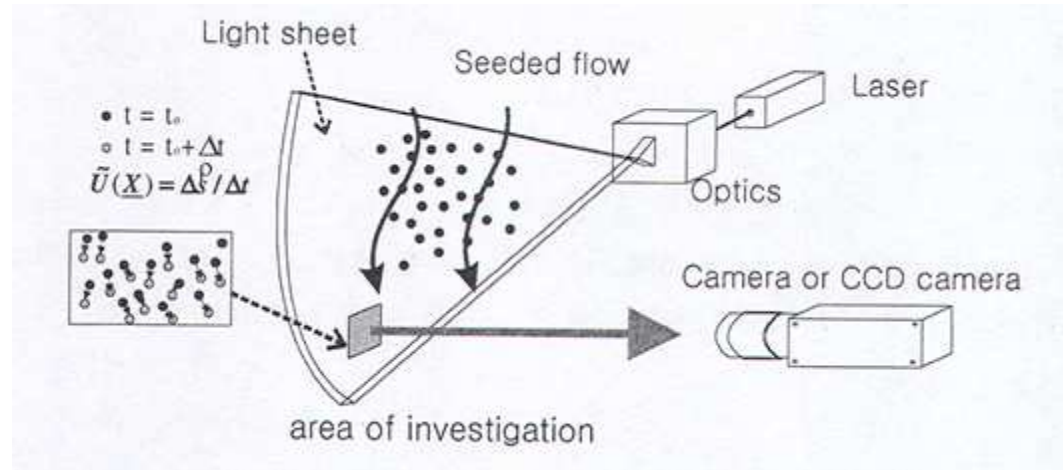
Figure 3.2 General configuration of a PIV system (Lee, 2001)

The concentration of particles in the recorded images determines the type of algorithm used for velocity estimation. For low seeding concentrations, PTV processing algorithms are used to detect individual particles, estimate their displacement in time, and determine their velocity with equation 3.1. The such-obtained velocities can be used to quantify the dynamics of the underlying flow or variables associated with the particulate transport in the flow (particle concentration, fluxes). For high particle concentrations, the tracking of the movement of individual particles becomes difficult. In contrast, PIV algorithms quantify the flow movement by tracking patterns formed by groups of particles suspended in the flow. Use of PIV is associated with the detailed characterization of the turbulence structures in various flows. A short discussion of each of the image velocimetry step is provided below.

Seeding. Although image velocimetry is categorized as a non-intrusive technique, the flow subjected to measurements has to be visualized by the addition of minute quantities of flow tracers, a.k.a. seeding particles. Ideally, the particles must be neutrally buoyant so that they can follow the direction of the flow including the finer flow structure driven by turbulence. From this perspective, the particles should be light and small. At

the same time, particles should be sufficient bright for the recording devices to be able to get accurate images of the particles within the illuminated flow field. Tracer particles for use with water flows are most often nearly neutrally buoyant glass or plastic microspheres, but metallic powders or natural particles (pollen) may also be used (e.g. Raffel et al., 2007).

Illumination. Flow field illumination is typically accomplished with a combination of spherical and cylindrical lenses that produce a thin laser sheet as illustrated in Figure 3.3. The actual illumination consists of short but intense light pulses fired in the flow at a high rate (Westerweel et al, 2013). Capturing these pulses will require a fast speed camera with high rates of recording.
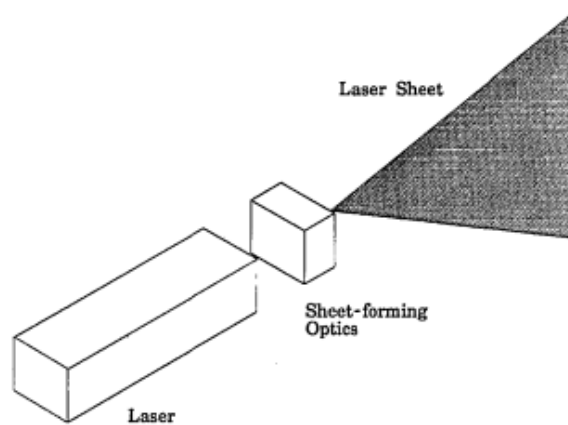
Figure 3.3 Illumination (Lourencoet al. 1994)

Image recording. The most often used contemporary image velocimetry recording devices are the coupled charged device (Raffel et al. 2007). Recording can be made in several ways: single frame with single, double, and multi-exposure; double frame with single exposure; and multi-frame with single or double exposure as shown in Figure 3.4. In order to make sure that both the maximum and minimum velocities are captured, the operator has to anticipate the flow features, define the measurement

objectives, and to appropriately design and operate the illumination-recording

sequencing. With appropriate camera settings, images are successively acquired at time

intervals commensurate with the goals of the measurement. For PIV measurements this

sequencing is stricter as the velocity evaluation is based on the assumption that the

patterns formed by the particles remain the same in image pairs (i.e., there is little or no

relative change in the positions of the particles within the pattern).
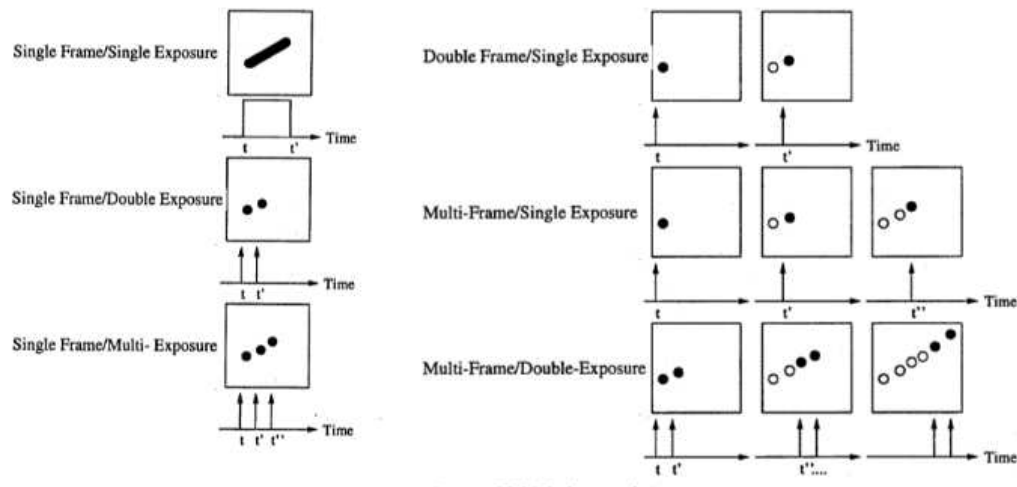
Figure 3.4 Single/Double frame exposure (Raffel, 1998)

Image processing. Following the acquisition, the images are processed using

statistical tools to determine velocities. While PTV and PIV have many commonalities in

terms of configuration, setup and operations, there is a considerable difference in their

image processing algorithms. As both techniques are used in the present study, the basic

elements of the two processing algorithms are briefly presented below.

PTV. Figure 3.5 provides a flow chart that describes a typical PTV methodology

(Admiraal, 2017). To the right of the flow chart, progression of the methodology is

demonstrated using subsections extracted from a pair of PTV images. As shown in Figure

3.5, the PTV process begins with the collection of a pair of particle images. The quality

of the seeding and of the illumination-recording sequencing are critical for PTV as for

37

locating the particles, their image has to contain more than one pixel. Furthermore, large particle-image diameters should be avoided to optimize fidelity of the velocity measurements in locations with strong temporal or spatial velocity gradients. After the PTV images are collected, some initial processing may be required to make sequences of images more uniform (brightness adjustments, background filtering, setting thresholds for particle identification, etc).

Once individual tracer particles are found, the centroids of the tracer particle-images are calculated based on the contiguous pixels that form the tracer. After particles and their centroids are identified in consecutive images, an attempt is made to match pairs of particles in adjacent images that eventually lead to the estimation of the particle displacement in time. The estimation of the potential displacement for each particle is made with various statistical algorithms (e.g., nearest neighbor, cross-correlation) applied to identical-sized particle candidates (Lloyd *et al*., 1995). After estimating velocities for each particles (using Equation 3.1), various filtering are applied to the velocity estimates to remove the effect of possible errors. The velocity vectors estimated with PTV are randomly located throughout the flow field based on the positions of the tracer particles when the images are collected. It is usually desirable to know the velocities at selected points in the flow, so the PTV vector data must be combined to form weighted average vectors at the selected points. Such vectors may be time averages of data collected from many PTV realizations or instantaneous averages of all of the tracers within a known radius of the point of interest (Admiraal, 2017). Admiraal (2017) makes reference to a Large-scale PTV that operates with identical features just that the imaged area is much larger than the one used in the conventional PTV (typically of order of 20x20 cm).
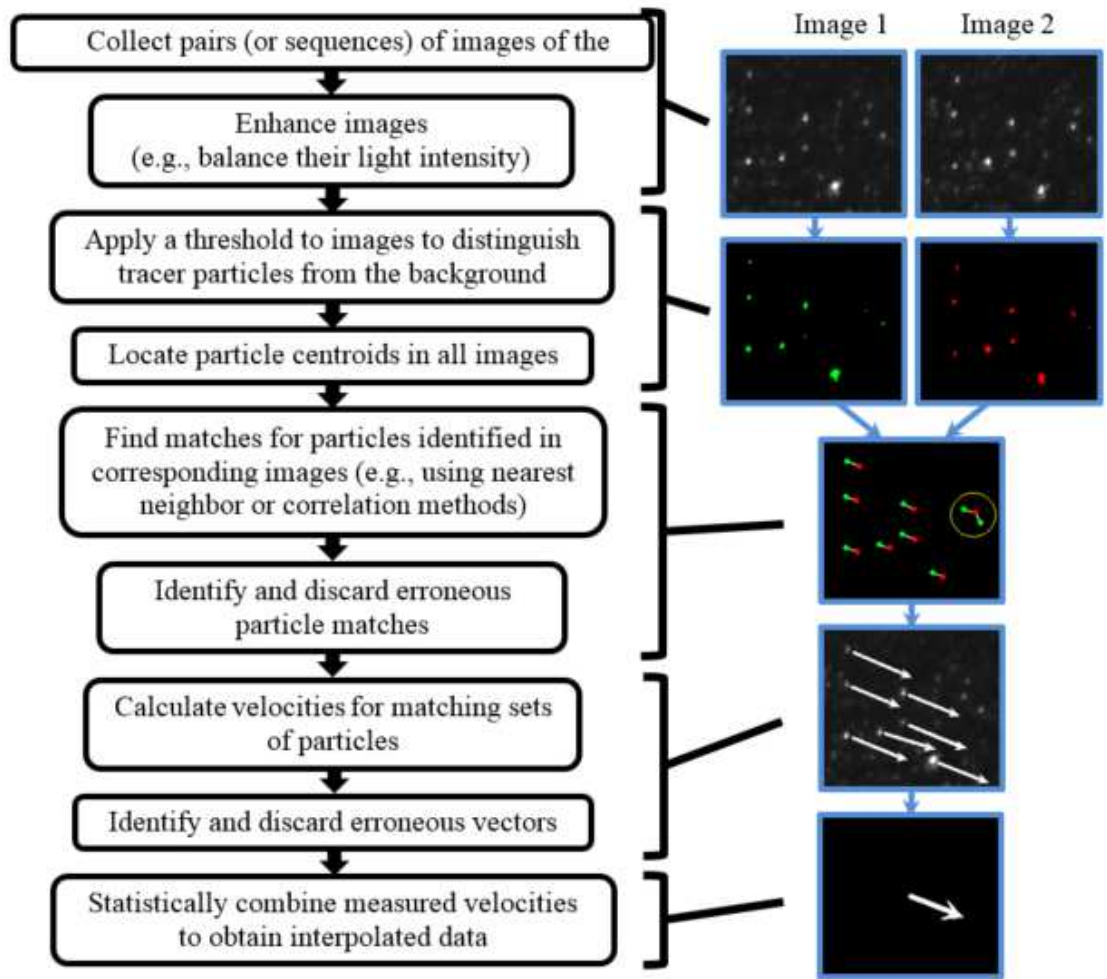
Figure 3.5 Flow chart illustrating the PTV methodology (Admiraal, 2017)

__PIV.__ Prior to apply the image processing leading to the velocity vector field, the

recorded image are binned into small interrogation areas (IA), a.k.a interrogation spots, or

interrogation windows. For each individual interrogation area, statistical approaches are

applied to a larger-size search areas (SA) centered on the IAs to determine the possible

direction and magnitude of the possible IA displacement. During the evolution of PIV,

several image processing algorithms were developed, driven by the technology available

at the respective times. The first PIV systems used single frame/multiple exposure

recordings that required autocorrelation-based algorithms for evaluation of the velocities

(Adrian, 1991). Subsequently, with the increase in camera frame rates, double frame/single exposure recordings have emerged (Raffel et al., 2007), leading to the development of cross-correlation methods for the evaluation of velocities (Raffel et al., 2007).

Currently, the cross-correlation technique is the dominant contemporary PIV interrogation technique. Several reasons explain why the cross-correlation method is being increasingly applied for image processing. Not only because it can resolve the velocity direction as well as its magnitude, but also that the processing of cross-correlation algorithms are more robust and easier to obtained than auto-correlation which needs to use other software to determine shifting of exposure. Given its extensive use and that fact that the Large-Scale Particle Image Velocimetry subsequently presented is based on the same algorithm, only cross-correlation velocity estimation algorithm is presented here.

The cross-correlation approach used in our study is described in Muste et al. (2008). In essence, a pattern matching technique is applied to image intensity distribution in a series of images as illustrated in Figure 3.6. The similarity index for patterns enclosed in a small interrogation area (IA) fixed in the first image is calculated for the same-sized window within a larger search area (SA) selected in the second image. The window pair with the maximum value for the similarity index is assumed to be the pattern's most probable displacement between two consecutive images. Once the distance between the centers of the respective small window is obtained, velocity can be calculated by dividing it with the time difference (dt) between consecutive images. This searching process is applied successively to all IAs in the image. The end result of image

processing is a velocity flow filed covering the entire processed area with a velocity density that is decided by the user.
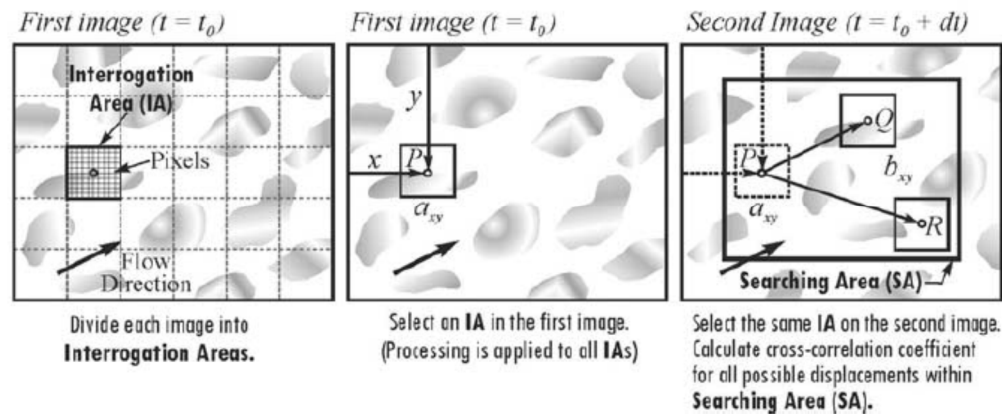
Figure 3.6 General procedure for PIV measurement (Muste et al., 2008)

3.2.2 Large scale particle image velocimetry (LSPIV)

An extension of the traditional PIV was created for estimating velocity covering large scales flows by Fujita et al (1998). This innovation, labeled Large Scale Particle Image Velocimetry (LSPIV), was firstly implemented for non-intrusive measurement of the velocity at the free surface of open-channel flows. LSPIV entails all the components of conventional PIV, i.e., seeding, illumination, recording, and image processing. However, given that large size of the imaged area, often recorded from a tilted angle, requires an additional step before processing the images for estimation of the velocities (Fujita et al, 1998b). The differences between conventional PIV and LSPIV are synthesized in Table 3.1.

Table 3.1 Similarities and differences between conventional PIV and LSPIV (Muste et al., 2004)

Component	Conventional PIV	Large scale PIV (LSPIV)	LSPIV Additional Procedures/Features
Illumination	- small image areas (up to 0.20m^2)	- large areas (up to 100 m^2)	- elimination of light reflections on the flow free surface and uniform distribution of the light intensity over the imaged area
	- strong illumination sources (CW or pulsed lasers)	- conventional illumination: white natural or artificial light	
Seeding Particles/ Material	- micron-size, neutrally buoyant , uniformly dispersed in the flow	- cm-size, lighter than water density	- seeding material color needs to contrast background color (Muste et al., 1999)
Recording	- high-resolution or high-speed cameras	- video-based cameras (low resolution, low speed)	- special image processing algorithms required
	- recording of a reference grid for scaling	- recording of images to include marker points (known coordinates) needed	- geodetic survey of the marker points for image-to-real-coordinate transformation
		-	
Pre-processing	- not needed	- removal of image distortion due to lens aberrations and perspective effects -	- image reconstruction using geometrical mapping (Fujita and Komura, 1994)
Processing	- reliance on individual particle images	- flow tracing made on local image patterns formed by groups of particles	- use algorithms designed to process for low resolution images (Fujita et al., 1998)
	- 2-D autocorrelation or cross-correlation of image pairs, usually with Fast-Fourier Transform (FFT)	- 2-D cross-correlation applied to image pairs in real space	- flexibility in chosing the interrogation area shape and size
		- de-coupling of the interrogation area from its fixed location in the first image of the pair to any arbitrary location in the second image of the pair	- eliminates velocity bias and improves processing of vortical flows (Fincham and Spedding, 1997)

As shown in Table 3.1, LSPIV entails an extra processing step: the image ortho-rectification. In order to extract accurate flow data from images recorded from oblique angles, they have to be rectified by an appropriate image transformation scheme (Muste et al., 2004). This transformation requires to survey at least six Ground Reference Points (GRPs) that are included in the flow video frames at the time of image acquisition, as illustrated in Figure 3.7a. The control points are surveyed in the field using specialized equipment. The GRPs selection is often dictated by what is accessible out in the field (e.g., trees, power line poles, building corners, etc.) rather than what is desirable. These points are subsequently used in conjunction with a conventional photogrammetric

relation that maps the GRP coordinates in the physical space $(X, Y, \text{and } Z)$ with their

image (x and y) coordinates, as shown in Figure 3.7b.

a)

b)
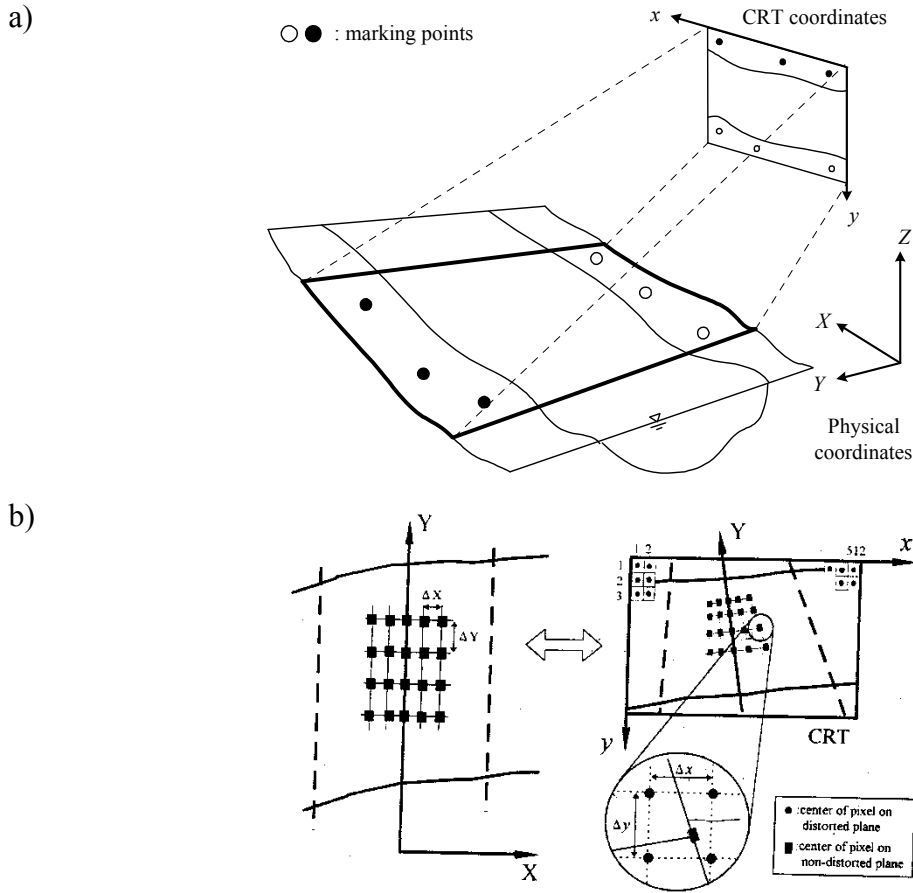
Figure 3.7 Image ortho-rectification: a) imaging of the GRPs; b) mapping of the GRPs from physical coordinates to camera coordinates (Fujita et al., 1998b)

Similarly to PIV, LSPIV requires "seeding" in order to visualize the water body

movement. The step-by-step procedure to determine LSPIV velocities is schematically

shown in Figure 3.8. Seeding in the LSPIV context is defined as groups of particles

floating at the free surface that collectively create image patterns that are distinguishable

in the recorded images. Attaining uniform and adequate seeding over large areas is

difficult for both controlled (lab) and natural environments. Consequently, most of the

seeding of the free surface in natural conditions is non-uniform and in rare situation

adequate.
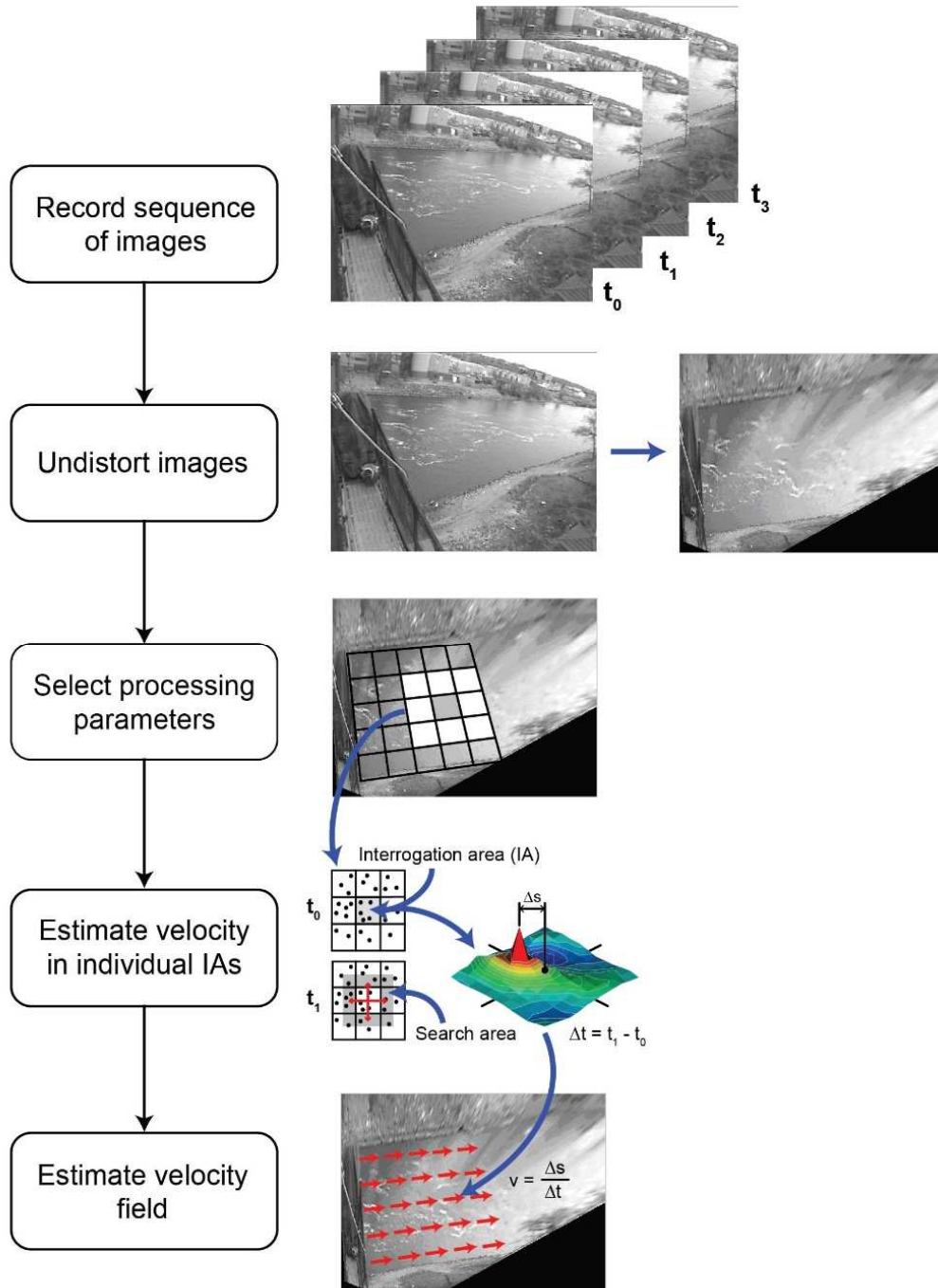
Figure 3.8 The LSPIV procedure for estimation of velocities in an open channel
flow (Muste et al., 2014)

To counteract for the limitations associated with seeding in natural-scale environments, the present authors adopt an image processing algorithm that can estimate velocities from low-resolution images, such as those captured by standard video cameras from far distance. The algorithm is similar to the correlation imaging velocimetry of Fincham and Spedding (1997) that considers each pixel in the interrogation area equally weighted in the interrogation process such that the background image is just as important as the pattern images.

The LSPIV algorithms for estimating velocities are the same with those used in conventional high-density-image PIV (Adrian, 1991), see also Figure 3.8. The LSPIV measurement outcome are instantaneous vector fields. Each IA encompassed in the original free surface image has a vector attached. The LSPIV vector field obtained makes it possible to conduct Langrangian and Eulerian analysis for determining spatial and temporal flow features such as the mean velocity field, streamlines, and vorticity as other velocity-derived quantities.

3.2.3   Photogrammetry

The main purpose for photogrammetric survey is to use photographs to quantify the terrestrial space in three dimensions and also replicates its texture as a continuum. Kunapo (2005) defines photogrammetry as the art and science of constructing reliable three-dimensional (3-D) landscapes from 2-D photographs. While in photography the three dimensional object is captured in a two-dimensions, in photogrammetry the process is reversed, working from two dimensional images to three dimensional objects being measured. This is accomplished by using two or more overlapping two-dimensional images so that it is possible to triangulate on the object points, as illustrated in Figure 3.9.

Multiple cameras are positioned with different angles and aimed at the object in order to recreate the object, the combination of two or more photos from the same object is also called stereoscopy. This method is able to determine the height of the object.
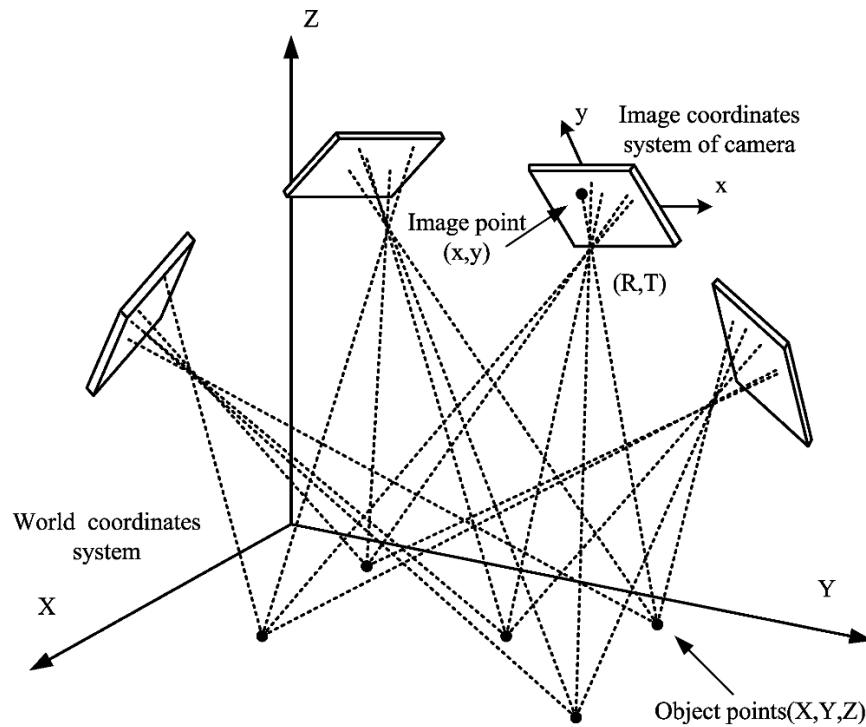
Figure 3.9 Principles of photogrammetry survey when creating a three dimensional model (Tang, 2012)

Photogrammetry comprises two main operational steps: acquisition of photographs and metrology. There are two types of image acquisitions used in photogrammetry: traditional (aerial) and non-traditional (close-range) depending on the location of the camera during the image recording. In aerial photogrammetry, the camera is mounted underneath an aircraft and images are acquired with camera oriented vertically downward. In non-traditional close-range photogrammetry (CRP), the camera is positioned closer to the object and typically set on the steady pole or tripod. (Matthews, 2008). CRP is typically reconstructing the actual terrain topography using a pair of

photos of the same area (or object) taken from slightly different locations. However, the more overlapping images are taken from different angles, the better resolution of 3-D reconstruction of the object can be generated (Kraus, 1992; Wolf and Dewitt, 2000; Cooper and Robson, 1996).

Regardless of the type of image acquisition, high photogrammetric outputs can only be obtained with high quality photographs. The three main elements involved in capturing high quality images are camera settings: the focus, exposure time, and field of view. Cameras have to be adjusted to focus on the object/image plane in order to enhance the resolution of the texture used for photogrammetric reconstruction. The exposure time has to be long enough to allow to distinguish multiple features of the recorded background surfaces. The camera field of view determines the range of visibility of the images related to the focal length. In other words, the areas of the imaged surfaces that are outside the field of view appear blurred in the recordings and cannot be efficiently used to reconstruct the 3D image.

The second component of photogrammetry is metrology, i.e, the reconstruction of the three-dimensional space from combining two-dimensional images. In this step, a triangulation method is applied to a set of points that are recognized in the multiple images of the overlapping areas of the photogrammetric survey. In order to scale the 3-D location of each object point in the images, it is required to conduct a survey of few reference points at the measurement site (Basnet, 2015). These, so-called ground reference points (GRPs) are specified by the operators and can be marked by using paints, tapes, or stakes. GRPs actual coordinates need to be associated with the image coordinates and typically each sets of images needs at least three GRPs as illustrated in

Figure 3.9. With the lines and points overlapping, pixels representing same point in different images will be recognized, the triangulation principle will be able to determine the accurate location/depth of the object. These overlapping points within the covered area by the multiple photographs are generated by the sophisticated photogrammetric software (i.e. Agisoft) and identified as tie points. The more tie points generated results in higher probabilities to recognize the same location of the surface in the images. Tie points are used along with the physical coordinates of GRPs in order to scale and evaluate the geometry quantitatively (Basnet, 2015). Agisoft software then generated the cloud of tie points (typically thousands) with the known accurate coordinates as the final output data which is plotted in Agisoft software for the quantitative visualization of the volume. Several additional steps are involved in reconstruction of the final three dimensional model: aligning the photos to auto-detect the tie points, building dense cloud to identify the amount of the tie points, building a mesh in order to connect the points to generate polygons surface, and build texture to define the appearance and color for each polygons.

The final output of CRP is an easily understandable 3-d representation of the landscape not the typical topographic visualization of the terrain (i.e. not similar to a map with iso-contours). The final product does not need any additional technical knowledge as it is the form that is close the human visual perception. Photogrammetric surveys are increasingly used due to some distinct advantages: cost efficiency as they only require camera and software; reduction of the safety risk compared to the actual field survey measurement; relative ease to obtain data remotely without the need to access the site.

3.3 Instrumentation and preliminary tests

3.3.1 Summary of instrumentation and software used in this study

3.3.1.1 Image-based techniques for snow velocity and sizing

Two different image techniques, PTV and PIV, were applied in this study for determining the study targeted variables. PTV was used to quantify the snowfall whereas PIV was used to determine the horizontal transport of snow particles in the form of snow drift. The summary of the PTV and PIV features for the present study is presented in Table 3.2.

Table 3.2 Summary of different image techniques used for tracking particle velocity

| Image Technique | Role | Image velocimetry Components | | | | Software |
		Seeding	Illumina-tion	Recording	Processing	
PTV	Measurement of snowfall (vertical)	Snowflakes	Natural/ Artificial light	Sony 4K video camera	Cross-correlation	EDPIV
PIV (as used in LSPIV)	Measurement of snowdrift (horizontal)	Snowform migrating on the snow deposits	Natural/ Artificial light	Sony 4K video camera	Cross-correlation	FUDAA

As shown in Table 3.2, PIV and LSPIV recordings were made with the same camera. Acquiring photographs for dynamic flow field with particulate transport with variable velocity is challenging from several respects: sufficient lighting (day and night conditions), high resolution camera with adjustable optics to focus the camera field of view, and high speed capabilities to capture the high velocity of snowflakes carried by wind gusts.

Testing camera settings. Prior to establish the measurement protocols with PIV and LSPIV the evaluation of the proper setting on the camera were tested and establish anticipating various measurement scenarios. More testing was needed for the snowfall measurement where PTV was used for processing. For PTV the recording were made with camera adjusted manually for focus, shutter speed and frame rate. The main reason to use manual focus rather than auto focus with default values was to accurately image individual snowflakes as sizing and concentration measurement are also needed for measurement of snowfall. If the camera is used auto focus, it wouldn't be able to focus on the moving particles as the auto focus is adjusting automatically for various planes according on what individual particle dominates the image plane. The adjustment of the shutter speed of the camera is mandatory to get the image particle with higher accuracy. Shutter speed controls the time of exposure of image sensor to the imaged object; i.e., if shutter speed is large, less light goes into the camera through the aperture. If the shutter speed is low, the particle images are captured in motion leading to particle images as short segments rather than individual snowflakes. The length of the particle-driven streaks depends on the camera shutter speed setting and the wind velocity. Preliminary measurements are made to check the proper shutter speed for the given wind conditions, display in Figure 3.10. The reduction of the shutter speed is inherently leading to less sensor exposure so the possibility to not image smaller particles at all. A tradeoff between illumination conditions, snowflake particle size, and velocity of the wind has to be made to get to an optimum shutter speed for a specific situation. For safety, the recording of each test was done with a minimum of three shutter speeds to be able to select the best combination during post-processing.

Shutter Speed: 1/60	Shutter Speed: 1/180
Shutter Speed: 1/250	Shutter Speed: 1/500
Shutter Speed: 1/1000	
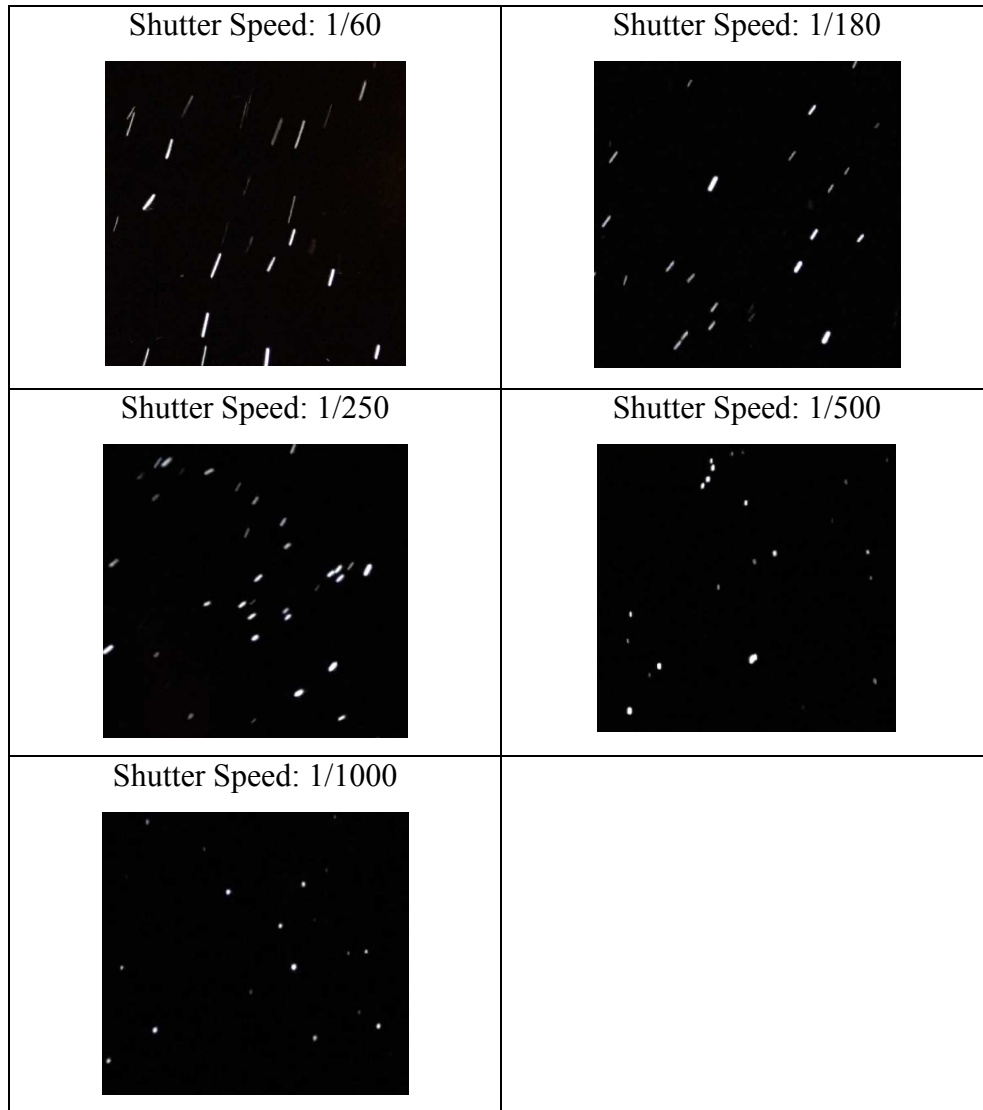
Figure 3.10 Sensitivity of shutter speed

3.3.1.2 Instruments and technologies used for mapping of snow deposits

Photogrammetry. The images for the photogrammetric survey were acquired with an unmanned aerial vehicles (UAV): DJI Inspire 1 model with the Zenmuse X3 Gimbal camera attached (see Figure 3.11). DJI inspire 1 model has the ability to take 4K resolution videos or 12.4 megapixel size photos and store them on a micro SD card. The camera focal length is 20mm. The drone can operate with a maximum speed of 49 mph under the temperature range from -10 to 40°C; the average flight time per battery is 18

minutes. (http://www.dji.com/inspire-1/info). The images taken from the UAV are then inputted into Agisoft software. Agisoft software has the ability to generate the cloud of points with the known coordinates surveyed by RTK and from the images covering the whole study area to extract the 3-D terrain data and to map the object. Table 3.3 summarize the individual components used for carrying out the photogrammetric survey.

Table 3.3 Summary of the components associated with the photogrammetric surveys

Image technique	Role	Camera	Survey	Software
Photogrammetry	Reconstruct terrain/snow deposits	Zenmuse X3 Gimbal camera	Aerial (UAV)	Agisoft

Figure 3.11 DJI Inspire 1 unmanned aerial vehicles

Real-time kinematic (RTK) satellite navigation is a surveying technique used for georeferencing the locations of the GRPs need in the photogrammetric surveys in this study. RTK is a GPS -based positioning system capable of recording the real-time horizontal and vertical elevation of [x,y,z] coordinates. During the measurement, RTK is consecutively placed on the top of each reference points to get the final reading. The three main devices contributing to the RTK instrument: receiver, hand-held data collector, and phone used for the wireless communication is shown in Figure 3.12a. The

instrumentation uses the wavelength of the signal to connect to the satellite in order to locate the accurate coordinate. Therefore, the good results would occur if the geometry of satellites are in place (RTK, 2003). The RTK accuracy continued to improve over time such that today the RTK accuracy for locating a survey point is sub-centimeter in the horizontal plane and of the order of few cm in the vertical. Results of preliminary runs conducted with the RTK to familiarize with its usage and refining the survey protocols are shown in Figure 3.12b and 3.12c.

Figure 3.12 Real-time kinematic: a) components; b) testing location; c) mapping result

Real-time communication web camera. This imaging instrument used for monitoring the snowdrift experiment was a Moultrie P180i video camera (Figure 3.13a). The monitoring scope was two-fold: to observe the dynamics of the snow accumulation at the fence and to check the integrity of the equipment deployed in the field. The camera is equipped with the ability to take 180 degree panoramic view at full 4K resolution

images. The camera was set to record images every hour under time-lapse option and store the images into the external memory card. The camera was attached to a communication unit (modem) shown in Figure 3.13b in order to transmit the images recorded with the camera to the Moultrie Mobile server. Both camera, modem, and external battery to supply the power were bundle inside a weather-proof case for convenience and safety purposes as shown in Figure 3.13c. In this configuration, this camera system is a stand-alone, self-power and real time data transmission device. The client user interface and a sample image taken from Moultrie camera are provided in Figures 3.13d and 3.13e respectively.

a)　　　　　　　　　　　　　　b)　　　　　　　　　　　　　　c)

d)　　　　　　　　　　　　　　　　　　　　e)
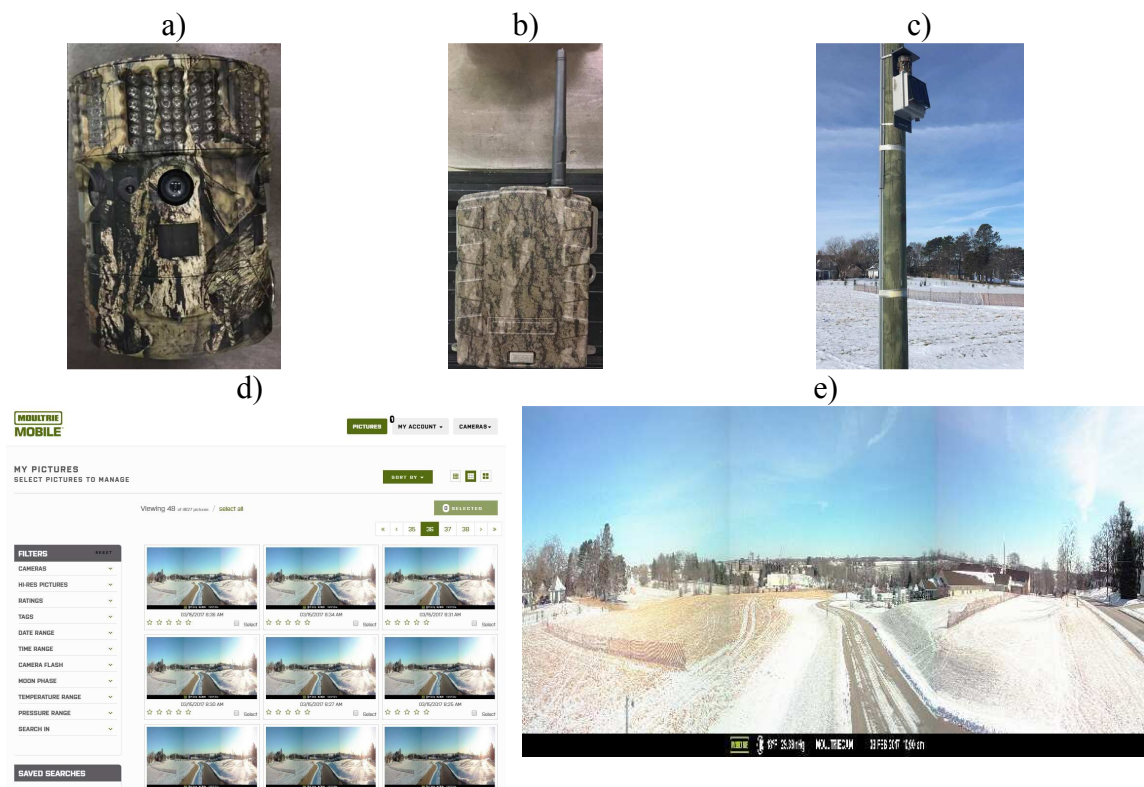
Figure 3.13 a) Moultrie Camera P180i; b) Moultrie Modem MV1; c) Site with the Moultrie products installed; d) User interface of the real time monitoring system; e) Sample image taken from Moultrie Camera

An additional webcam was installed at the same experimental site (see Figure 3.14a). This prototype webcam with real time communication was built from Iowa Flood Center (IFC), and was deployed as backup in case of failure of the Moultrie camera and, possibly to gather more information. The camera is fitted with the external battery to supply the power, and it is programmed to sample images at a 1 image/hour rate and transmit the images to the server. A sample image taken with the IFC webcam is provided in Figure 3.14b. The overall set up of the Moultrie and IFC camera assembly deployed at the snowdrift experimental site is shown in Figure 3.15. The Moultrie Mobile and IFC webcams are not used for quantitative mapping of the snow deposition; rather they are used to observe the site and plan trips and to capture the dynamics of the snow deposits during and in between storm events.

a)   b)

Figure 3.14 a) IFC webcam; b) Sample image taken from IFC webcam

Figure 3.15 Front and side views of the Moultrie and IFC web-cameras

3.3.1.3 Wind measurements

Three anemometers for measurement of the local wind velocity were installed at various experimental sites and tested: Vaisala anemometer, Youngs anemometer and Davis Vantage Pro2. The Vaisala anemometer is a custom-made instrument assembled by IIHR-Hydroscience & Engineering in 2012. It is a stand-alone unit contains its own house-made cell modem in order to transmit the signal and connect to an IIHR server, and a 12V external battery attached to the solar panel, as displayed in Figure 3.16a. The Vaisala anemometer measures the wind by using the speed of the sound to determine the wind intensity. The wind sensor has three equally spaced ultrasonic transducers. To determine the wind speed and wind direction, it measures the time the ultrasound takes to travel from each transducer to the other two.

The Youngs anemometer wind monitor model 05103 (Figure 3.16b) is
commercial stand-alone anemometer connected to a Campbell Scientific CR10X
datalogger. The anemometer can be adjusted for sampling time, duration and the type of
output data. The recorded wind data is stored internally on a memory unit. Both Vaisala
and Youngs anemometers were programmed to sample every 15 seconds and transmit the
wind data every hour to the database. The measurement output for the two anemometers
entails wind magnitude and direction.

Figure 3.16 a) Real time Vaisala anemometer; b) Youngs Anemometer

The Davis Vantage Pro2 anemometer (Figure 3.17) is a meteorology station
containing the Vantage Pro2 console which monitors various weather parameters: wind
intensity, wind direction, temperature, humidity, barometric pressure, and daily and
monthly precipitation data. The data is stored internally in the station but is very limited
in terms of adjusting the data sampling parameters.

Figure 3.17 Davis Vantage Pro2 [1]

3.3.2 EDPIV-PTV software

The PTV experiments for this study were processed with a customized software EDPIV (http://lcgui.net). EDPIV stands for "Evaluation software for digital particle image velocimetry" and was developed at IIHR – Hydroscience & Engineering by Lichuan Gui. The software contains a wealth of PIV and PTV processing algorithms that can be engaged in complex measurement conditions to overcome issues associated with limitations in one or more image velocimetry components (e.g., illumination or flow seeding quality, etc.,). The software ingests only black & white images in 8-bit Windows Bitmap format that are obtained with additional software (Adobe Photoshop). Beyond robust PIV and PTV spatial analysis algorithms, the software includes several image conditioning steps such as: image conversion, removal of background disturbances and background noise and evaluation.

Setting image processing parameters. With a given set of recorded images, a trial- and- error approach is needed before to process the snow experiment data. it is

---

[1] http://www.davisnet.com/product/wireless-vantage-pro2-with-standard-radiation-shield/

essential to select the interrogation and searching area when doing the post processing in PIV. Since the interrogation areas is able to detect each individual vector, it cannot be too large to eliminate the velocity gradient in order to reach its maximum spatial resolution. On the other hand, the expected particle movement from the images has to be determined before applying the size of searching area to optimize the velocity vectors. When the statistical algorithm is implemented, there will be some error predicting the accurate velocity vectors if the average particle movement is bigger than the searching area, in which case the algorithm will not successively observe the peak distribution. However, setting the searching area larger than the expected particle displacement also reduces the accuracy of the algorithm. Typically, another filter option is then be applied for setting up the correlation. Users are asked to input the minimum correlation to eliminate the outlier vectors. Therefore, by estimating the average displacement of the particles between images in order to create the right searching area size and applying the correlation factor to exclude the deviation, the final results of the instantaneous velocity vector field will be dramatically improved.

The main steps in using the EDPIV for our snow experiment are summarized in Figure 3.18.

b)

c)

d)
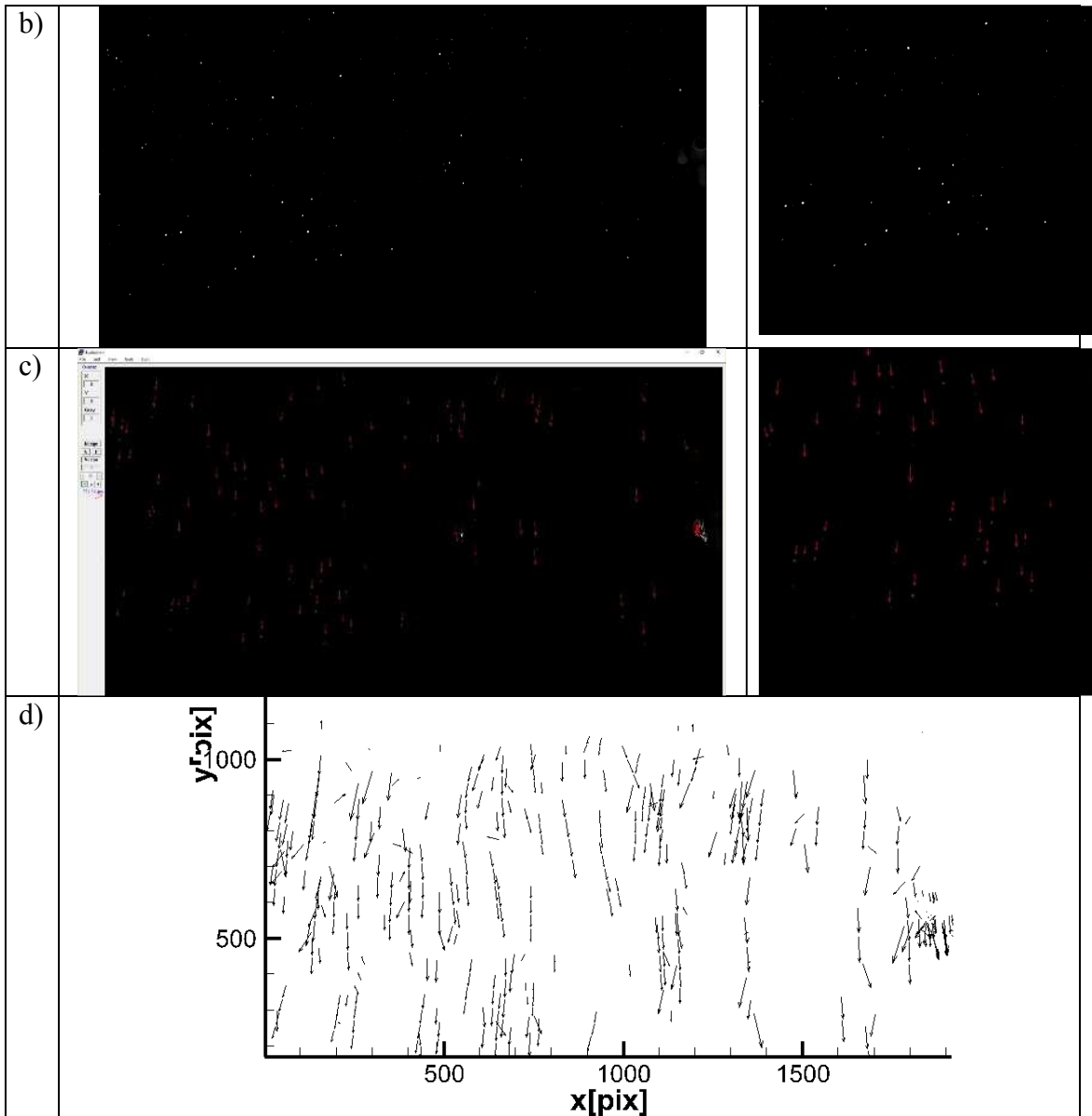
Figure 3.18 Selected screen shots of the EDPIV software applied to snow fall measurements: a) sample raw (color) image from a snow fall event; b) sample image after removing background noise and applying the size-filtering; c) instantaneous velocity field plotted within EDPIV software interface; d) Tecplot file of the averaged velocity field for 200 processed images.

3.3.3 FUDAA-LSPIV software

The alternative image-based method used for quantification snow transport dynamics is LSPIV. The LSPIV experiments data were processed with an open-source customized software labeled FUDAA-LSPIV (https://forge.irstea.fr/projects/fudaa-lspiv). FUDAA-LSPIV was developed by ElectricitÃ © de France Company (EDF) and IRSTEA (national research institute for Environment and Agriculture). The software is fit with user-friendly graphical interfaces for applying the LSPIV process and calculating the final velocity vector field. This software intakes the 256 grey level format using VirtualDub software to covert the videos into images and specific format. Fudaa-LSPIV software is fitted with a Java interface atop of a Fortran executable that allows user to: ortho-rectify the images, calculate the surface velocities of tracers movement from the statistical analysis, apply filters to time-average velocities, and finally to visualize the velocity vector field.

Testing of the LSPIV Software was made to track the snowfall movement. Experimental setup for preliminary tests was set to have a contrasting background (canvas) with the snow particle and with the artificial light to enhance the particle. The orientation of the canvas background was developed by using a hand-held anemometer to ensure that the backgrodevelopund was align with the dominant wind direction. Eight points were also marked/painted for the use of reference point purpose. Figure 3.19a shows the experiment set up for the preliminary runs and Figure 3.19b shows the images taken during the snow event.
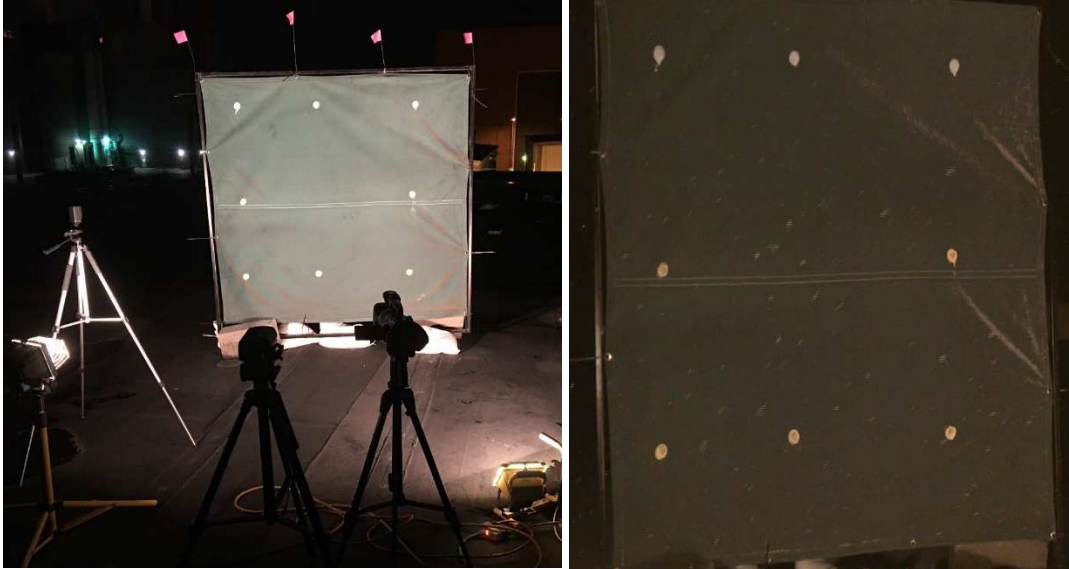
Figure 3.19 a) Experiment set up for preliminary LSPIV testing; b) image taken during November 20, 2015 event

The final velocity vectors result shown in blue was obtained from the FUDAA-LSPIV software and displayed in Figure 3.20. The technique was originally intended for quantification of snow drift but during the preliminary measurements it was concluded that the technique is not adequate for quantifying snow fall. Later on in the study, field observations lead to the conclusion that this technique is suitable for measuring snow drift, hence it was maintained as one of the study tool. Using FUDAA-LSPIV software doesn't obtain well results when tracking the vertical snowfall velocities, therefore, FUDAA-LSPIV software would be used for quantifying the horizontal snowdrift calculation in the study.
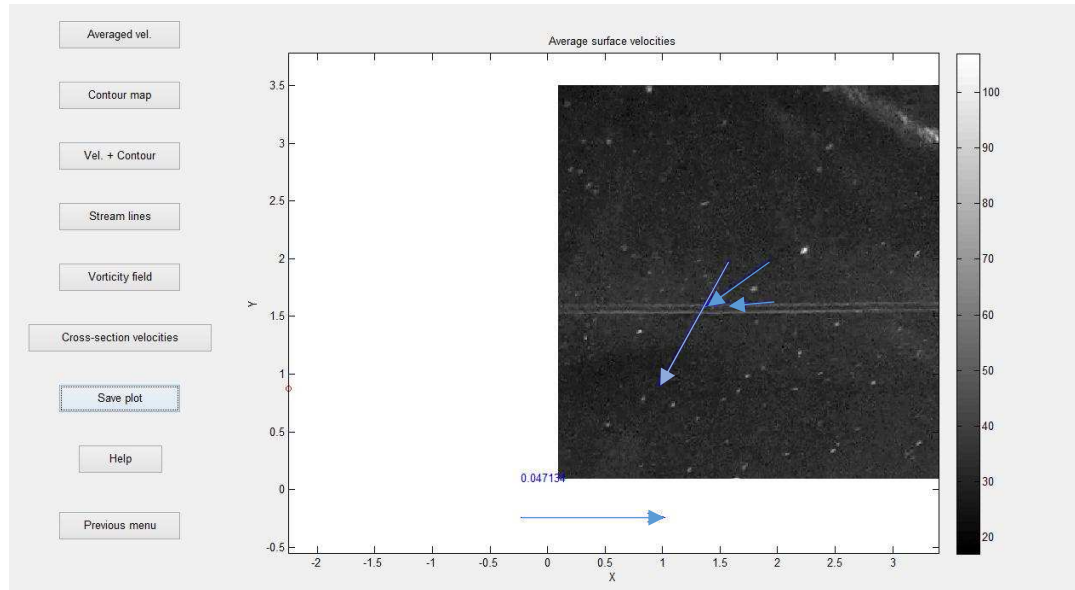
Figure 3.20 Final results computing by FUDAA-LSPIV software for preliminary tests

3.3.4 Photogrammetric survey

Photogrammetry survey was introduced in this study being able to measure the deposition of the snow. The traditional aerial photogrammetry is applied here for the applications of the photogrammetry survey. Multiple images were taken at various angles with the unmanned aerial vehicles (UAV) DJI Inspire 1 with the camera attached underneath pointing straight down to image around the object/field and with overlapping reference points. A sample example of photogrammetric survey result was illustrated in preparation of the winter snow experiment. Figure 3.21a shows the DJI Inspire 1 drone taking images overhead of the three-box culvert with the image framing covering an area of $1500m^2$. Fourteen ground reference points were marked by temporary paints and then surveyed by Real Time Kinematic (RTK) as indicated in Figure 3.21b in green and red dots for the post processing purpose. Although Agisoft software generated tie points, it does not visualize the tie points used. Figure 3.21c shows an example cloud of tie points created by the previous experiment's software (ERDAS) for the reconstruction process.

63

The final results output from Agisoft is displayed in Figure 3.21d. This sample example

shows the high-resolution and an accurately recreated 3-D model using the

photogrammetric survey technique of the culvert. However, since the culvert contains a

broader spectrum of color and texture gradient, careful attention is required when

applying the photogrammetric survey technique to the snow surface images.

a)

b)

c)

d)
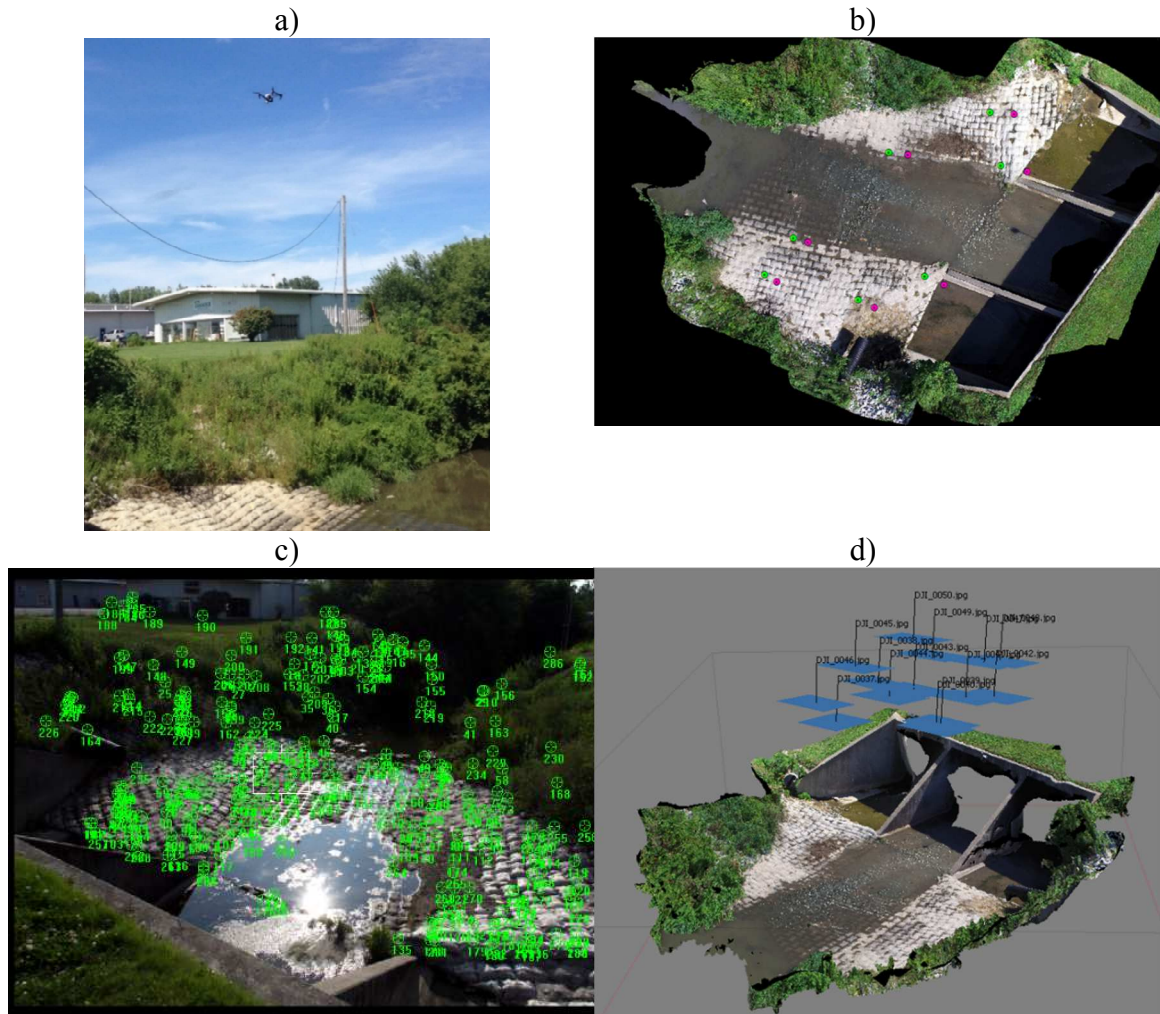
Figure 3.21 a) UAV mapping the three-box culvert; b) Covered area for

photogrammetry survey; c) Clouds of tie points generated by software; d) 3-D

reconstruction of culvert using photogrammetry method

CHAPTER 4 PROTOCOLS FOR METHODOLOGY VALIDATION

Three experimental sites were chosen to validate the methodologies used to quantify the snowfall and snowdrift velocities. Both snowfall and snow drift sites were intentionally selected close to Iowa City, Iowa to allow deployment of the instrumentation as soon as a storm event occurs.

The snowfall experiment was assembled on the rooftop of IIHR-Hydroscience & Engineering, which is indicated by a red dot in Figure 4.1. The experiment was conducted using the PTV technique described in Chapter 3.

The goal of the snowdrift experiment was to visualize and quantify the horizontal movement of the snowflakes near the ground. The LSPIV technique was used for this analysis. The snowdrift measurement site is located along a railroad. Its position is indicated by the green dot in Figure 4.1. There is a free fetch for the wind to pick up at the measurement site. The site is situated in a relatively flat area, where wind is practically undisturbed by the presence of buildings.

Lastly, the in-situ snow drifting site located in Shueyville, Iowa was suggested by the Johnson County Secondary Roads' Maintenance Superintendent to evaluate the snow relocation coefficient (SRC) and to map the volume of snow deposited at the fence during the winter season.

Figure 4.1 Location of the snowfall and snow drift experimental sites

4.1 Snowfall measurements (2015-2016 winter season)

4.1.1 Experimental arrangement

The snowfall experiment was conducted on the rooftop of the IIHR building which is located in Iowa City, Iowa, on the bank of the Iowa River. The building is fairly isolated from the other buildings on the university campus, hence precluding the interference of flow disturbances (e.g., wakes) induced by the presence of other buildings. The vertical distance from the sidewalk to the rooftop, where the snowfall experiment was conducted, is 14.33 m, as shown in Figure 4.2.

Figure 4.2 IIHR - Hydroscience & Engineering building where the snowfall experiment was conducted

The experimental set up of the snowfall experiment is shown in Figure 4.3. In this study, a snowboard, as recommended by meteorological standards (white board) was used to measure the snow depth. A Vaisala anemometer (the yellow dot in the same figure) was used to measure the local wind velocity at the site. A Sony 4K video camera (FDR-AX100) (the black dot in the same figure), which was attached to the handrail of the ladder, was used to record the snowflakes movement continuously during the snowfall event.
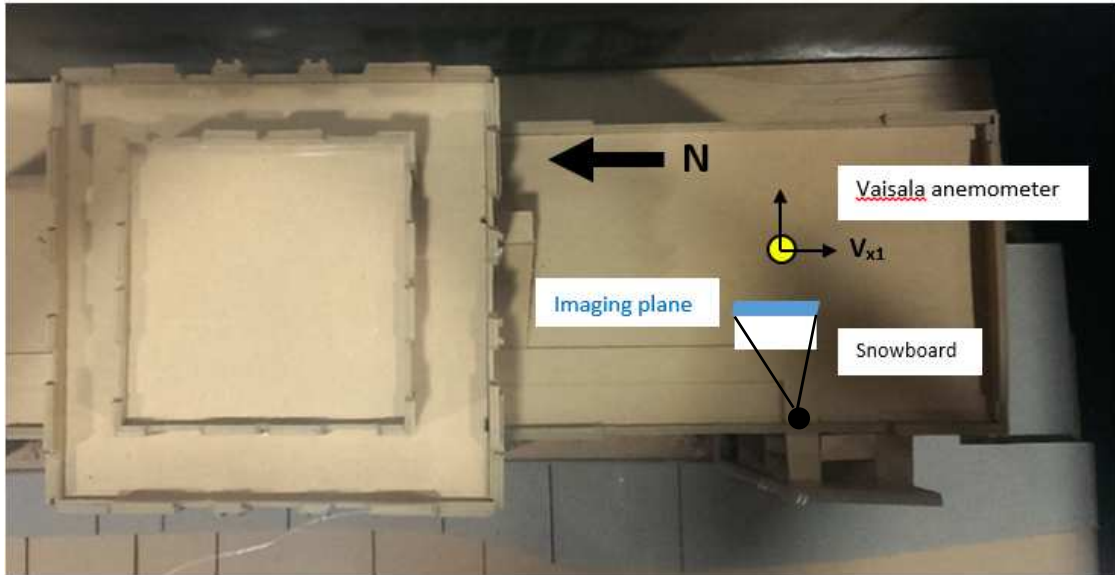
Figure 4.3 Experimental set up used for the snowfall experiment

The standard procedure used by the Community Collaborative Rain, Hail & Snow Network (CoCoRaHS) recommends that a snow measuring board using a 16" by 16" piece of ½" or ¾" plywood is employed. The board installed on the rooftop of IIHR was a 3' by 5' plywood with ½" depth that allowed to measure the "in-depth" snow, as shown in Figure 4.4. This difference in the dimensions of the plywood was inconsequential to the results.

Figure 4.4 Snow measurement board used to measure snow accumulation as part of the rooftop experiment

The camera's field of view entailed a rectangular plane with dimensions of 0.73 m by 0.43 m (W x H), as presented in Figure 4.5. The imaging plane was orientated parallel to the local dominant wind direction and perpendicular to the camera. A ruler was attached to the experimental set up to estimate the relative scale of the image. Given the close distance between the camera and the imaged field and the normal-to-image angle, it was unnecessary to correct for image distortions when the PTV processing algorithm was applied to the recorded images. This approach is called large-PTV technique, as the image is large, irrespective if the images are distorted or not. The method is described in detail by Admiraal et al. (2017).

Figure 4.5 Sketch showing the vertical plane in which the movement of the snowflakes was visualized

A Vaisala anemometer was chosen because it measures the wind magnitude and wind direction in two dimensions, labeled herein as V_{X1} and $V_{Y1,}$ respectively. The x-direction of the rectangular plane shown in Figure 4.5 is co-directional with Vaisala anemometer's V_{X1} direction (see Figure 4.3). A comparison of wind velocity estimates

given by three different types of anemometers will be presented in chapter 4.1.3 as part of assessing the Vaisala's anemometer accuracy to measure wind velocity.

Using the recorded videos of the snow events in conjunction with the image velocimetry EDPIV software, the individual snowflake velocity vectors can be obtained. The EDPIV processing procedure described in chapter 3.3.2 provides snow particle velocities in the V_X and V_{Y1} directions. The V_X velocities obtained using EDPIV were compared to the wind data output from the Vaisala anemometer, V_{X1}, to determine the relationship between these two velocity vectors. The main assumption is that the snowflakes behave as 'good' air-flow tracers as they are relatively light and small.

Once the snowfall experiment site was chosen, several issues regarding optimization of the recording process had to be addressed. In order to track the particles with the image-based technique, the background color of the image has to contrast with the snow particles' color for accurate particle identification and specification estimation for sizing purposes. The University of Iowa's power plant located across from the IIHR building has a red brick walls. By placing the camera toward it, the needed background was created. Using this experimental set up, it was easier to identify the snow particles and to track them during daytime measurements. Given that during the 2015-2016 winter season the majority of the snowfall events occurred during the night, a Rigidhorse 42 inches 240 W straight Philips LED light was deployed (Figure 4.6) and placed in front of the snow measurement board in order to create a light sheet shining upwards (Figure 4.7). The light sheet created by this source was effective in illuminating the particles during night time, as shown in Figure 4.8. The raw images were adequate to be processed by the EDPIV software after more pre-processing steps were applied to the raw images.

70

Figure 4.6 Rigidhorse Philips LED light used for night-time illumination

Figure 4.7 Rigidhorse Philips LED light used to conduct night-time snowfall experiments

Figure 4.8 Sample of enhanced images of the snowflakes obtained using the EDPIV software

4.1.2 Measurement protocols

Several protocols were tested and then deployed for efficiently capturing the particle movement during the snowfall experiments. The first step was to monitor and document the weather conditions using data provided by local meteorological stations (weather.com). This step is needed to identify possible events and trigger preparation of the experiment whose purpose is to measure snowfall during a snow event. Once a high chance of snow precipitation was forecasted, the various devices needed to perform the experiment (video camera, lighting, power for instruments) were deployed at the site. During each snow event, a camera was attached to the tripod, which was connected to the handrail on the top of the IIHR building. Once the camera was in place, several parameters had to be adjusted: zoom level to aim to the area of interest, manual shutter speed to optimize the image quality, and manual focus for the camera lens to focus on the image plane. For each storm event multiple recording segments ranging from 30 seconds to 60 seconds were captured to provide a mean description of the snow falling movement. In most cases recordings were taken over three segments. This data was then used to obtain

an averaged value of the total snowfall velocity for each event. After the recording process was finished, the next step was to estimate the snow depth using the snowboard device and the snow flake size using the black cardboard and information on the snow type (Figure 4.9). This was needed because the snow flake shape and density are a function of the surrounding pressure, temperature and precipitation type (see Garrett et al., 2012 and McClung et al., 1993)

Figure 4.9 Picture showing snowflakes on the cardboard. The picture is then used to infer the snow flake characteristic

4.1.3 Wind data acquisition

Three anemometers were tested during the 2015-2016 winter season: the Vaisala anemometer, the Youngs anemometer and the Davis Vantage Pro2 device. The locations of the three anemometers are shown in Figure 4.10. The purpose of this comparison was to identify the optimum wind-measurement instrument for the experiments. An essential feature of the instruments used to measure the wind velocity was to be able to record continuously the data and store it for subsequent retrieval.
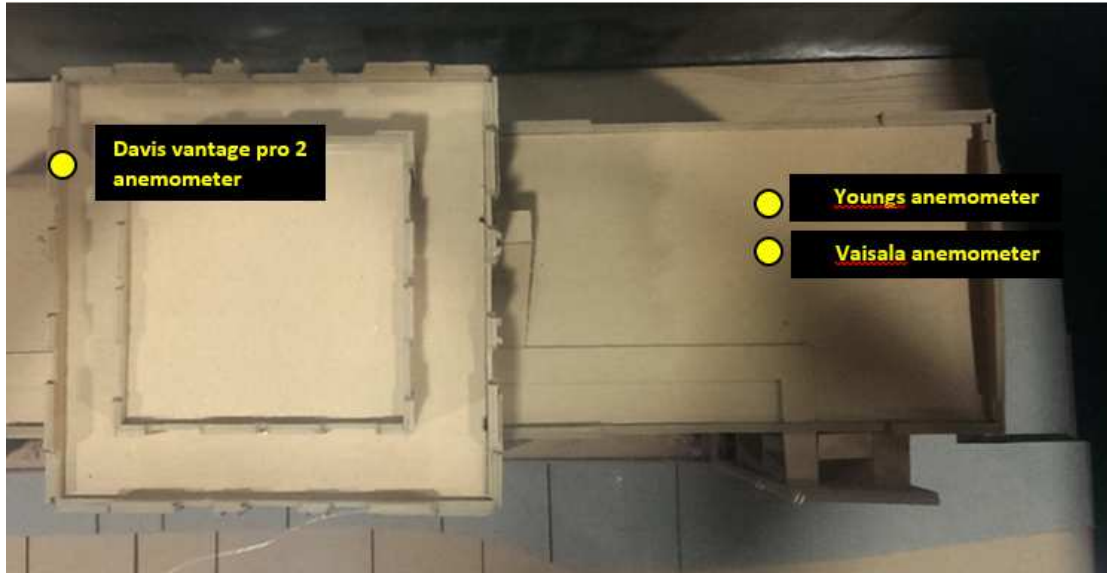
Figure 4.10 Location of the three anemometers used to measure wind velocity during the snowfall experiments

During the deployment, each of the three anemometers were aligned with the true North direction and were marked with an arrow printed underneath each sensor. This was needed to insure the measurement instruments obtained measurements in the same coordinate system. The output of the Vaisala and Davis Vantage Pro2 anemometers contains various weather parameters including: wind mean direction (D_m), wind maximum direction (Dx), wind mean speed (Sm), wind maximum speed (Sx), ambient temperature (Ta), relative humidity (Ua), barometric pressure (Pa), rain accumulation (Rc), rain duration (Rd), rain intensity (Ri), and rain peak (Rp). The Youngs anemometer was programmed to output only wind mean speed and mean direction. The essential variables that need to be measured in the present experiments are the wind mean direction in degree and wind mean speed in meters per second.

The Vaisala and Youngs anemometers were deployed on the rooftop and placed side by side to test the variation and similarity of the wind data (see Figure 4.11). Both

instruments were programmed to have a sampling time of 15 seconds over a recording period of 10 minutes for a total of 40 outputs. Because the Davis Vantage Pro2 anemometer could not be programmed to sample every 15 seconds, the data had to be catalogued every 15 seconds in real time and then compared with data from the Vaisala and Youngs anemometers for shorter time spans.

Figure 4.11 Setting of the Vaisala & Youngs anemometers on the roof of IIHR building

Two experiments were conducted to compare the measurements of the three anemometers. The experiments were conducted on February 19 and 22, 2016. The wind intensity and direction during these two experiments are plotted in Figure 4.12a and 4.12b, respectively.
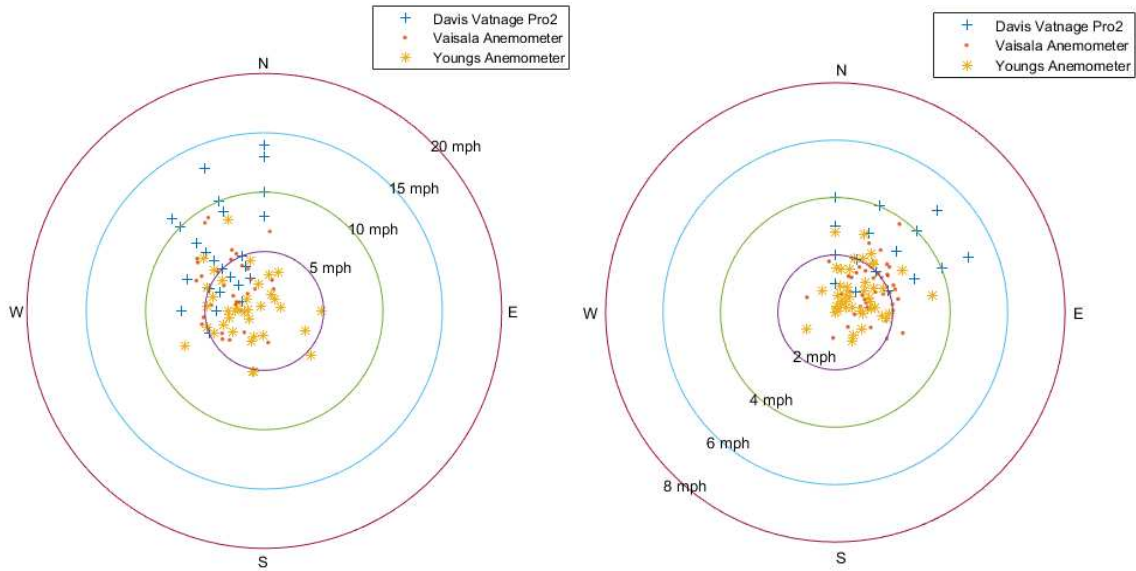
Figure 4.12 Comparison of data recorded by the three anemometers on a) February 19, 2016; b) February 22, 2016

Wind intensities measured by the Davis Vantage Pro2 anemometer were always biased high compared to measured values given by the other two anemometers. This can be attributed to the fact that the Davis Vantage Pro2 anemometer was installed at the highest elevation at a location where no obstruction can affect the measured data. However, due to the design of the IIHR building, both the Vaisala and Youngs anemometers' data could have been interrupted if the wind field was affected by the presence of some obstruction near the anemometers. The comparison of the measured data showed that the Vaisala and Youngs anemometers captured relatively well the wind variables during the snowfall event. The average differences for the wind intensity and direction between measurements conducted with these two anemometers are not statistically significant.

Another concern for the experimental arrangement was to ensure that the position of the test section is not subjected to artificial effects induced by the building geometry.

Specifically, the test section was located on the lower roof of the building where the

presence of the central, more elevated, part of the building could induce the development

of a wake region with large-scale turbulence and changes in the mean wind direction.

Sensitivity tests were conducted on February 27th, 2016. During these tests, the Vaisala

anemometer remained in the middle of the rooftop site, while the Youngs anemometer

was placed at five different locations to measure the wind variables under various wind

directions. Figure 4.13 shows the location of the Vaisala anemometer and the five

locations where the Youngs anemometer was placed.
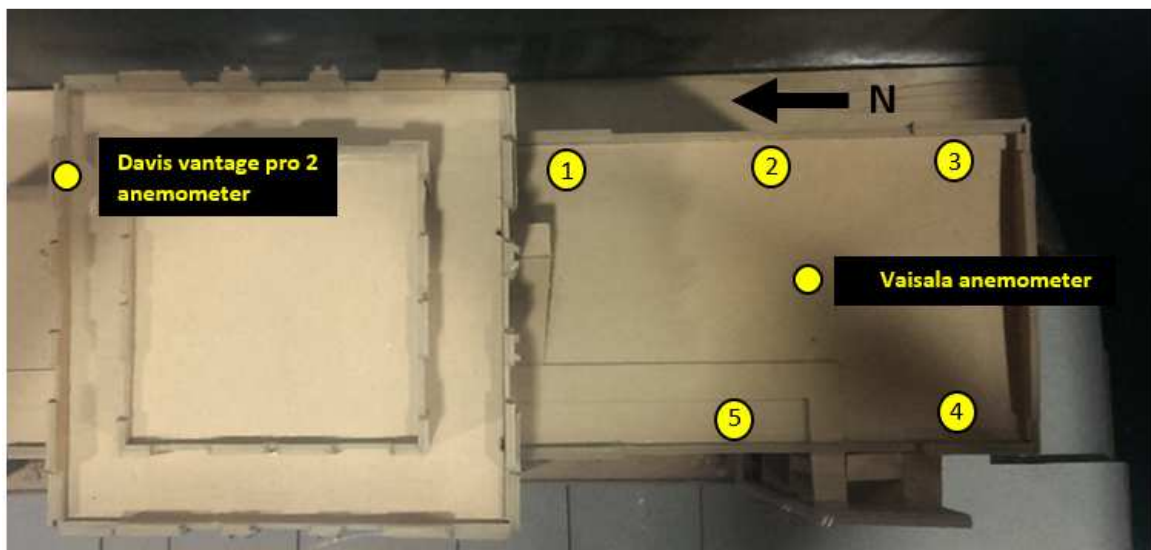
Figure 4.13 Sketch showing the locations of the Davis Vantage Pro 2 and Vaisala
anemometers and the five locations where the Youngs anemometer was placed on the
roof of the IIHR building

The results of placing the Youngs anemometer are five different locations are

shown in Figure 4.14. The wind recordings are different for each of the five locations.

However, for most of the time a good agreement between the Vaisala and Youngs

anemometer readings is observed.

Following these tests where three anemometers were used to measure wind variables, the

Vaisala anemometer was chosen as the reference device to measure wind velocity and

orientation. Another reason for this decision was that the Vaisala anemometer has

capabilities to store large amounts of measured data in the server. By comparison, the

Youngs anemometer requires manually retrieving the data with a computer or a laptop.

Figure 4.14 Comparison of wind specifications acquired using the three anemometers. Results are shown for measurements conducted with different locations of the Youngs anemometer
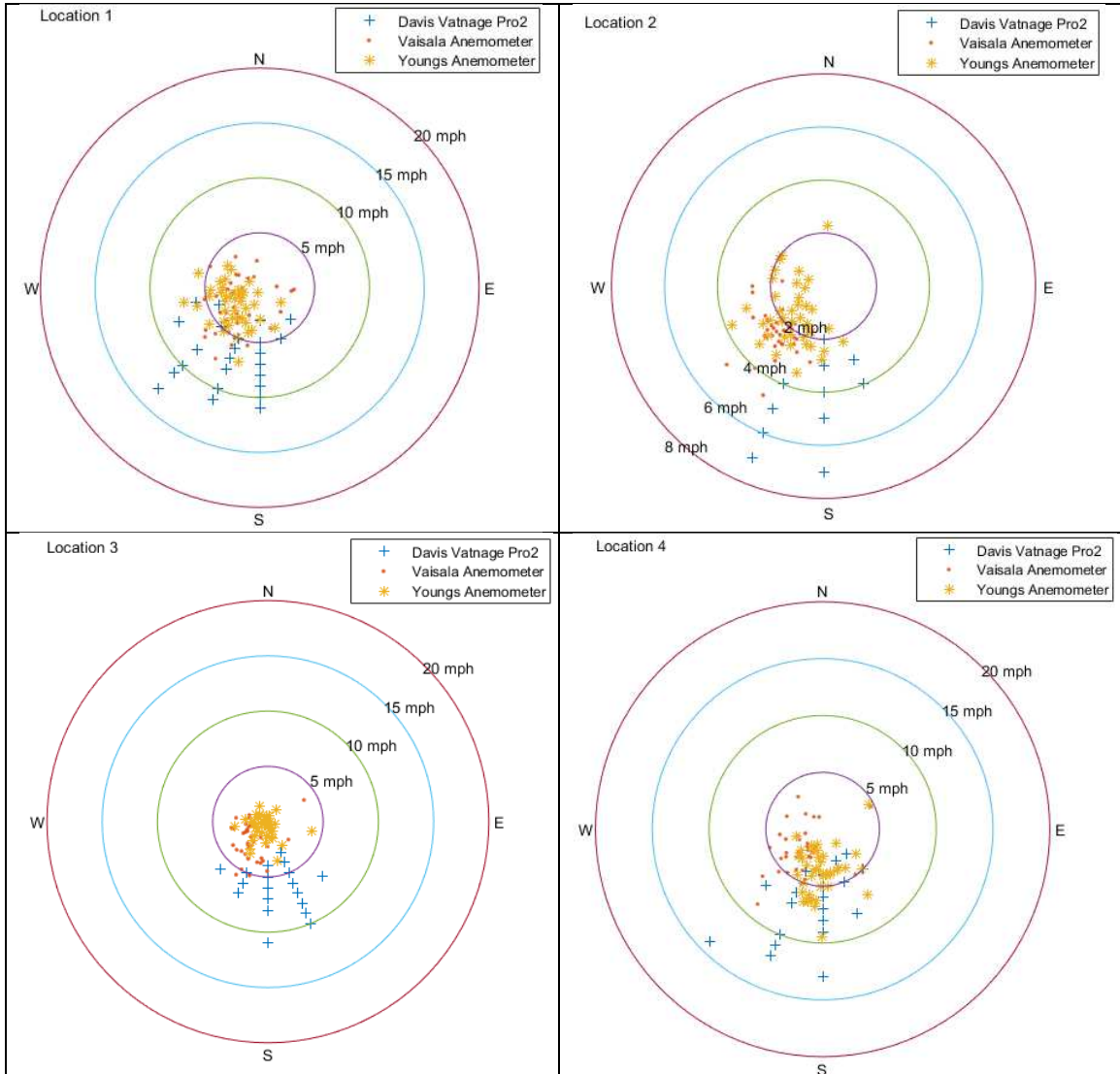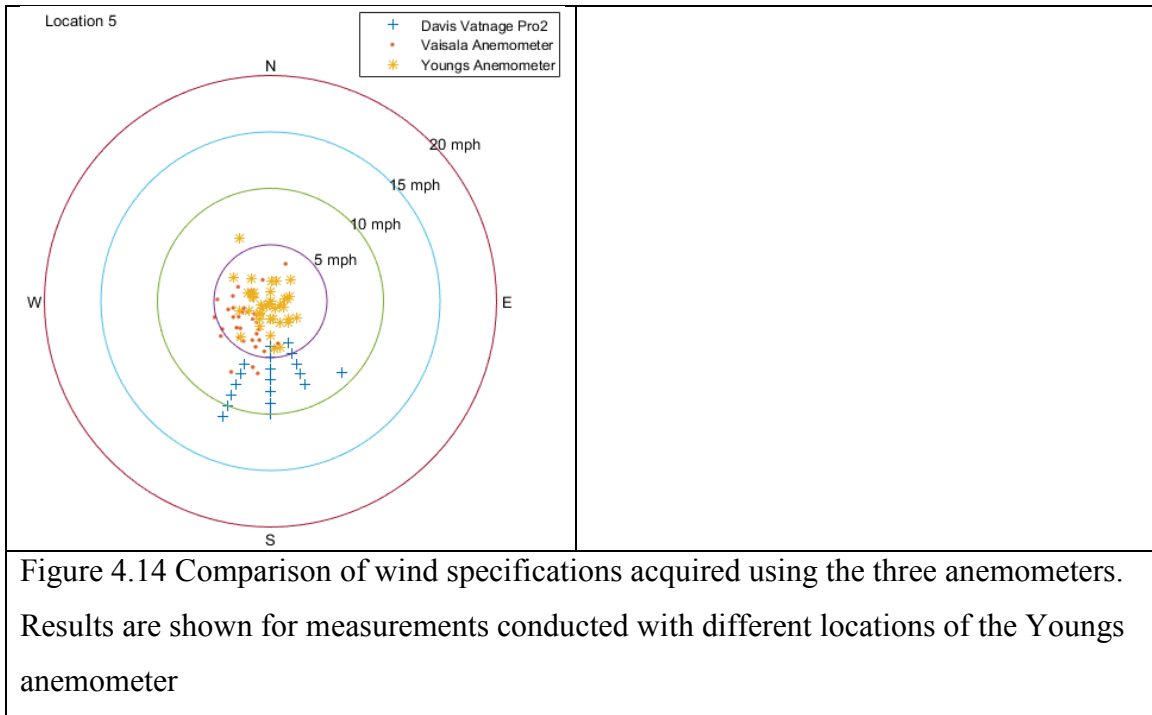
4.2 Snow drift estimation

4.2.1 Experimental arrangement

4.2.1.1 In situ tests

The measurement of the snow drift required much more experimental testing prior to establishing a working measurement protocol. These measurements brought critical challenges for the image-based methods from several perspectives: lack of background for the snowflakes moving close to the bed in a similar background, highly random snowflake behavior as they approached the fixed snow layer, as well as during their rolling along the snow bed. Moreover, the area of interest for determining the snowdrift is located near the bed (for low winds the process is confined within 2 feet height from the fixed snow layer). This leaves few choices for setting the camera in a position that allows recording from an angle normal to the image plane. To accomplish the desired results, four different approaches, labeled herein as experimental arrangement (EA) 1 to 4

were implemented during the snow events that occurred during the 2016-2017 winter season. These arrangements are presented below with their strengths and weaknesses.

The EA 1 approach uses a mobile station that contains a LED light and a 12V external battery placed about the chest height. The illuminated area is aligned with the dominant wind direction. The main arrangement goal was to capture the snowdrift movement at less than a men's height (Weather Online) to trace the snow drifting movement. A video camera with manual focus was used to focus on the image plane, as shown in Figure 4.15a. The sample image obtained using this approach is also shown in Figure 4.15b.
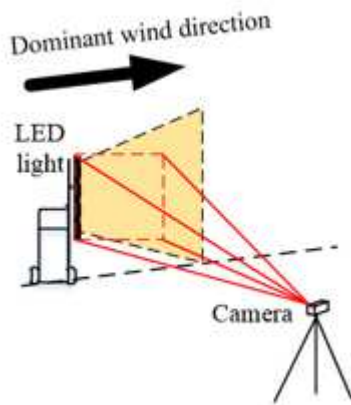
Figure 4.15 Experimental arrangement EA1: a) experimental set up; b) sample image

The EA 2 set up is similar to EA 1, but the LED light is positioned lower. This allows focusing on the near-bed movement. The EA2 set up is shown in Figures 4.16.
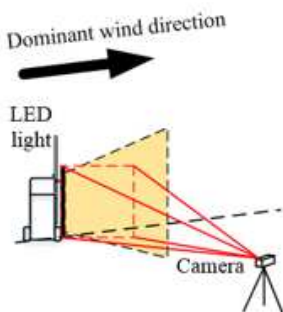
Figure 4.16 Experimental arrangement EA2: a) experimental set up; b) sample image

In the EA 3 set up the LED light was placed horizontally with respect to the bed. The light shines up. This allows visualizing the entire vertical profile of the snow movement (see Figure 4.17). The set-up of the EA 4 experiment was similar to that of EA 2, but retained the ability to visualize the horizontal boundary layer (see Figure 4.18).
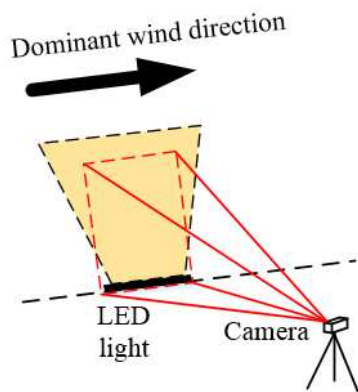
Figure 4.17 Experimental arrangement EA3: a) experimental set up; b) sample image
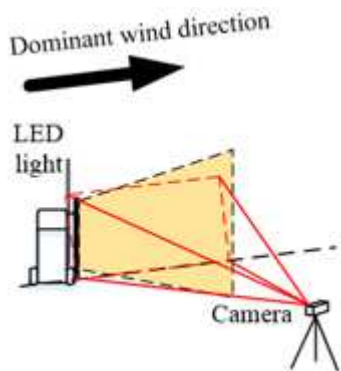
Figure 4.18 Experimental arrangement EA4: a) experimental set up; b) sample image

Another concern about the snow drifting experiment set-up was that the mobile station was on the same side as the dominant wind. Under this circumstance, the near the ground movement might be disturbed since the instrument could potentially block the snow transport. The aforementioned four set-ups for the camera and light assembly with

respect to the direction of the dominant wind near the ground were tested progressively and used to develop the new protocols for snow drift measurement.

Taking into consideration the lesson learned from the previously described tests, two new arrangements, EA 5 and EA 6, are proposed for performing future measurements that can accurately measure the snow fall and snow drift with a mobile station. EA 5 is similar to EA4 but the station is placed against the dominant wind direction, such that the snow drift area subjected to the measurements is not disturbed by the instrument deployment (see Figure 4.19). To be able to perform more precise measurements near the bed, the LED light will be placed horizontally, but pointed down and focused on the bed. The goal will be to track the snow sheet and the movement of the snow-surface bedforms as a pattern instead of the movement of individual particles using particle image velocimetry techniques. This method is the best approach for quantifying snow drift since most of the snow transport contributing to the formation of the snow bedforms is associated with the movement of snow sheets that slowly advance over the stationary layer of snow deposited on the ground. Moreover, this method can be deployed even without the presence of active snow fall, when only the drifting snow process is active, as shown in Figure 4.20.
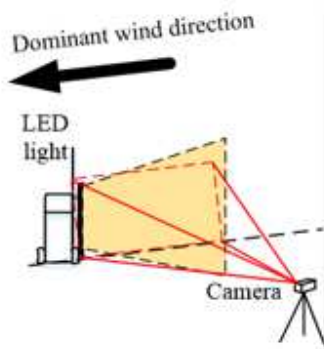
Figure 4.19 Experimental set up for EA 5   Figure 4.20 Experimental set up for EA 6
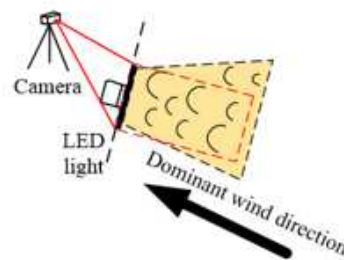
4.2.1.2 Laboratory tests

Due to the insufficient amount of major snow events during the 2016-2017 winter season, the performance of the EA 6 experimental set up was tested in laboratory conditions. The snow flakes and snow bedform movement were simulated by melamine plastic particles. These particles were identified through several preliminary tests aimed at replicating the snow drift movement over fixed snow deposits. This measurement arrangement and the ancillary experiment and processing protocols were first introduced as the so-called Acoustic Mapping Velocimetry (AMV) by Muste et al. (2016). The implementation of the non-intrusive AMV technique for the snow transport case is readily applicable as sand transport in the boundary layer over a loose bed in open channel flow is similar to snow transport over a layer of deposited snow.

The new AMV implementation was tested using the experimental arrangement shown in Figure 4.20a. The experimental flume was 6-m long, 0.75-m wide and 0.4-m deep (Figure 4.20a). The testing area was 0.6-m long and 0.4-m wide (Figure 4.20b). The entrance of the channel was connected to a Viper Racer 3-speed, transportable, 1/3 horsepower carpet fan to create a uniform wind intake. The wind conditions were controlled by setting three different speeds (~10, 12, and 14 m/s) of the fan. Four ground reference points were made and painted in green. A trapping system extending over the whole width of the channel was designed to collect the particles moving as 'bedload' associated with particle drifting.

The Sony 4K camera was mounted on top of the flume (see Figure 4.21c). It features a multi-angle positioning system that fulfills the needs of both LSPIV and photogrammetric analyses. The multiple angles are required to reconstruct the 3-D

model of the bedforms and snow dunes, as described in Chapter 4.2.2.2. Illumination was

created by pointing the light at a low position toward the direction of flow to visualize the

shadow from the dunes. This approach is readily usable for in-situ night conditions and

also during day time if a stronger light source is used for illumination to add the shadow

effect. As demonstrated by Muste et al (2016) and in the next section, this experimental

arrangement allows combining LSPIV and photogrammetry for tracking the dynamics of

the snow bedforms and eventually estimating snow drifting fluxes.

a)   b)

c)
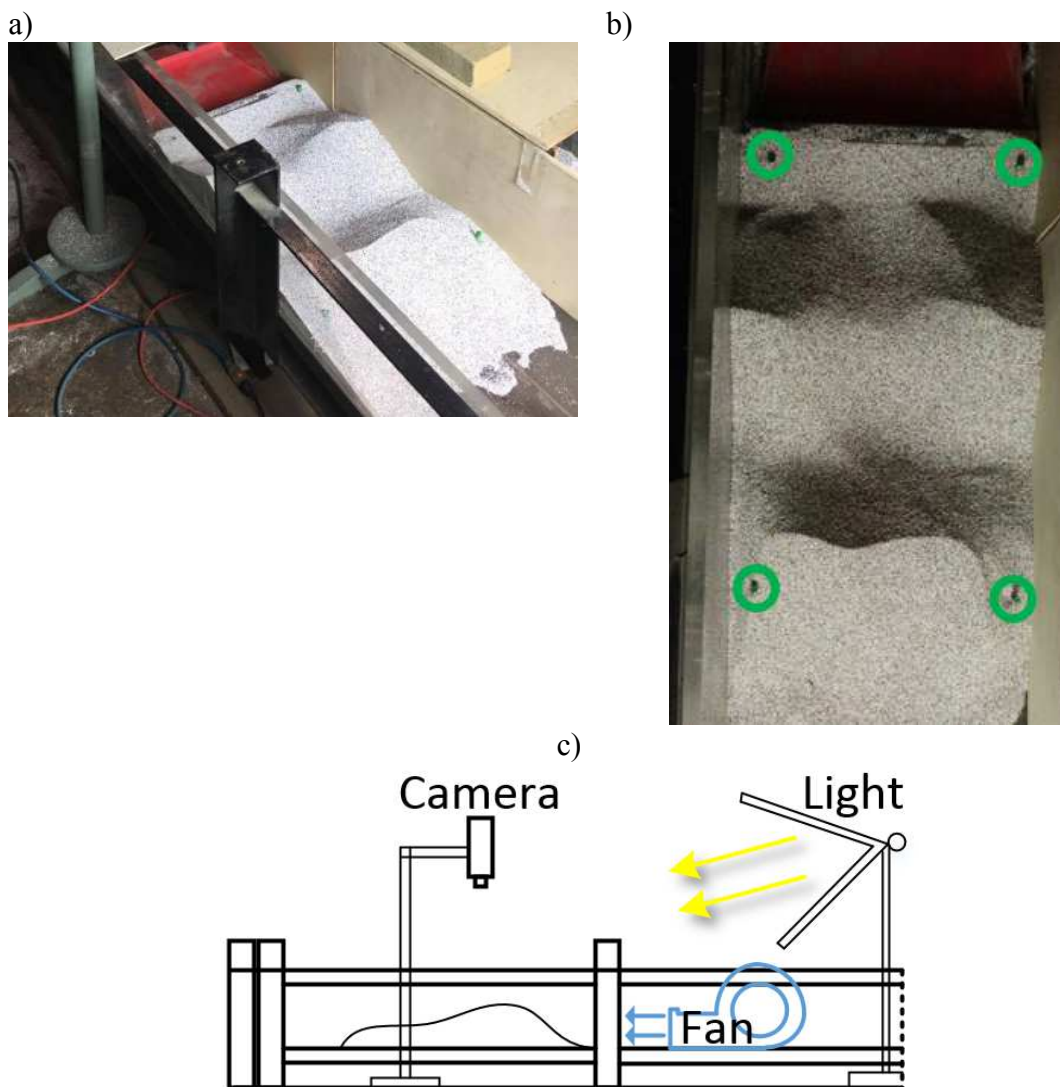
Figure 4.21 Experiment to simulate snow drift; a) sketch of the experimental set up; b)
view of the experimental flume; c) view of the test area as captured by the video camera

4.2.2 Experimental protocols

The measurement protocol for measuring the snow drift focused on the moving layers migrating atop of the fixed snow deposits rather than on the suspended snowflakes. The fraction of snowflakes in suspension are also an integral part of the snow drift but it represents a small fraction of the volumes retained by the snow fence. This assumption is based on two considerations: a) the concentration of snow in suspension is decreasing rapidly with the distance from the bed; and b) the mobility of the snow in suspension is considerably higher compared to that of the rolling bedforms approaching the snow fences. From a practical perspective, the later process has the most negative influence on road visibility. Moreover, after snow starts being trapped by the snow fence, the suspended snow is travelling atop of the trapped layer of snow and contribute little to the volume of snow trapped by the snow fence. From this perspective, the adoption of the AMV measurement protocol as developed by Muste et al. (2016) should capture the main part of the snow transport relevant for snow fence design.

The AMV is in essence a combination of two techniques introduced in Chapter 3: image velocimetry and snow deposit mapping. The principle of the method to be used for snow-deposit mapping obtained using acoustic instruments is illustrated in Figure 4.22. The raw bedform maps were obtained by scanning the channel bed with a linear arrangement of sensors while the flow in the channel was running. If bedform scanning is conducted with a sufficient density of data points, the discrete depth values acquired by each sensor can be interpolated to obtain a map of the channel bottom, as illustrated in Figure 4.22. Subsequently, acoustic maps are created as a continuous depth-data layer covering the target area of the channel bottom by interpolating the measured depths. This

step is the basis for all sounding techniques and produces the conventional bathymetric maps. The acoustic maps provide a full 3-D description of the geometry of the bed forms. In the second step, the acoustic maps are converted to "image-equivalent" maps by resampling the raw information in pixel coordinates (Muste *et al.*, 2015). Images obtained at different time steps are subsequently processed using an image velocimetry technique (Muste *et al.*, 2008). Bedload rates are obtained by combining the outcomes of the acoustic mapping carried out in the first step along with the velocity fields obtained in the second step using analytical relationships for predicting sediment transport rates for the bedload (Vanoni, 2006).
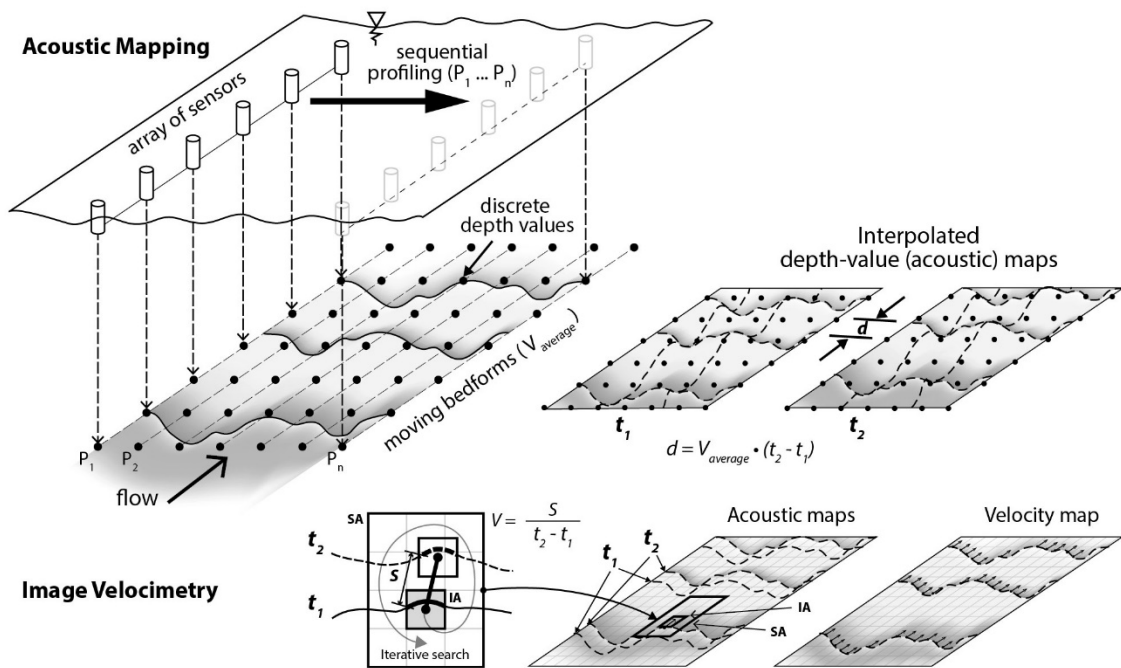
Figure 4.22 Example of time sequenced bathymetry of a dune field obtained by acoustic mapping velocimetry (adapted from Muste et al., 2016)

4.2.2.1 In situ tests

An attempt to make measurements with real snow was made, by choosing a site in Northern Iowa, after a snow storm occurred in the area. A wind blower and actual snow were used in the experiment, as shown in Figure 4.23. Despite of several tests conducted in the field, the snow was not moving similar to drifting, as the compactness of the deposit and the high local temperatures have consolidate the snowflakes. The snow particles aggregated and subsequently moved as larger snow balls in the test area.

a)

b)   c)
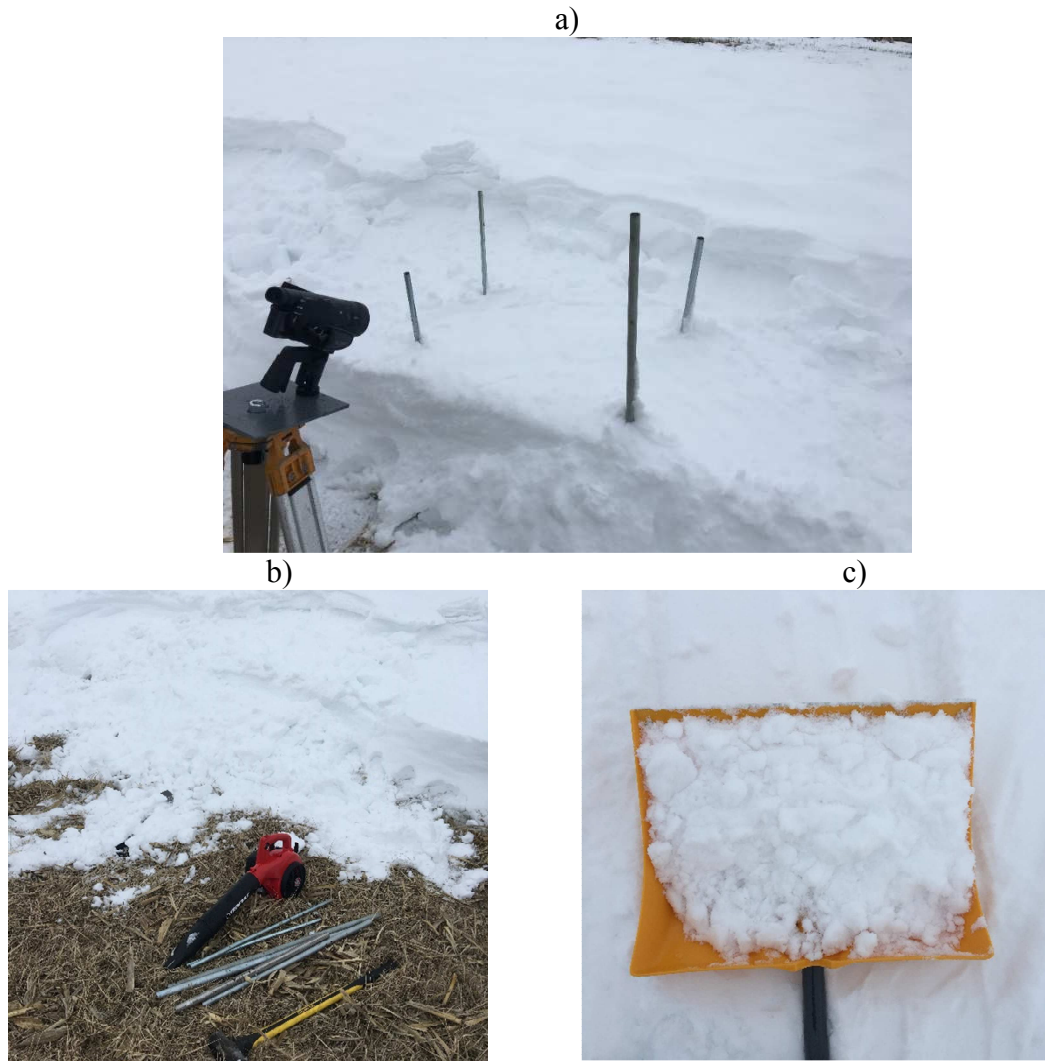
Figure 4.23 Attempt to measure snow drift in situ: a) test section; b) snow blower used for entraining the snow; c) aggregation of snowflakes due to compactness in the snow layer and high temperatures

Several auxiliary variables need to be measured in conjunction with the snow drift estimation in the laboratory test, i.e., wind speed, volume of deposit and weight of the melamine plastic particle. Prior to the experiment, artificial dunes were created as the initial condition (time = 0 minute). A total of six images were taken after the dunes formed for the Photogrammetry technique mapping purposes. One continuous recording was taken to process the velocity vector field using the LSPIV technique. In total five cases (time = 1, 2, 3, 4, and 5 minutes) were completed and used and used to infer dune displacement for each case. The same procedure of taking six images with a different angle (Figure 4.24) was applied after each individual case was completed to plot it and map the propagation of the dunes for all the cases.

Position 1	Position 2	Position 3
Position 4	Position 5	Position 6
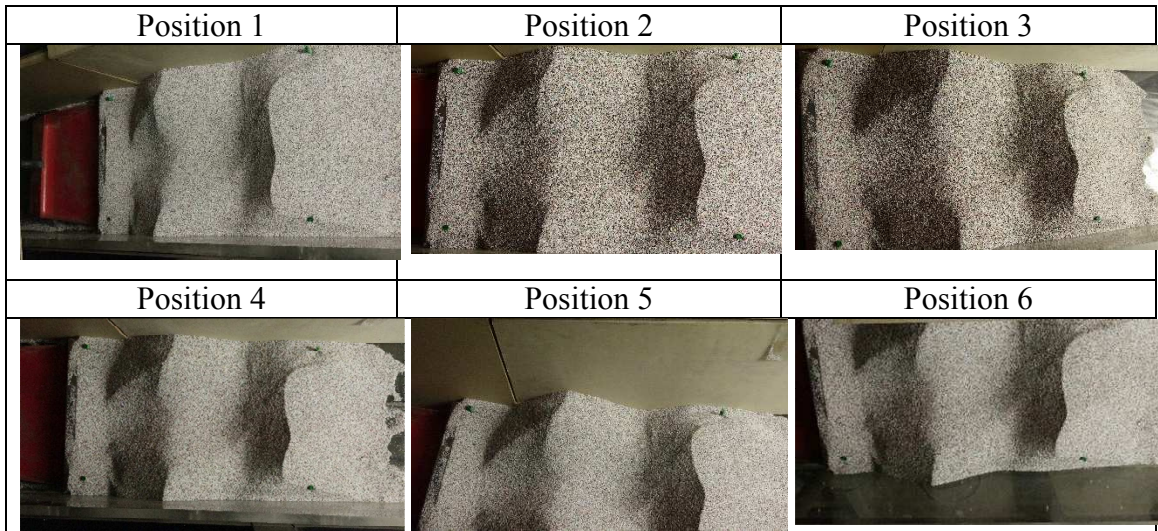
Figure 4.24 Temporal evolution of the dunes during one laboratory experiment. Six images are processed per case

4.3 In-situ snow deposit tracking at snow fences

4.3.1 Long-term observations of the snow fence site

This experimental field site is located in Shuelville, IA. Two snow fences are located near the Shueyville United Methodist Church. The present investigation focuses on the snow fences situated on the west side and left side of the school driveway situated near the church. The site location was chosen after consulting with the Johnson County Secondary Roads' Maintenance Superintendent. Following his recommendation, several visits at the site were done during the 2015-2016 winter season. This specific location was found to match all the needs for the present project research.

During the 2016-2017 winter season (from December 2016 to March 2017), measurements of the snow fall and snow drifts were conducted at this site. The measurements were conducted outside of the school perimeter, on the left side of the school driveway, as indicated in Figure 4.25. Two real-time cameras and one anemometer were deployed at the site next to the electrical poles (see Figures 3.12 to 3.15). All three instruments are self-powered with solar panels and do not require any supervision or maintenance. Images of the fence taken last winter are also included in Figure 4.26. The measured variables for the deployed instruments include time series of images and wind velocity characteristics, as discussed in Chapter 5.
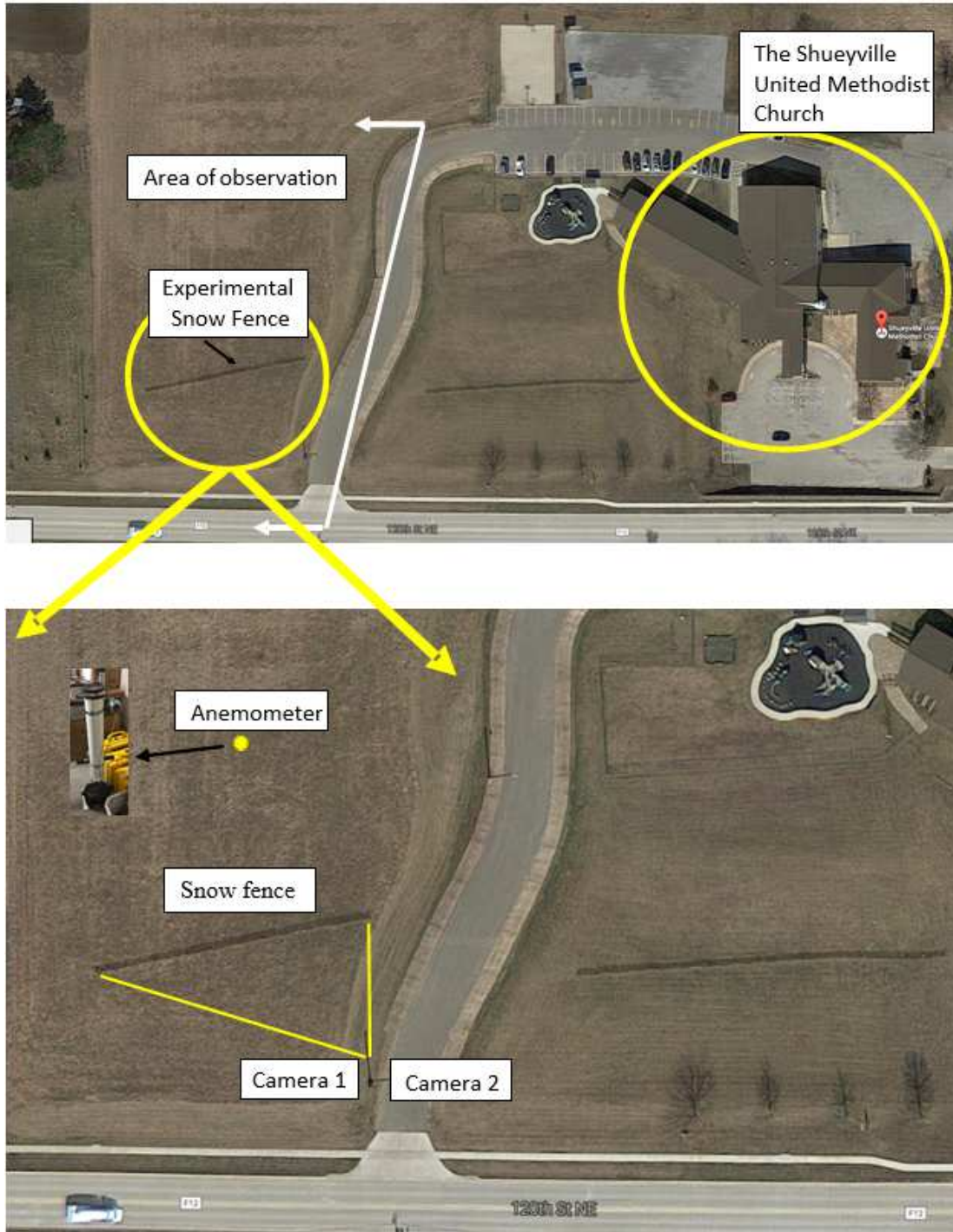
Figure 4.25 Experimental field site in Shuelville, IA containing a snow fence. Also shown the position of the cameras and instruments used to measure wind

Figure 4.26 Visualization of the snow fence on the west side at the Shueyville experimental site

4.3.2 Event based observations of the snow fence site

Another type of in-situ snow drifting tracking experiments was perform to observe snow deposition following a storm event. The original intention was to apply drone-based photogrammetric survey as described in Chapter 3. However, due to the new regulations proposed by the Federal Aviation administration (FAA), the photogrammetry survey using a drone could not be conducted. Another type of photogrammetric survey was attempted using close-range photogrammetry, as described in Keshav et al. (2015).

Images from this survey (this was the only survey performed given the lack of major storm events in the 2015-2016 and 2016-2017 winter seasons) are shown in Figure

4.27a. The survey was conducted following the March 14, 2017 snow storm. Images

were consecutively taken from several positions surrounding the area of interest. Prior to

acquire these images, a GRP survey, as required by the photogrammetry method, was

conducted downwind and upwind of the fence, as shown in Figure 4.27b and 4.27c. The

GRPs were obtained by spray painting the snow in several places. The results of the

survey are shown in Figures 4.27d and 4.27e.

a)

b)

c)

d)

uw1 uw6 uw7 uw12 uw13 uw18 uw19 uw25

uw24

uw2 uw5 uw8 uw11 uw14 uw17 uw20 uw23

uw3 uw4 uw9 uw10 uw15 uw16 uw21

p1 p2 p3 p4 p5 uw21 p6

dw3 dw4 dw5 dw6 dw7 dw8 dw9 dw10 dw11

dw2

dw12

dw1 dw20 dw19 dw18 dw17 dw16 dw15 dw14 dw13

e)

Church

UW25 ●
0.0555 m

UW1 ● UW6 ● UW7 ● UW12 ● UW13 ● UW18 ● UW19 ●
0.111 m 0.0587 m 0.1 m 0.084 m 0.081 m 0.0714 m 0.05715 m

UW24 ●
0.0778 m

UW2 ● UW5 ● UW8 ● UW11 ● UW14 ● UW17 ● UW20 ● UW22 ●
0.1286 m 0.1238 m 0.117 m 0.1508 m 0.06 m 0.1159 m 0.1318 m 0.1095 m

UW23 ●
0.10795 m

UW3 ● UW4 ● UW15 ● UW16 ● UW21 ●
0.1254 m 0.146 m UW10 ● 0.1095 m 0.1063 m 0.1555 m
0.1317 m

UW9 ●
0.146 m

P1 P2 P3 P4 P5 P6
0.092 m 0.065 m 0 m 0 m 0.0254 m 0.0365 m

DW4 ● DW5 ● DW6 ● DW7 ● DW8 ● DW9 ● DW10 ● DW11 ●
0.224 m 0.1556 m 0.1698 m 0.184 m 0.144 m 0.143 m 0.162 m 0.141 m

DW3 ●
0.111 m

DW12 ●
0.0635 m

DW2 ●
0.094 m

DW13 ●
0.0571 m

DW1 ● DW20 ● DW19 ● DW18 ● DW17 ● DW16 ● DW15 ● DW14 ●
0.0698 m 0.092 m 0.0794 m 0.0968 m 0.0556 m 0.0683 m 0.06 m 0.06 m

EAST FENCE

Figure 4.27 Event-based mapping: a) the survey site following the March 14, 2017 snow storm; b) downwind area of the fence with marker points; c) upwind area of the fence with marker points; Frames d) and e) show the results of the survey

Two to four images were acquired from each position to allow stitching the images for 3-D reconstruction. To avoid the difficulty of identifying the tie points required by photogrammetry on the snow deposits, artificial "seeding" was applied using dry leaves. Figure 4.28a showed the instruments (a power generator and a leave blower) used for seeding. The results after the seeding was applied are shown in Figures 4.28b (upwind area) and 4.28c (downwind area).

The results obtained using photographic mapping is provided in Figure 4.29. However, due to the relatively small deposition heights observed during the snow event, the results are within the accuracy of the photogrammetric survey.

a)

b)

c)

Figure 4.28 Seeding used for supporting the photogrammetric survey: a) instruments used to conduct the seeding (power generator and leave blower); b) view of upwind area of the snow fence; c) view of downwind area of the snow fence
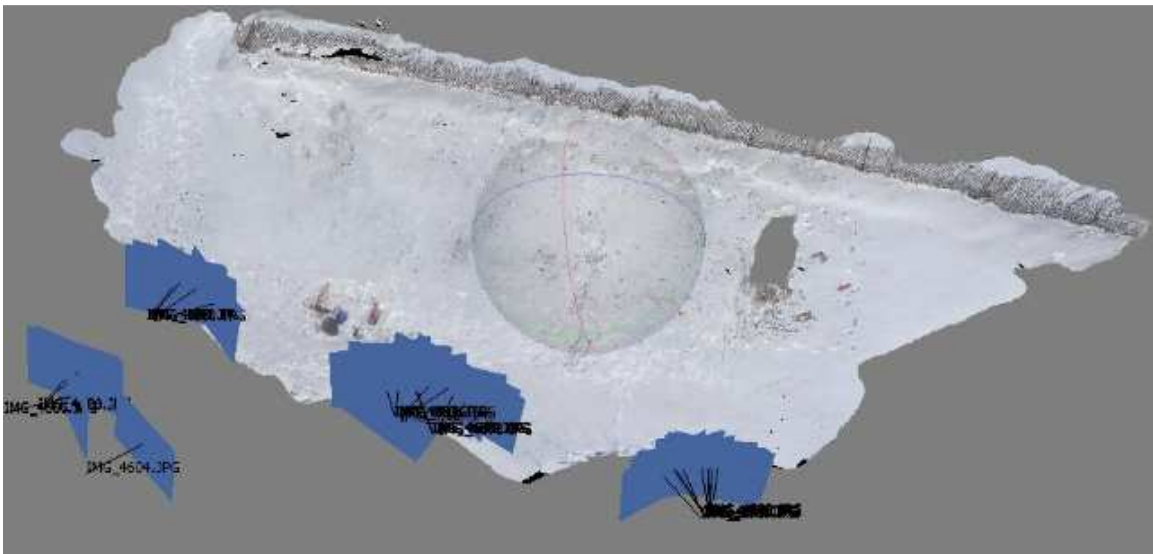
Figure 4.29 Photogrammetry result for snow deposit mapping

CHAPTER 5 EXPERIMENTAL RESULTS

The main goals of this research are to propose a set of protocols for local

measurement of snow fall and snow drift at a site, as well as for mapping snow deposits

at snow fences. A large part of this research was devoted to selecting the appropriate

instruments, proposing appropriate measurement and processing methods, developing

and optimizing the experimental arrangements and measurement protocols. Following

the finalization of each of the new measurement protocols, attempts have been made to

implement the research outcomes through proof-of-concept experiments. Unfortunately,

the last two winter seasons were milder than usual and there were few major storm events

recorded in Central Iowa during these two winter seasons. Given this situation, the

measurement of snow drift was tested in the laboratory using synthetic snow, an

experiment that was not included in the original research plan. Reported below are the

laboratory and field experimental results that were used to validate the proposed

approaches to measure snow fall, snow drift and snow deposit at snow fences.

5.1 Snowfall measurements using PTV

5.1.1 PTV results for storm events

Following the initial experiments whose main purpose was to propose a new

methodology to measure the snow fall, a series of snow fall events were document with

the developed PTV experimental protocol. The in situ measurements were collected with

the instrumentation and protocols described in Chapters 3 and 4. A sample of the

meteorological conditions during the monitoring of a snow fall event is provided in

Figure 5.1. Overall, the wind intensity and temperature reported in the figure are typical

for the snow storms that took place during the 2015–2016 winter season. The output files

containing wind data are given in the following format: f (001,1980-01-09,21:35:23.1,71,D_m,D_x,S_m,S_x,T_a,U_a,P_a,R_c,R_d,R_i,R_p) where 001 is the number of measurements in each transmit sampling time of 5 minutes, date: year-month-date, time: hh:mm:ss, and 71 is the Vaisala serial number. The definitions of the remaining variables are provided in section 4.1.3.For the 2015-2016 winter snow fall experiment, the dominant wind direction was between the Northwest/Southeast direction and the Northeast/Southwest direction. At most times, the wind velocity was below 10 mph.
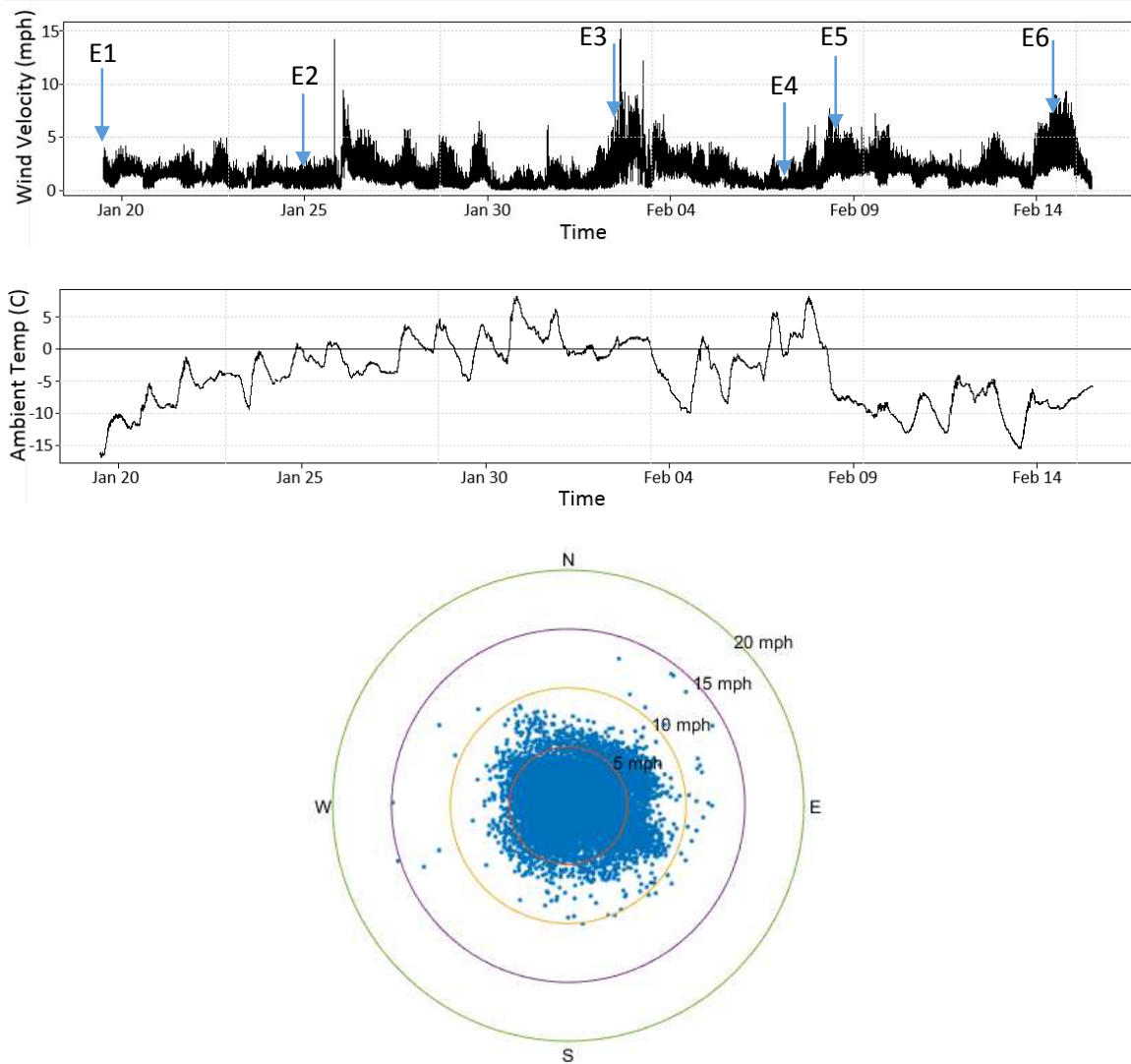
Figure 5.1 Sample of wind velocity, wind direction and temperature time series recorded during a snow fall event during the 2015-2016 winter season.

Several videos of snow fall events were recorded during January and February, 2016, resulting in a total of 6 different observed snow events. The individual snow events are listed in Table 5.1 with the corresponding date, event duration, number of recordings, and event descriptions. For event number 5, there are three recordings done throughout the day, which are labeled S1, S2 and S3.

Table 5.1 Summary of snow fall events monitored during 2015-2016 winter season

#	Date of the event	Event duration	# recordings/ event	Event specifics
1	Jan 19, 2016	2 hrs	1	Moderate snow, night time
2	Jan 25, 2016	2.5 hrs	1	Small snow, night time
3	Feb 2, 2016	1 hr	1	Mix of snow with rain, daylight
4	Feb 7, 2016	0.5 hr	1	Small snow, night time
5	Feb 8, 2016	8 hrs	3	Moderate snow, day & night time
6	Feb 14, 2016	4.5 hrs	1	Moderate snow, night time

Each time of observation was matched with the wind data provided by the Vaisala anemometers, as stored on the server. After determining the desired time period, the mean wind direction (D_m), and mean wind speed (S_m) were calculated. In summary, the calculated wind direction and intensity for all six storm events are shown in Table 5.2.

Table 5.2 Summary of mean wind velocity and wind direction during the snow fall events

Event	Total averaged wind velocity (m/s)	Average wind direction measured with respect to the North (°)
1	1.991	97
2	1.670	272
3	3.576	84
4	0.610	274
5 – S1	3.800	318
5 – S2	2.600	346
5 – S3	1.000	316
6	3.620	115

The instruments used to perform the measurements are described in Section 3.3.1.3. The measurement protocols are provided in Section 4.1.1. Using EDPIV software applied to successive video recordings, the snowflakes' velocity vectors can be inferred. Following the processing procedure described in Section 3.2.3, the components of the velocity vector of the individual snowflakes can be estimated in in the x and y directions (V_X and V_Y). The wind data output from the Vaisala anemometer also provides the V_{XI}, V_{YI} wind velocity components. The measurements and calculations performed for event 1 (2016/01/19) are summarized in Figure 5.2. The full analyzed results for events 2 to 6 are presented in Appendix A. In each individual event, the video recording range from 30 seconds to 1 minute. Within each recording, three bursts were calculated on the first 4 seconds, middle 4 seconds and last 4 seconds of the recording segment. Once the x and y components of the velocity vectors for each burst are decomposed and analyzed, the average of these values is assumed to be the final velocity in the x and y directions for the event.

Event 1: 01/19/2016 – 2 hours

S1_Start: 239 images, 149 snowflakes

S1_Middle: 240 images, 184 snowflakes

S1_end: 245 images, 115 snowflakes

Total snow velocity for the three PIV samples

Total snow fall velocity during Event 1
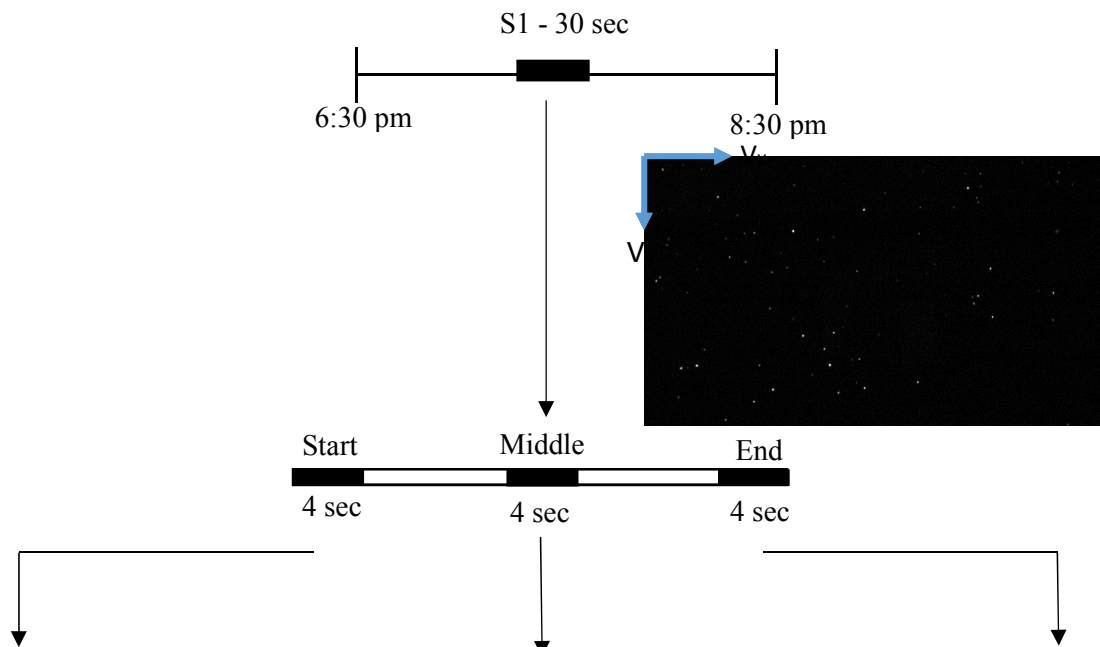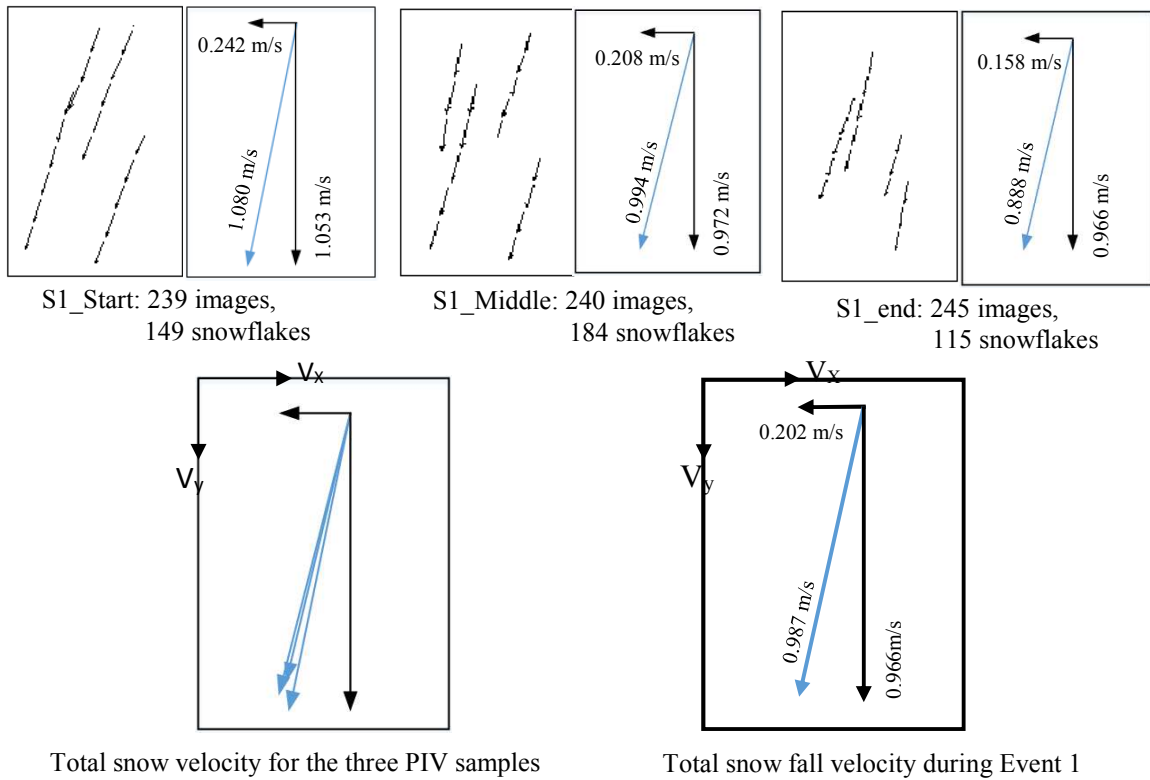
Figure 5.2 Processing stages leading to estimating the components of the velocity vector of the snowflakes during event 1.

Another essential variable used to estimate the snow relocation coefficient is the flux of snow in vertical and horizontal directions. The flux can be estimated if the particle velocity and concentration are determined, which is possible using a PTV based measurement technique. Previous studies concluded that snowflakes can be assumed to be of spherical shape (Muramoto et al., 1995). Based on this assumption, one can use the tracked particle size (in pixels) output from the EDPIV software to determine the average particle diameter. The concentration of the particles (snowflakes) can be subsequently determined by dividing the sum of the areas occupied by the individual particles to the image area. The results obtained for event 1 that characterize the type of snow and the snow fall dynamics are summarized in Table 5.3.

Table 5.3 Summary of wind velocity predictions during snow event 1

Event 1	V_x (m/s)	V_y (m/s)	Total Velocity (m/s)	Avg. Particle Snow Flake (pix)	Concentration (%)
E1_S1_Start	-0.242	1.053	1.080	25.73	0.144
E1_S1_Middle	-0.208	0.972	0.994	29.04	0.178
E1_S1_End	-0.158	0.874	0.888	22.28	0.131
E1_S1_Average	**-0.202**	**0.966**	**0.987**	**25.68**	**0.151**

As this specific example shows, a snow flake size of 25.68 pixels is equivalent to a diameter of 3.12 mm based on the relative pixel size. The inferred diameter of the snowflake is then used to calculate the snow flux. The horizontal velocity, V_{X1}, measured by the Vaisala anemometer was interpolated by decomposing the resultant vector, as shown in Table 5.4.

Table 5.4 Summary of observed wind condition for event 1

Event 1	Angle from North is 97°		
	V_{x1} (m/s)	V_{x2} (m/s)	Total Wind Velocity (m/s)
E1_Wind	-0.246	-1.976	1.991

5.1.2   Comparison of Vaisala anemometer and PTV predictions of wind velocity

Since these experiments focused on the horizontal movement of the snow particles, the predictions of the x-component of the mean snowflake velocity vector given by the PTV (V_X) and the Vaisala anemometer (V_{X1}) are compared in Table 5.5 for the six events. The vertical component of the snow fall is typically larger than the horizontal one, hence the measurement protocol accuracy is better tested by considering the smaller horizontal component.

Table 5.5 Summary of PTV predictions of snowflakes related variables and comparison with the Vaisala anemometer prediction of the horizontal velocity component

Event	V_x from PTV result (m/s)	V_{x1} from Wind result (m/s)	Total Wind velocity (m/s)	Wind Angle from North (°)	Avg. Particle snowflake diameter (mm)	Concentration (%)
1	-0.202	-0.246	1.991	97	3.12	0.151
2	0.044	0.058	1.670	272	1.14	0.007
3	0.306	0.374	3.576	84	2.06	0.254
4	0.026	0.043	0.610	274	0.72	0.001
5 – S1	2.561	2.824	3.800	318	3.20	0.254
5 – S2	0.854	0.970	2.600	346	2.49	0.091
5 – S3	0.603	0.719	1.000	316	2.61	0.070
6	1.444	1.530	3.620	115	2.84	0.011

One should emphasize that the main assumption that made this comparison possible is that the snowflakes are closely following the wind dynamics. In addition to velocity, PTV measurements include the diameter of the individual snowflake particles. PTV also provides estimates of the velocity and snowflake concentration as instantaneous values. By taking the product of the two quantities one can estimate the snowfall flux by correlating the measured wind velocity with the observed resultant motion of the snowflakes. The results for the x-direction velocity calculated based on EDPIV (V_X) and the Vaisala anemometer (V_{X1}) show a strong relationship. This result basically validates the proposed image based method to measure particle velocity. The PTV velocity measurements   are slightly smaller than those obtained using the anemometer due to some uncertainties. Overall, the comparison between the two methods shows that the non-intrusive measurement protocols developed for measuring the snowflake velocities are in agreement with independent direct measurement of the wind velocity using standard instruments (anemometer).

5.2 Snowdrift measurements

5.2.1   In situ measurements

The snow drift measurements can be only quantified in the context of the boundary layer transport processes, as described in Chapter 2. In terms of the horizontal flux of snow, the region of interest for snow fence design is situated in between the ground and a distance of 6-8 feet above it (Weather Online). Measurements performed along the vertical within this region combine the effect of wind acting on the falling snowflakes with the effect of suspension of the snowflakes entrained from the bed by wind currents. Unfortunately, it is not possible to split the flux into two components associated with these two effects. From this perspective, taking measurements in the absence of snow fall is the best approach for quantifying snow drift as in this case only the second effect is present. Moreover, most of the snow transport contributing to the formation of the snow dunes is associated with the movement of "snow sheets" that slowly advance over the stationary layer of deposited and compacted snow.

The intertwined nature of snow transport processes necessitates separate measurement strategies for the snow fall and the snow drift. In summary, for snow fall, measurements should be taken above the boundary layer (at least 6-8 ft. above the ground), while for the snow drift, measurements should be acquired at less than 6-8 ft. from the ground, preferably after the snow fall stops and the snow moves only via entrainment from the deposited snow on the ground. For a quick estimation of the snow drift flux, a good surrogate measurement is to quantify the movement of the snow sheets advancing over the stationary layer of deposited snow.

Sample snow drift in-situ measurements were obtained using PTV and LSPIV techniques during a snow drift event on December 16th, 2016. The presented results are only marginally relevant as they were acquired during the development of the protocols for in-situ measurement of the snow drift leading to experimental arrangement EA6 described in Section 4.2.1.1. The mild snow storms that took place during the 2016-17 winter season have not offered more opportunities to perform *in situ* measurements at the location where the PTV - LSPIV setup was installed. The alternative of mobilizing the recording and illumination equipment using forecasted storms at various locations where snow drifting occurs is feasible for the developed measurement protocols. However, the limited resources available for this research did not allow us to pursue this alternative. Based on the previous arguments, the results reported in this section only discuss the dynamics of the snow dune movement. The full protocol for snow drift measurements is presented in the next section.

The protocol for measuring snow movement above the bed utilizes the PTV approach for estimating the velocity of the individual snowflakes moving near the bed, as illustrated on the right side of Figure 5.3a. The movement of the snow dunes as they migrate over the layer of compacted snow is more accurately quantified by LSPIV rather than PTV. This is because the LSPIV is based on grey-level pattern recognition while PTV is more accurate when the goal is to capture the movement of individual particles.

a)

0.89404 →

b)

0.16057 →
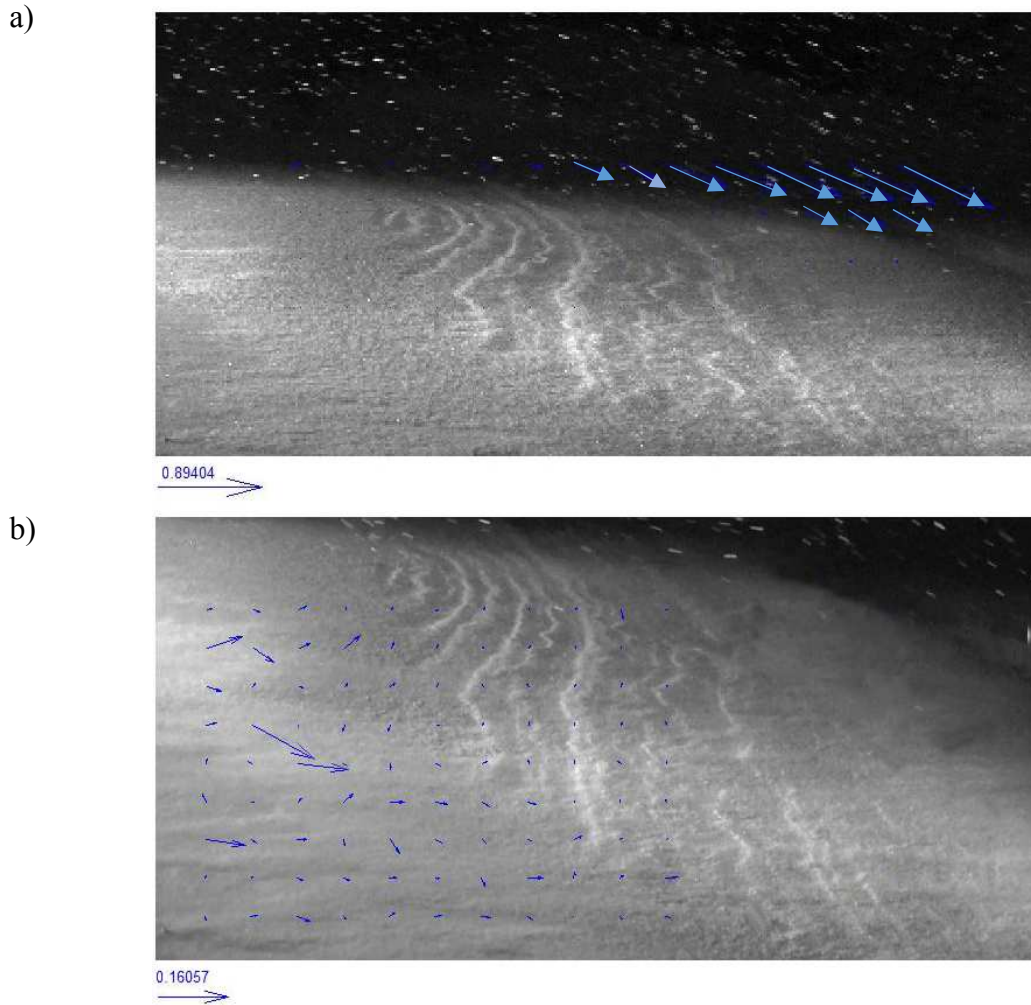
Figure 5.3 Illustration of measurement results used to quantify snow movement above the top of the layer of compacted snow a) velocity of snowflake particles moving near the bed; b) velocity field over the snow bedforms

Limitation of the PTV techniques for cases when a high concentration of tracked particles is present, which is the case for snow particles moving as bedforms (see ripple like bedforms in Figures 5.3a and 5.3b). The snowflake velocities obtained from PTV measurements using images taken at the same time are approximately one order of magnitude higher that the velocity of the snow bedforms migrating over the fixed layer of snow. It is the latter component of the total snow flux that is essential to be accurately quantified for the design of snow fences.

5.2.2   Laboratory measurements

The facility and measurement protocols for estimating snow drift in laboratory conditions were described in Sections 4.2.1 and 4.2.2. Preliminary experiments were performed to evaluate several possible arrangements for the camera and the light assembly. Several preliminary arrangements were tested until the EA6 arrangement was reliably replicated in the experimental setup. The movements of the melamine particles modeling the snowdrift in laboratory conditions were first mapped using photogrammetry. Their dynamics was then studied based on LSPIV data. LSPIV was applied to 6 bedform maps, as illustrated in Figure 5.4. The time interval between the maps was 1 minute. Bedform migration was induced using a blower that covered the whole test section in the spanwise and streamwise directions. The velocity magnitude in the streamwise direction found to rapidly decay as the planar air jet was not confined, as it is the case in standard wind tunnel experiments.
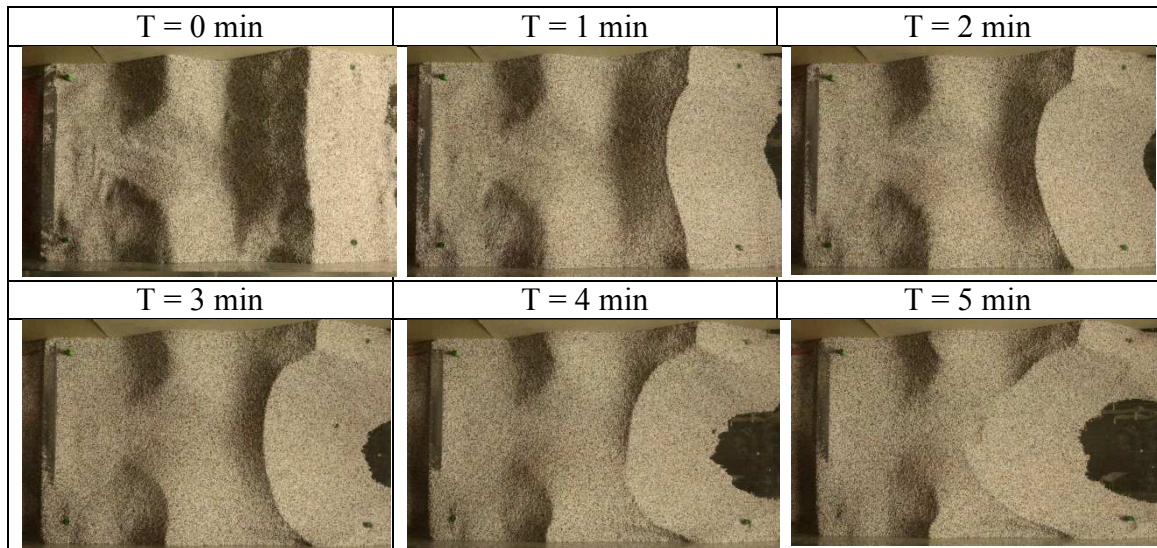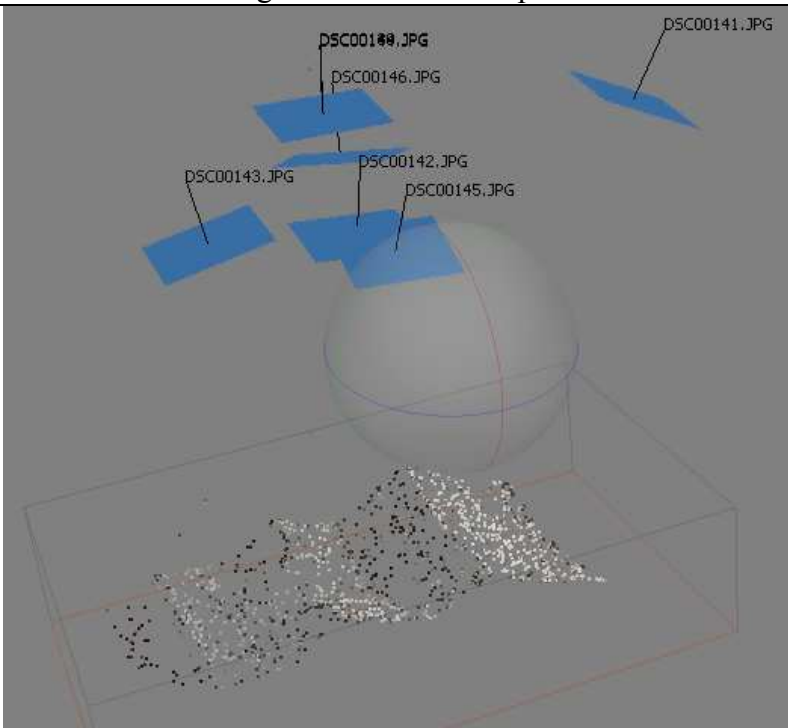
Figure 5.4 Visualization of the temporal evolution of the bedforms over a period of 5 minutes in the snow drift experiment

5.2.2.1 Photogrammetry results

One of the procedures available to map snow deposition is photogrammetry (see Section 3.2.3). On average, 6 images were taken from various angles. Four ground reference points were used for scaling and image correction purposes. The present study used the Agisoft Photoscan software to process the images and obtain the coordinates of each photo. Then, the overlapped GRPs were observed. Four steps were needed to reconstruct the 3-D model using this photogrammetric approach: align photos, build a dense cloud, build a mesh and apply texture to the image. The sequence of steps and their output, as applied to the validation laboratory test, are illustrated in Figure 5.5.

Steps	Agisoft Photoscan output
Align photos & Build dense clouds	
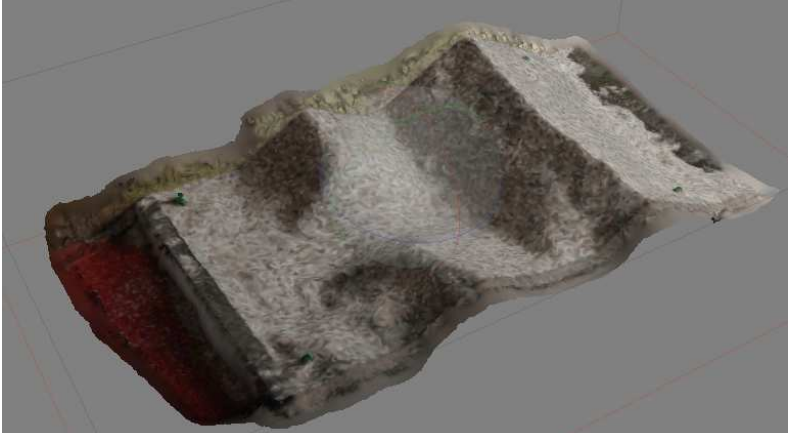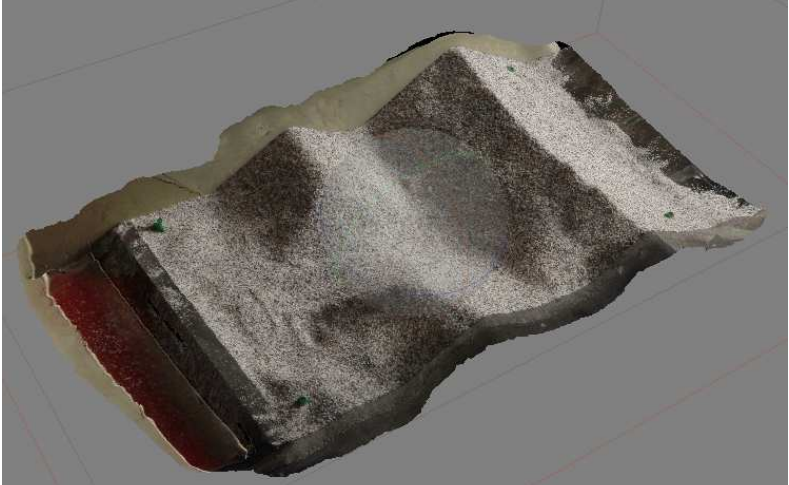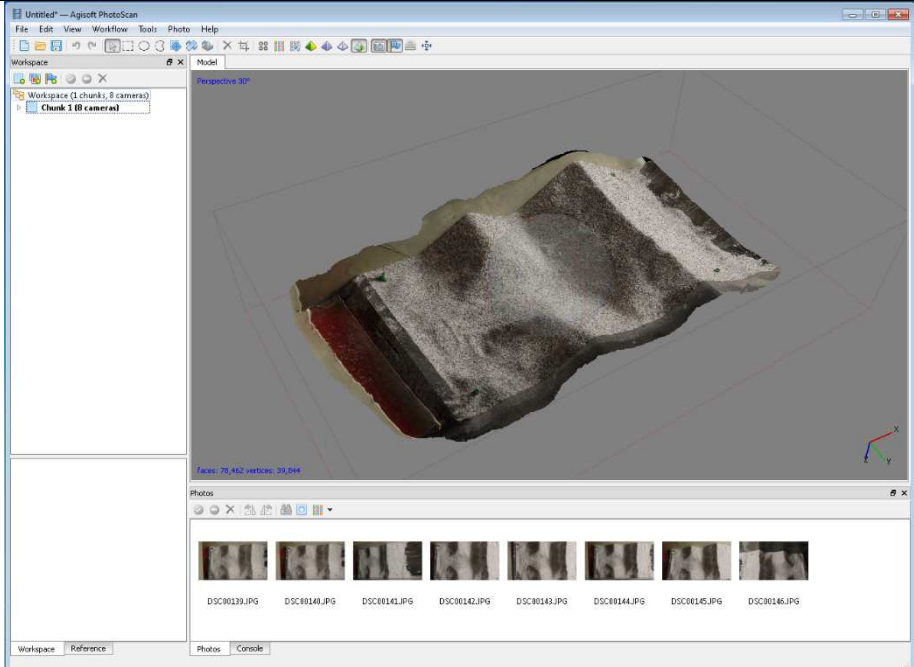
Build mesh	
Build texture	
Agisoft interface	

Figure 5.5 Main steps of the procedure used to reconstruct the 3-D model using the Agisoft software

In the first step, the images from various angles are stitched. Using the ground reference points set in the experimental test section, the proper photo alignment is carried out across all the acquired images. Software workflows are available to subsequently create a rough layout of the mapped area. In the seldom case where the camera falls short of recording the coordinates, the software has the potential to locate all the reference points using the known locations of the camera successive shots.

Secondly, the software generates a dense point cloud. The main purpose of this step is to generate and gather all the points and use this information to advance the design process and obtain points acquired from raw information. The relatively smaller scale and simple structure of this experiment allow the majority of the points to be generated without any problems. However, some studies (Maiwald, 2017) provided more detailed information on how building dense clouds may not be sufficient to complete the detailed reconstruction of the model. For the field measurement protocols reported in Section 4.3.2, the building of the tie points was facilitated by spreading leaves over the texture less snow surface. In general, to improve the resolution and accuracy of the photogrammetry modeling it is recommended to take several images of the area to be surveyed. The higher the quality of the original image, the better is that of the constructed 3-D model.

The main goal of the next step is to create the smaller mesh between all the tie points generated from the dense clouds and to form a layer that links all the points creating the smooth surface. In the last step, the Agisoft Photoscan software identifies the surface texture and color in order to transfer and apply the texture layer on the top of the

mesh layer. This step matches the 3-D model with the actual object, giving the user the final control on the surface's appearance.

The results generated by the Agisoft Photoscan software were organized and compared side by side with the physical measurement. They are shown in Figure 5.6. The results demonstrate the high capability of reconstructing the 3-D model and its relevant details by using only 6 images. The obtained photogrammetry maps can be used as stand-alone three-dimensional representations of the snow deposited at any location in situ, including for mapping the snow volumes developed upwind and downwind of the snow fence. Using successively generated photogrammetry maps, the rate of volume change can be tracked and then used to characterize the dynamics of the bedform movement, an essential outcome for documenting snow drift dynamics.

In general, photogrammetry techniques   have the ability to recreate an accurate 3-D model of the objects. Several studies (Skarlatos, 2012; Kersten, 2006) concluded that such techniques are relatively cost efficient compared to techniques using laser scanning. Although the resolution and quality of the output might not be as precise as the one obtained using laser scanning, the Agisoft Photoscan software results are suitable for the purpose of the present research. A main advantage of this technique is the relatively rapid processing time of the data to obtain the photogrammetry maps.

Physical measurements	Agisoft Photoscan
T = 0 min	

T = 1 min
T = 2 min
T = 3 min
T = 4 min
T = 5 min
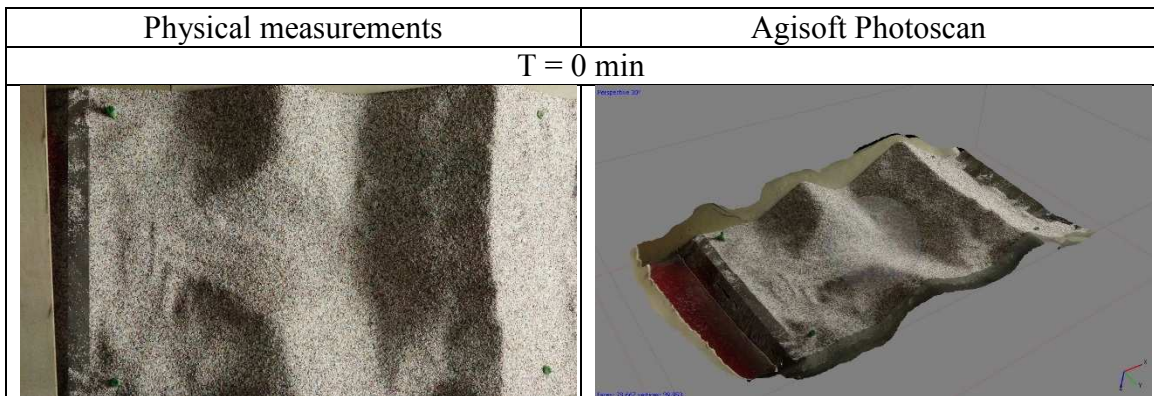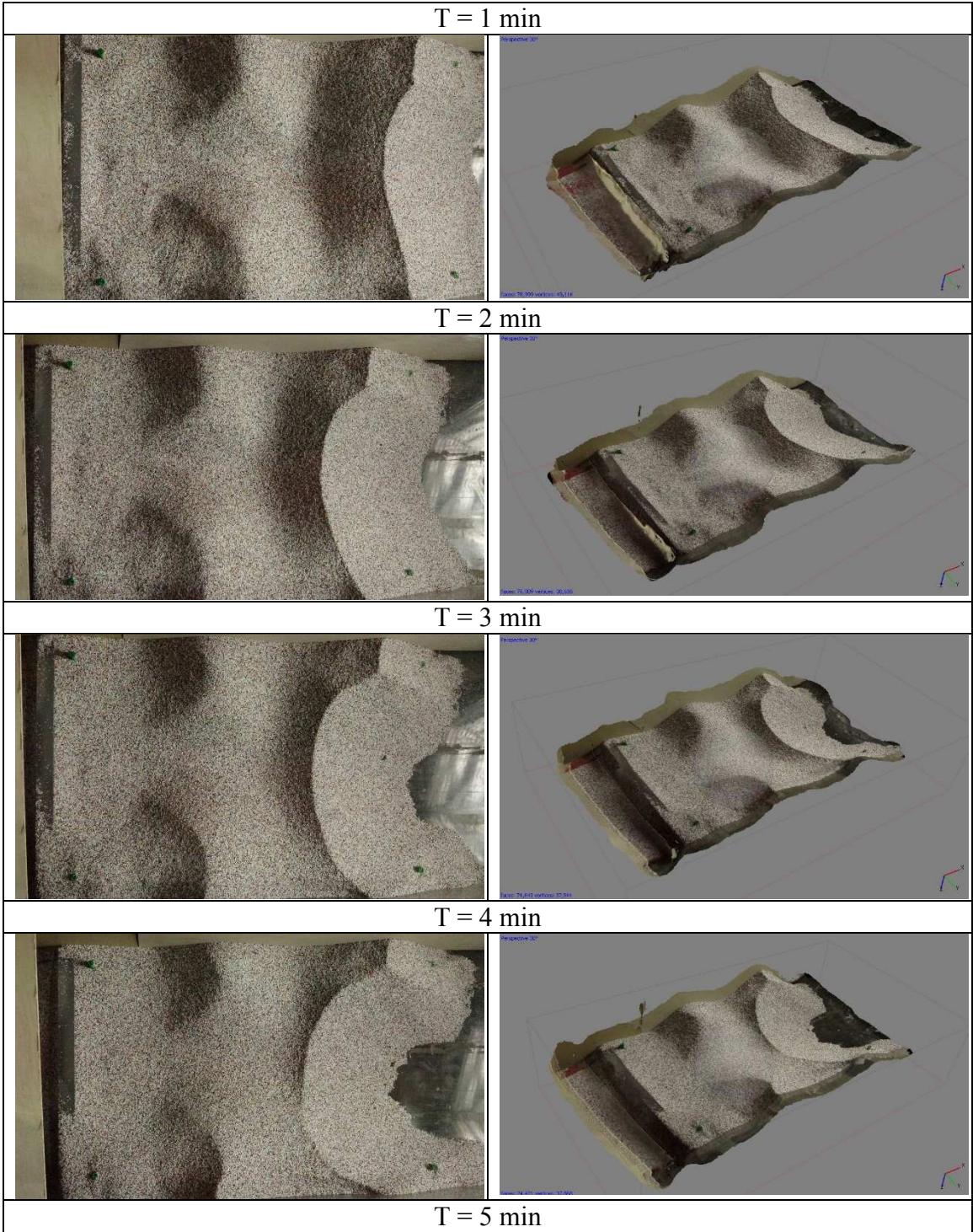
Figure 5.6 Comparison between Agisoft software 3-D maps output and physical measurements

5.2.2.2 LSPIV applied to photogrammetry-based maps

The sequence of repeated maps obtained using the photogrammetry technique is further used in conjunction with LSPIV to quantify the snow drift velocity. With this capability in place and estimation of the snow fall velocity/flux, as described in Section 5.1, direct estimation of the snow relocation coefficient is possible. After inputting the 6 images into the LSPIV software, a searching area (SA) and an interrogation area (IA) were selected commensurate with the size of the identifiable patterns and their speed of movement between successive images.

Several different combination of SA-IA were tested to obtain the best result in terms of capturing the bedform velocity migration. Using images, rather than another sensor output (acoustic or LIDAR) it is advantageous to quickly converge to an acceptable flow field, as visual observation is intuitive and does not require special training. Figure 5.7 shows the dune velocity vectors generated in the preliminary tests using different sets of SA and IA parameters. All the other processing parameters (i.e., minimum acceptable correlation coefficient of 60%, exposure time of 0.01667 s (1/60 seconds) were kept the same to isolate the impact of the targeted parameters.

a) IA 128 SA 32
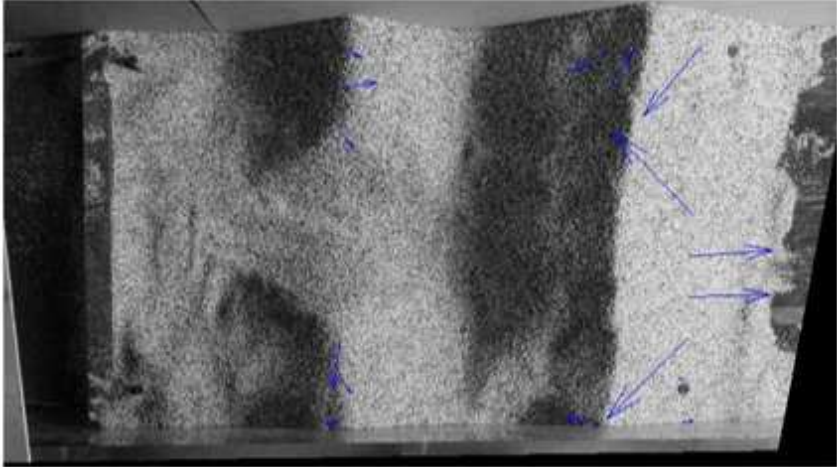
0.0074256

b) IA 256 SA 64
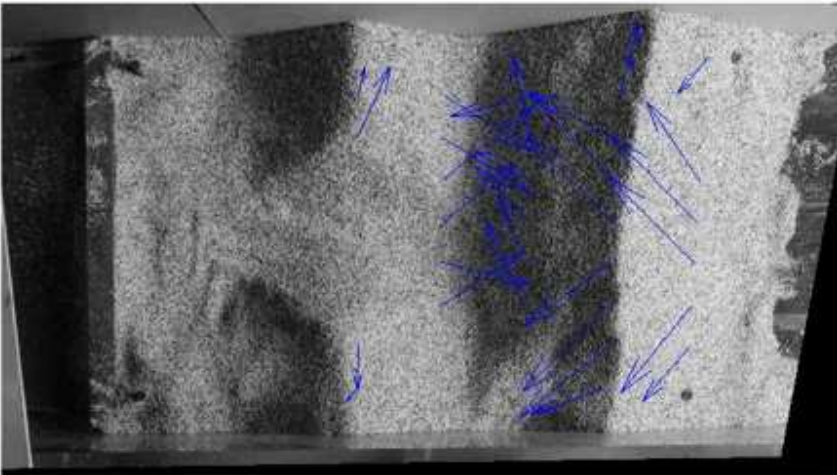
0.014968

c) IA 512 SA 128

0.028203
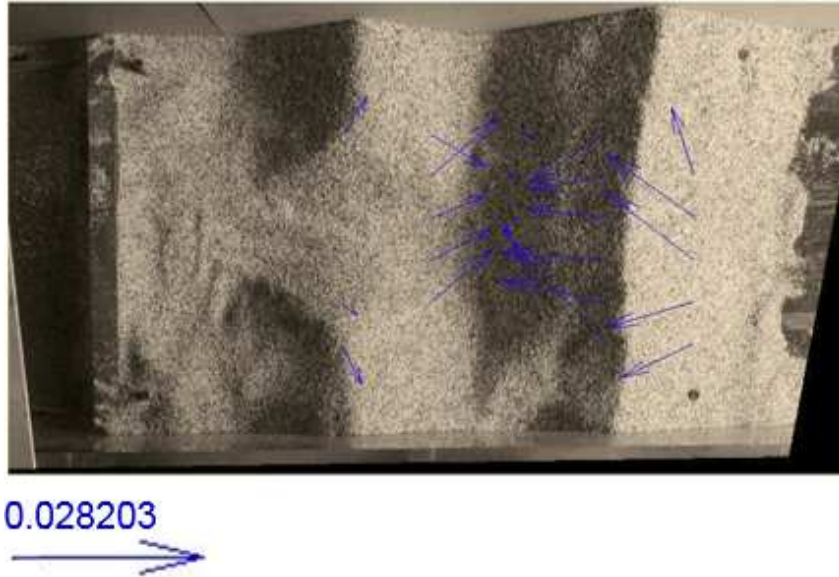
Figure 5.7 Dune propagation velocity vectors obtained using the LSPIV technique for different values of the main processing parameters. a) IA: 128 pixels, SA: 32 pixels; b) IA: 256 pixels, SA: 64 pixels; c) IA: 512 pixels, SA: 128 pixels.

Visual observation on the actual video recordings and bedform dynamics estimated using LSPIV indicates that the set up with IA: 128 pixels and SA: 32 pixels falls short of capturing the full motion of the simulated snowflakes and dunes. The high uncertainty in the velocity vectors' magnitudes affects the results. The other two cases using relatively larger values of the IA and SA parameters successfully demonstrated the capability of tracking the snowdrift movement. Both results agree with direct observations of velocity magnitude and direction of the dunes' movement. Part of this study three separate cases with varying parameters were evaluated. Only 6 images were used to track the movement. Due to the larger displacement within the 6 images, the estimated average displacement was chosen to have larger values of the parameters. One additional case was examined using a much longer series of images (~600 images) cut from a 10 seconds recording to test this procedure. Because the relatively small

displacement observed between frames collected every 1/60 second, the estimated

average displacements were selected using an IA value of 64 pixels and an SA value of

16 pixels. This was sufficient to track the propagating limbs of the individual dunes.

Figure 5.8a shows the estimated pixels for a value of IA equal to 64 (blue) and a value of

SA equal to 16 (red). This can provide a first good guess for the searching range and

interrogation areas. The final result is presented in Figure 5.8b.
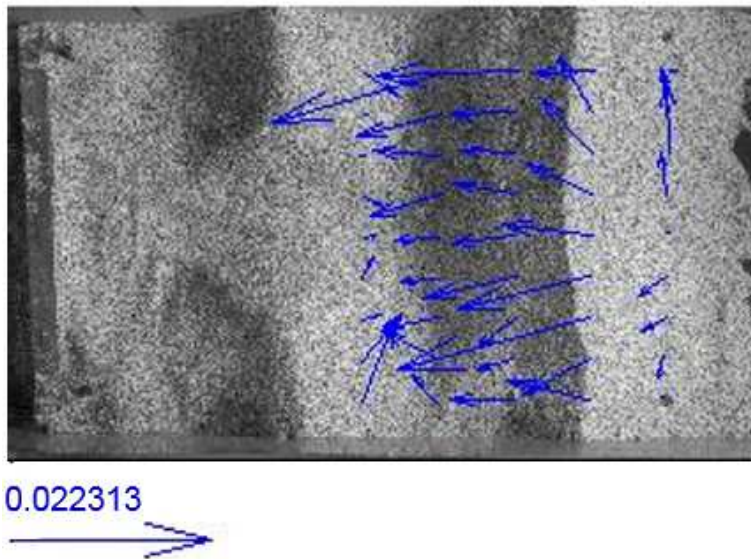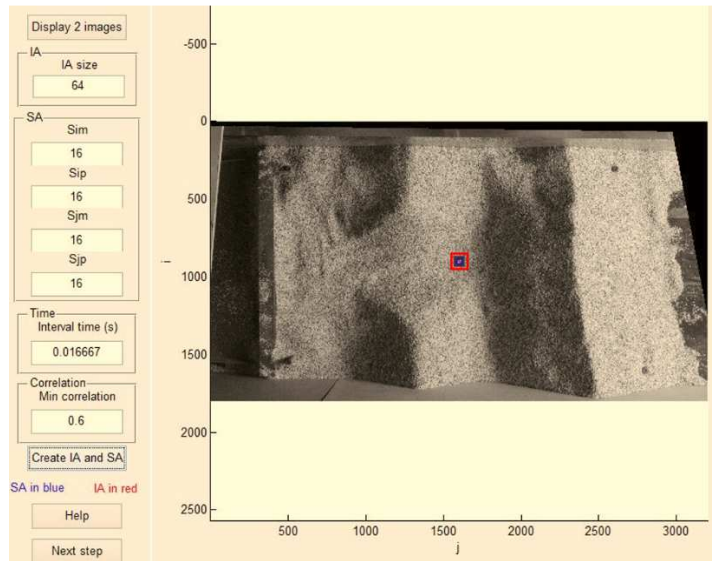
Figure 5.8 LSPIV velocity predictions obtained from a series of images: a) SA
and IA in pixels; b) dune propagation velocity vectors

5.3 In situ mapping of the snow deposits at fences during storm events

The measurements reported in this section were obtained during the 2016-17 winter season at the Shueyville site where two fences were deployed at the beginning of the winter season, as illustrated in Figure 4.25. The wind and temperature characteristics during the winter season are illustrated in Figure 5.9.
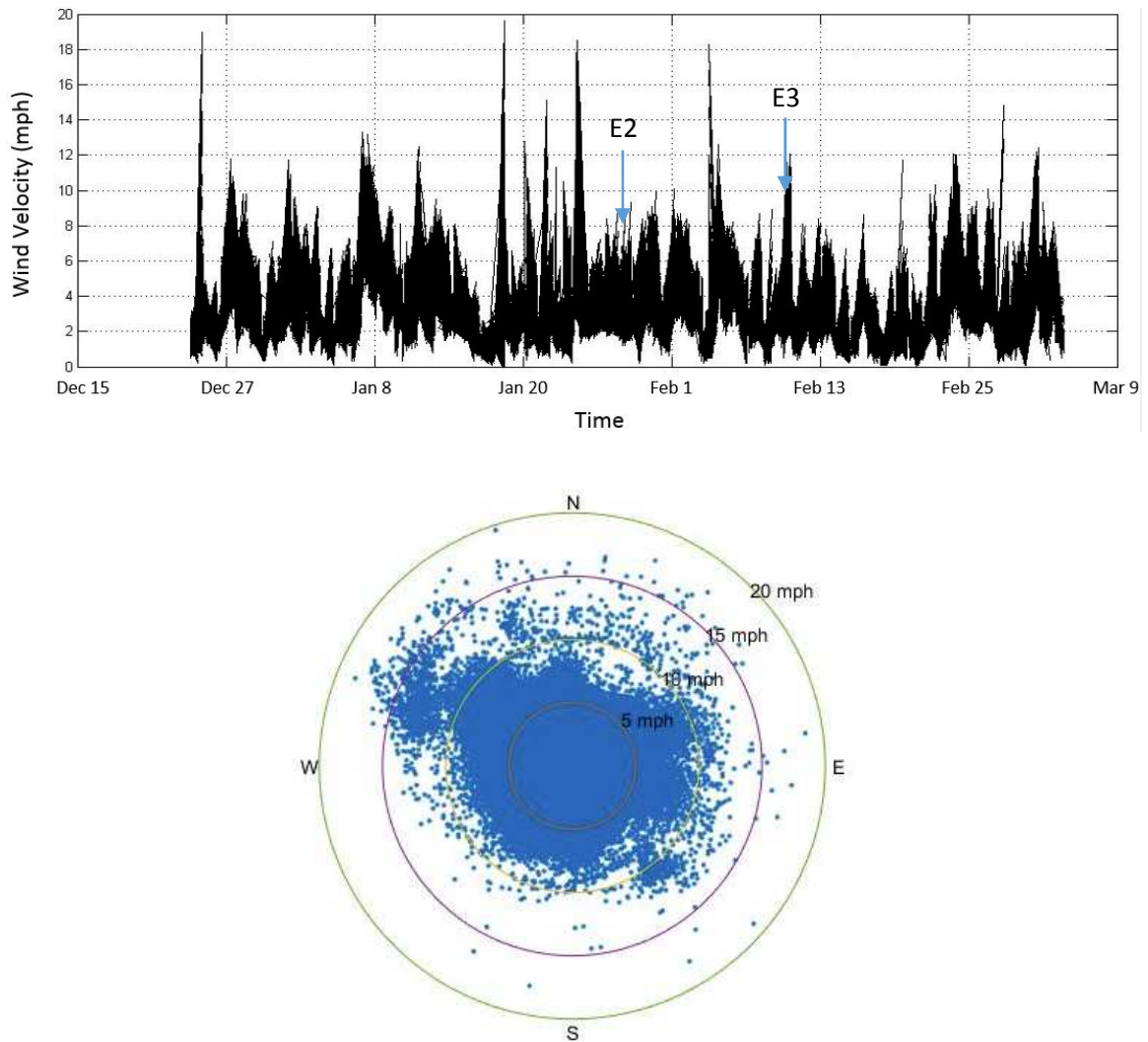
Figure 5.9 Sample of wind velocity and wind direction time series during the 2016-2017 winter season

Four larger storm events were monitored and measurements were performed at the Shueyville site. The first event occurred on December 15-16th, 2016; the second one (much milder) occurred on January 25-26th, 2017; the third one occurred on February 8th, 2017 and the fourth one occurred on March 12-13th, 2017 and it corresponded to the strongest storm. From the wind data represented in Figure 5.9, it is observed that at most time the dominant wind was oriented along the Northwest/Southeast direction. For these conditions, the two snow fences were active. When the wind speed was below 15 mph, no major snow deposition at the two fences was observed during the 2016-2017 winter season. A detailed analysis of the wind velocity and wind direction recorded by the Vaisala anemometer was performed for all four snow storm events. The metrological data for the March 12-13th, 2017 storm is provided in Figure 5.10 from weather.com. The wind intensity and direction measurements were conducted at the Eastern Iowa Airport situated 6 miles north of the Shueyville experimental site. This was done because the Vaisala anemometer server was down from March 4th to March 16th.

a) March 12th, 2017
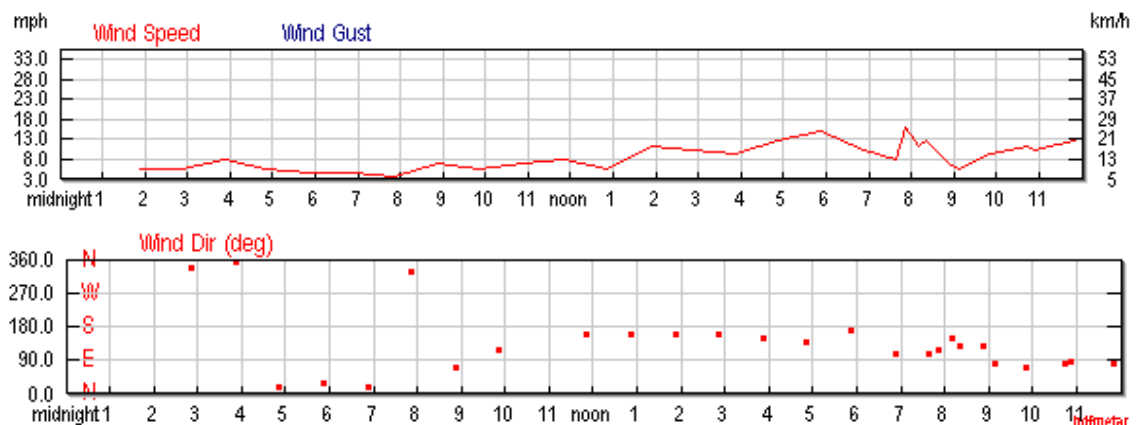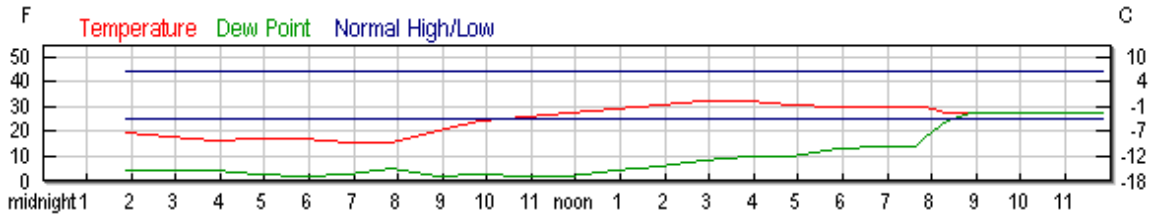
b) March 13th, 2017
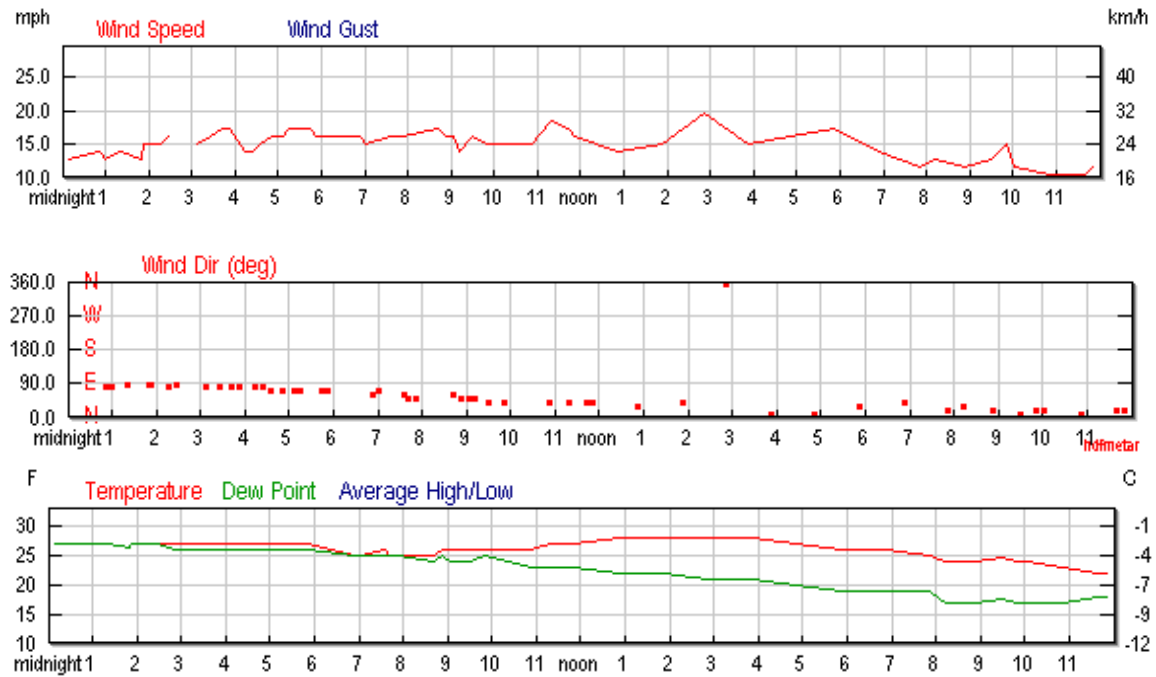
Figure 5.10 Wind intensity (mph), wind direction (degree), and temperature: (a) March 12th, 2017 event; (b) March 13th, 2017 event (Weather underground, 2016)

Series of images were also taken on both sides of the snow fences after the end of each storm to document the site condition. Figure 5.11 shows such images for the March 14th, 2017 storm. During this event, the amount of snow deposited on the downwind side of the two fences was relatively small. The other snow events that were monitored during the 2016-2017 winter season are documented in Appendix B.

Looking downwind
EAST FENCE – Looking upwind (on the right of the school driveway)
Looking downwind

Figure 5.11 Event monitoring for March 14th, 2017 storm

CHAPTER 6 CONCLUSION AND FUTURE WORK

Snow drifting and blowing are common phenomena in four-season areas exposed to intense snowfalls and winds during the winter season. Preventive actions against snow drifting and blowing are conducted both in the road design stage (by choosing suitable road alignment alternatives) as well as after road construction (through snow-retention infrastructure deployed at the site or maintenance activities applied when needed). Development of an effective snow-retention solution is preferred to maintenance activities, as the latter can become a large component of winter maintenance costs for states or local agencies. One of the most often used and reliable solutions for controlling snow drift is deploying snow fences along the roads in regions where severe snow drifting is reported. The cost of the snow fences including their installation costs is about an order of magnitude lower than that of mechanical snow removal.

The design of the snow fences is based on a set of local or regional weather conditions estimated over a long-term period and by taking into consideration the topology of the site where the snow fences are installed. This characterization is typically conducted through site surveys followed by the establishment of the orientation and geometry (e.g., height, bottom gap, porosity) of the fence and other design parameters needed to insure the structural integrity of the snow fence. Among the most challenging tasks for proper design of the snow fence is the thorough characterization of the meteorological conditions at the snow fence site. In the absence of this local characterization, an efficient design of the snow fence is practically impossible, as snow drifting is a process that is highly variable from location to location within the same climatologic area and also highly variable in time at the same location.

The present thesis addressed three critical aspects of snow fence design: estimation of the snow fall and snow drift fluxes and mapping of the snow volumes accumulated at the snow fence after its deployment at the site. The estimated snow fall and snow drift fluxes are used as input data in the software used for snow fence design, while the last variable is used to evaluate the efficiency of the fence after its deployment. Conventional methods for estimating these three variables are outdated. Most of these methods are intrusive, requiring deployment of instrumentation and personal at the site for extensive periods of time in a harsh winter environment.

The first important contribution of this thesis was to develop a number of non-intrusive measurement techniques that work independently or in combination to provide quantitative and accurate estimations of these three variables. The proposed measurement methods do not require permanent installation, are mobile and can be quickly operated to produce a wealth of qualitative and quantitative information readily usable for the design of the snow fences. Their non-intrusive features preclude extended exposure to frigid, and windy conditions that would pose a significant safety and health risk for the personnel conducting the measurements.

The **snowfall measurements** can be obtained continuously (day or night), with minimum preparation, using image-based techniques that are currently becoming remote sensing practice for many civil, industrial and research settings. The short-time video recordings acquired with off-the-shelf instrumentation are not interfering with the natural process of snow blowing in the vicinity of the ground. Locally-adapted strategies are needed for providing adequate illumination, setting the camera parameters and processing the raw information with commercially available software. This type of methodologies is

in sharp contrast and, doubtless more accurate, than the traditional ways of obtaining snow fall estimates using intrusive measurement techniques, currently in use at the majority of the meteorological stations (snow boards, anemometer arrays, etc). Moreover, the remote nature of image-based measurements does not interfere in any way with the plane where the image acquisition is made. The images collected with the videocamera are processes to provide: individual snowflake velocity and size. Subsequent post-procesing provides two-dimensional fluxes of snow passing the imaged plane. The image size is considerably larger than the size of the current snow boards used for measurement of snow fall, hence it can fully characterize the dynamics of the snow fall, instantaneously or over a certain time interval. By contrast, when using classical methods, information on snow flake velocity and size are obtained using different instruments.

The **snow drift measurement protocols proposed as part of the present research** also relay on image-based technologies (hardware and software). Concepts adopted from modern technology such as structure-from-motion (Westoby et al., 2012) and image velocimetry (Muste et al., 2004) have been assembled to propose, for the first time, a reliable non-intrusive method for estimating the drifted snow velocity and snow fluxes over the top of the fixed layer of compacted snow. The methodologies and protocols assembled for characterizing the snow drift at a site are providing multiple variables, i.e., velocity of snow sheets (ripples) moving along the bed (top of the fixed layer of snow), mean direction of motion over short and long time intervals, characterization of the wind-fetch distance. Obtaining quantitative information on the snow drift is even more challenging than measuring the snow fall. The snow drift flux is

rarely directly measured using intrusive methods (e.g., such measurements are usually performed using snow traps). Given the complexity of in-situ measurements of the snow drift flux, several empirical and semi-empirical relationships have been developed. These relationships are site-dependent, therefore they are not usable in other geo-climatologic areas other than those where they were determined.

Accurate estimation of the snow fall and snow drift fluxes is critical in defining the **Snow Relocation Coefficient** (SRC), a variable that is of great importance for the snow fence design (Tabler, 1994). Conventional SRC estimation is based on empirical relationships derived from regression models applied to snow mass flux and wind intensity measured intrusively at various heights above the surface bed. These empirical relationships are typically site-dependent and strongly correlated with the local meteorological and topological conditions. Therefore, the direct use of these relationships to predict the SRC at sites with different conditions is highly questionable. No corrections were proposed to easily adapt these relationships when used at sites with different conditions. Being able to measure more efficiently the main variables involved in estimating the SRC using a mobile measurement platform consisting mainly of a portable camera and illumination devices is a considerable advantage compared to conventional approaches. Such conventional approaches used to estimate the SRC require extensive labor and deployment time.

The SRC is also one of the main parameters used as input in snow fence design software used by state agencies. The snow fence design is highly dependent on the value of this variable. So, accurate information on the value of the SRC at a given site is critical for correct design of the snow fence that will be deployed at the site. Currently, design

engineers in state agencies are generally using a constant value for all cases based on Tabler's methodology developed for Wyoming conditions. Though they recognize this value is not the correct one, simple engineering judgment cannot predict the impact of multiple variable involved in the snow-drift process. Thus, they cannot a priori come with a more accurate estimate of the SRC for a given site location and conditions. Moreover, the methodology used for designing the snow fence is generally assuming a one-storm event occurring at the fence site. In principle, a snow fence should have a sufficiently high snow retention capacity to function well over a whole winter season, when successive snow storms can occur at a site. Multiple thermal processes are acting on the snow trapped by fences during and between successive storms. Such cases are not accounted for in the design. Moreover, the variability of weather conditions from storm to storm is not a parameter considered in standard snow fence design methodology used by state agencies. Further complicating the estimation of the SRC is its dependence on snow type and characteristics of the ground surface at the time of the snow storm event (e.g., the presence of tall vegetation results in a lower value of the SRC compared to the case a bare flat ground is present at the same site). Overall, it can be concluded that the availability of direct measurements of the SRC via the approaches and methodologies proposed in this research, should result in a significant improvement of the accuracy of the SRC estimated values. This should also result in more accurate predictions of the volume of snow retained by the fence and estimates of the risk of overtopping a snow fence during a given storm event. The proposed methods to estimate the snowfall and snow drift fluxes are not only useful for snow fence design. They can be equally useful for a range of meteorological applications. The instrumentation, measurement

methodologies and protocols developed as part of this research can create a new level

for this area of applications that has been left "frozen" for many decades.

The technologies and protocols developed for **mapping the snow deposition** at a

snow fence complete a suite of non-intrusive measurement approaches that can

efficiently support decisions related to snow fence type selection, size and fence position

in the design stage, but also in evaluating the design efficiency of the snow fence.

Quantification of snow accumulation at the fence site is the ultimate qualifier of the

efficiency of the snow fence design and its operational performance. Direct observations

of the capacity of the snow fence to retain snow during a whole winter season provide

critical feedback for continuously improving design guidelines for snow fences.

Conventional methods for quantification of snow accumulation are tedious, expensive,

and, given the harsh winter environment, risky, at times. The present research further

refines the use of close-range photogrammetry developed through previous work (Keshav

et al., 2015) for Fut. Implementation of the photogrammetry protocols for snow

deposition mapping required the development of new means to deal with the

"visualization" of the snow volumetric features. This was needed because in the absence

of visible patterns contained in the image recordings, the reconstruction of the imaged

area is difficult and of low accuracy, as the pattern recognition performed by the software

requires the presence of distinct, contrasting features captured in the images acquired for

mapping.

The proof-of concept experimental methodologies and protocols developed to

estimate critical variables for snow fence design have been barely demonstrated not

because of the limited resources available for the research (that is usually the main

obstacle), but mostly because of the absence of snow drift conditions at the monitored

sites over the two winter seasons this reasearch was conducted. This limitation led to use

of artifacts for some of the experiments and stretching the capabilities of the proposed

methods in areas where they are prone to errors. Despite these limitations, the

preliminary results for estimating the snow fall fluxes and mapping the snow deposits are

promising. The snow drift measurements results are better substantiated but only

demonstrated in laboratory conditions with modeled snow particles. The results of this

research can be used as a solid basis for a thorough step-by-step verification and

validation of the proposed methodologies through a systematically laid out program. The

following tasks are suggested:

- Use of the proposed methodologies and protocols for measurements of snow fall
  during extreme snow storm events, in areas where the wind is not obstructed (i.e.,
  open fields with low ground cover over which the wind velocity is high enough to
  initiate drifting and fetch distance that is sufficiently large such that the supply of
  driftable snow is practically unlimited). These measurements should be acquired
  at a minum of 1.5 m above the ground.

- Use of the prescribed methodologies and protocols for measurements of snow
  drift during strong events in areas of unobstructed wind. The snow drift
  measurements should be confined in a layer extending up to 1 m above the
  ground. This is needed becausesaltation of snow particles from the layer of
  deposited snow is the main contributor to the snow drift flux.

- Repeat the above measurements to confirm the robustness of the proposed
  techniques and consolidate the results in a set of data that can be compared with

available reference results (i.e., Tabler, 1994). The processing of the experimental data should substantiate the variability of the snow drift and snow fall measurements over the event duration at a site.Ideally such measurements should be conducted at several sites to capture the spatio-temporal variability of the snow transport processes.

- Performing the whole chain of measurement that generates the data required by the snow fence design software. Evaluate the design performance and compare the evaluations obtained using data collected directly at the snow fence site using the proposed methodologies and protocols with the design solutions obtaine based on the current methodologies used by state agencies .

- Development of standardized protocols for implementation of the proposed methodologies in current practice.

- Re-evaluating the available design standards and providing specific corrections that account for site characteristics and meteorological conditions.

OBSERVED SNOW STORM EVENTS: Measurement campaign 2015-2016

Event 1: 01/19/2016 – 2 hours

S1 - 30 sec

6:30 pm   8:30 pm

V_x

V_y

Start   Middle   End

4 sec   4 sec   4 sec

0.242 m/s   0.208 m/s   0.158 m/s

1.080 m/s   1.053 m/s   0.994 m/s   0.972 m/s   0.888 m/s   0.966 m/s

S1_Start: 239 images,   S1_Middle: 240 images,   S1_end: 245 images,

149 snowflakes   184 snowflakes   115 snowflakes
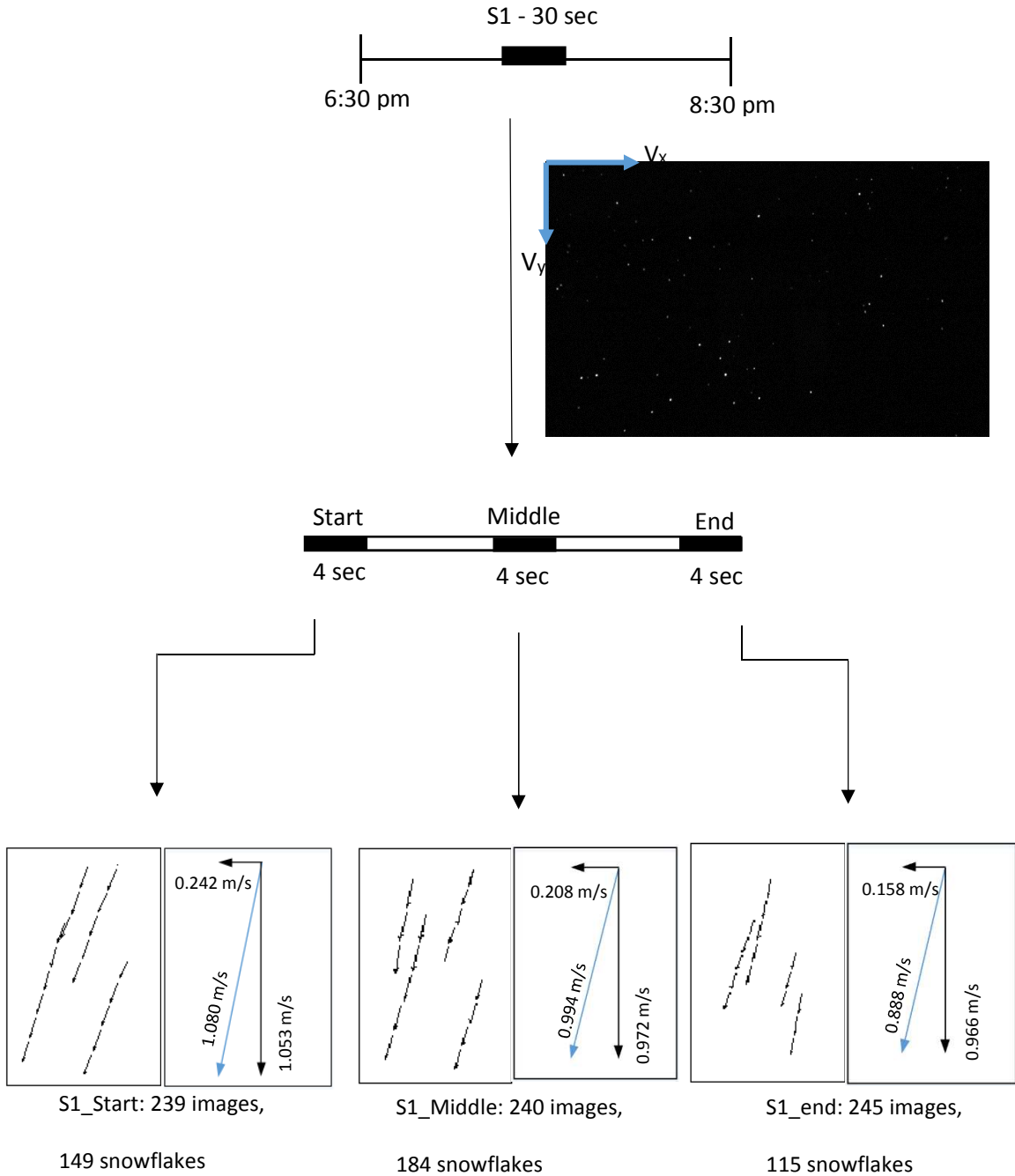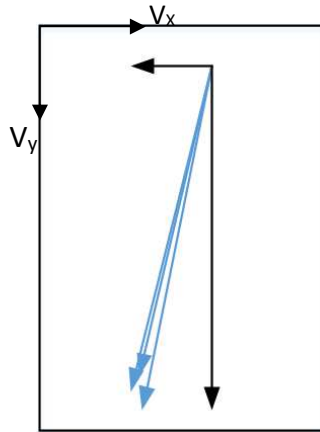
Total snow velocity for the

three PIV samples
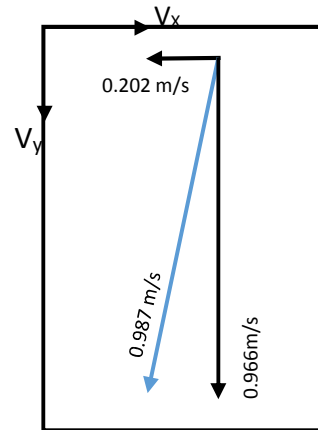
Total snow fall velocity

during Event 1

Event 1					
	V_x (m/s)	V_y (m/s)	Total Velocity (m/s)	Avg. Particle Snow Flake (pix)	Concentration (%)
E1_S1_Start	-0.242	1.053	1.080	25.73	0.144
E1_S1_Middle	-0.208	0.972	0.994	29.04	0.178
E1_S1_End	-0.158	0.874	0.888	22.28	0.131
E1_S1_Average	**-0.202**	**0.966**	**0.987**	**25.68**	**0.151**

25.68 pixels snow flake size = 3.12 mm in snow flake Diameter

Event 1	Angle from North is 97°		
	V_{x1} (m/s)	V_{x2} (m/s)	Total Wind Velocity (m/s)
E1_Wind	-0.246	-1.976	1.991

130

Event 2: 01/25/2016 – 2.5 hours

S1 - 30 sec

8:00 pm   10:30 pm

V_x

V_y

Start   Middle   End

4 sec   4 sec   4 sec

0.044 m/s

0.803 m/s   0.80 m/s
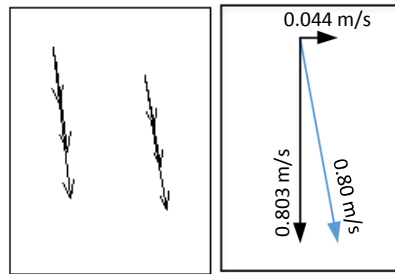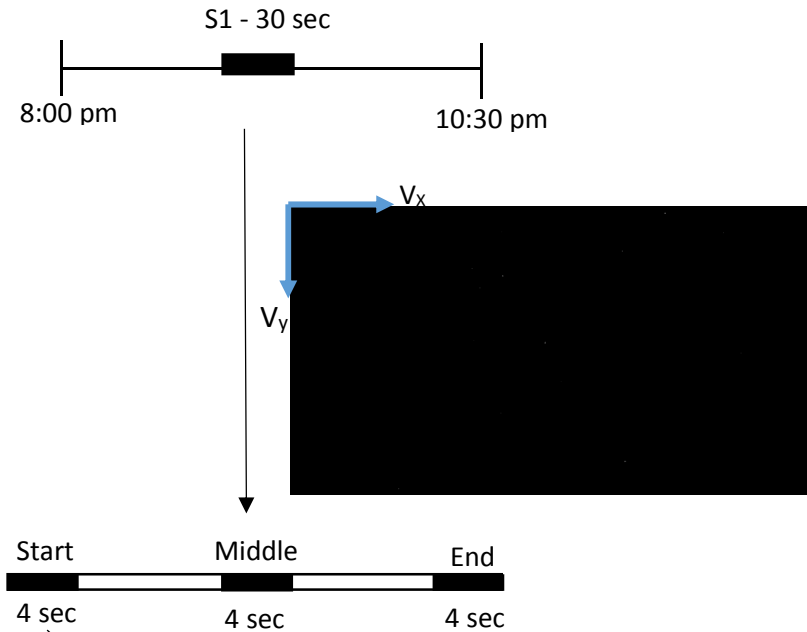
S1_Start: 239 images, 20 snowflakes

Event 2					
	V_x (m/s)	V_y (m/s)	Total Velocity (m/s)	Avg. Particle Snow Flake (pix)	Concentration (%)
E2_S1_Start	0.044	0.802	0.803	7.53	0.007

7.53 pixels snow flake size = 1.14 mm in snow flake Diameter

Event 2	Angle from North is 272°		
	V_{x1} (m/s)	V_{x2} (m/s)	Total Wind Velocity (m/s)
E2_Wind	0.058	1.669	1.670

Event 3: 02/02/2016 – 1 hour

S1 - 30 sec

8:30 am   9:30 am

V_x

V_y

Start   Middle   End

4 sec   4 sec   4 sec

0.31 m/s

2.64 m/s   2.66 m/s

S1_Start: 240 images, 360 snowflakes

Event 3					
	V_x (m/s)	V_y (m/s)	Total Velocity (m/s)	Avg. Particle Snow Flake (pix)	Concentration (%)
E3_S1_Start	0.306	2.644	2.661	28.34	0.254

28.34 pixels snow flake size = 2.06 mm in snow flake Diameter

Event 3	Angle from North is 84°		
	V_{x1} (m/s)	V_{x2} (m/s)	Total Wind Velocity (m/s)
E3_Wind	0.374	3.557	3.576

Event 4: 02/07/2016 – 0.5 hours

S1 - 30 sec

02:00 am   02:30 am

V_X

V_y

Start   Middle   End

4 sec   4 sec   4 sec

0.028 m/s

0.317 m/s   0.32 m/s

0.021 m/s

0.231 m/s   0.232 m/s

0.029 m/s

0.344 m/s   0.345 m/s
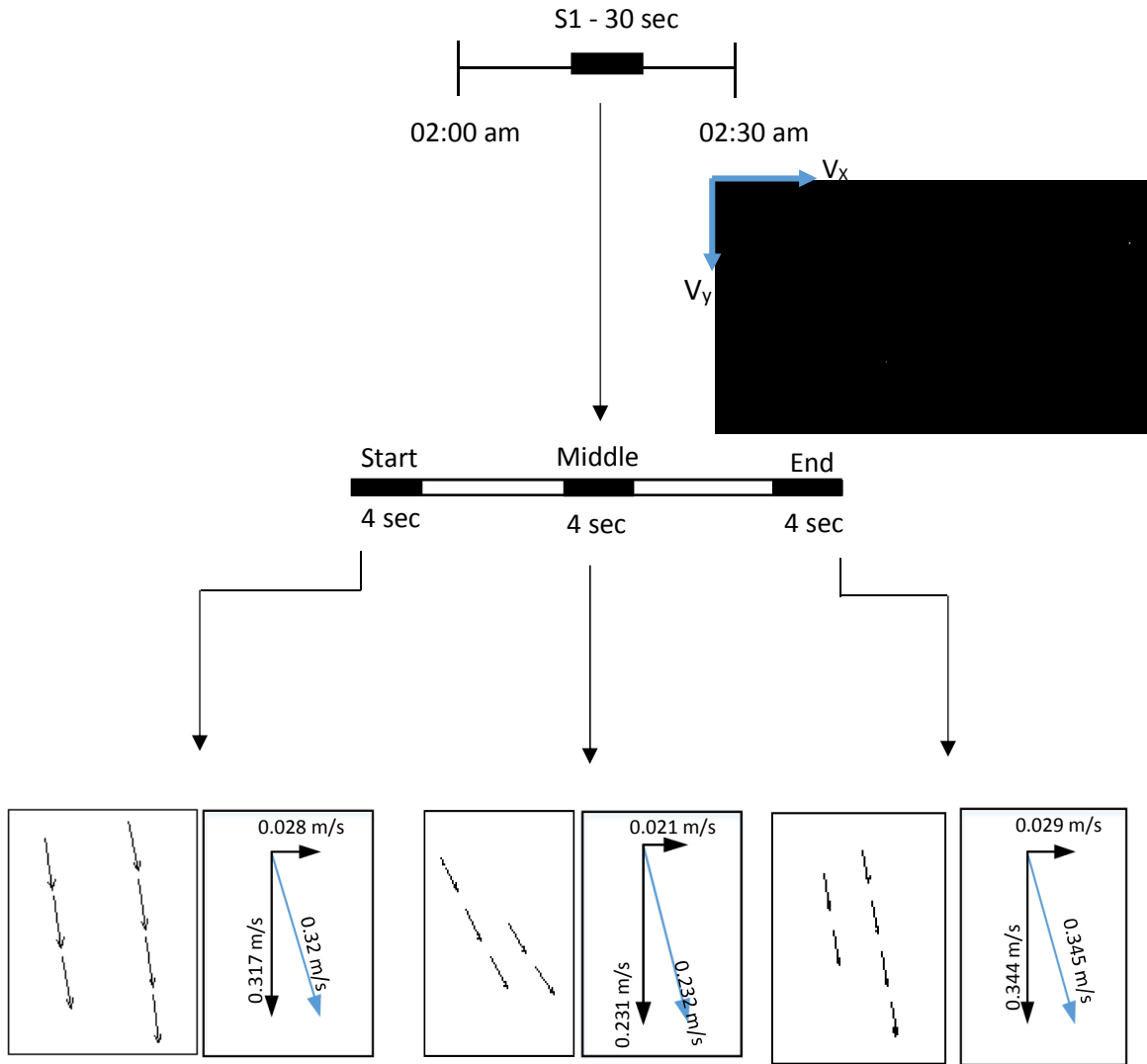
S1_Start: 290 images,

9 snowflakes

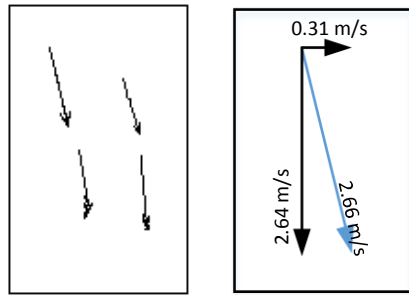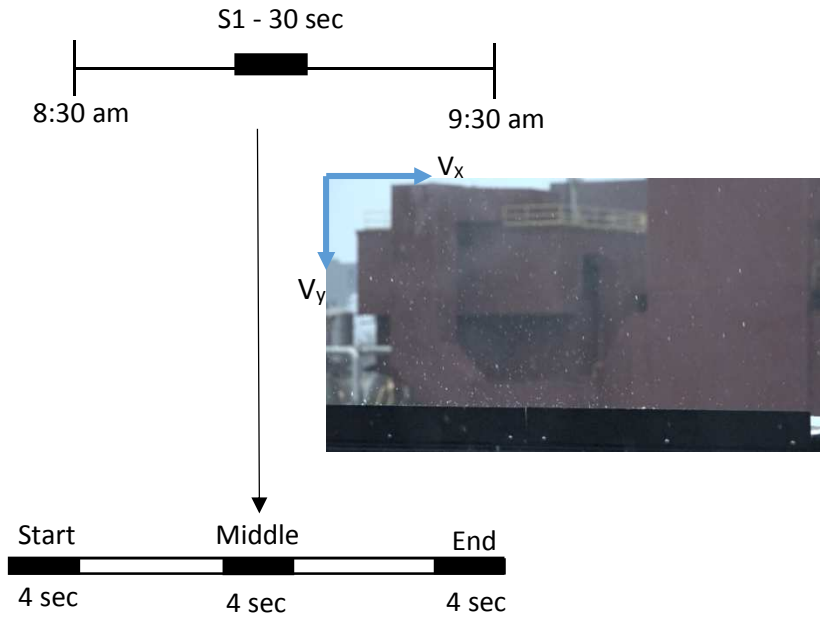S1_Middle: 227 images,

13 snowflakes

S1_end: 239 images,

10 snowflakes

Event 4	V_x (m/s)	V_y (m/s)	Total Velocity (m/s)	Avg. Particle Snow Flake (pix)	Concentration (%)
E4_S1_Start	0.028	0.317	0.319	3.68	0.001
E4_S1_Middle	0.021	0.231	0.232	3.66	0.001
E4_S1_End	0.029	0.344	0.345	2.90	0.001
E4_S1_Average	**0.026**	**0.297**	**0.299**	**3.41**	**0.001**

3.41 pixels snow flake size = 0.72 mm in snow flake Diameter

Event 4	Angle from North is 274°		
	V_{x1} (m/s)	V_{x2} (m/s)	Total Wind Velocity (m/s)
E4_Wind	0.043	0.609	0.610

Event 5 – S1: 02/08/2016 – 8 hours
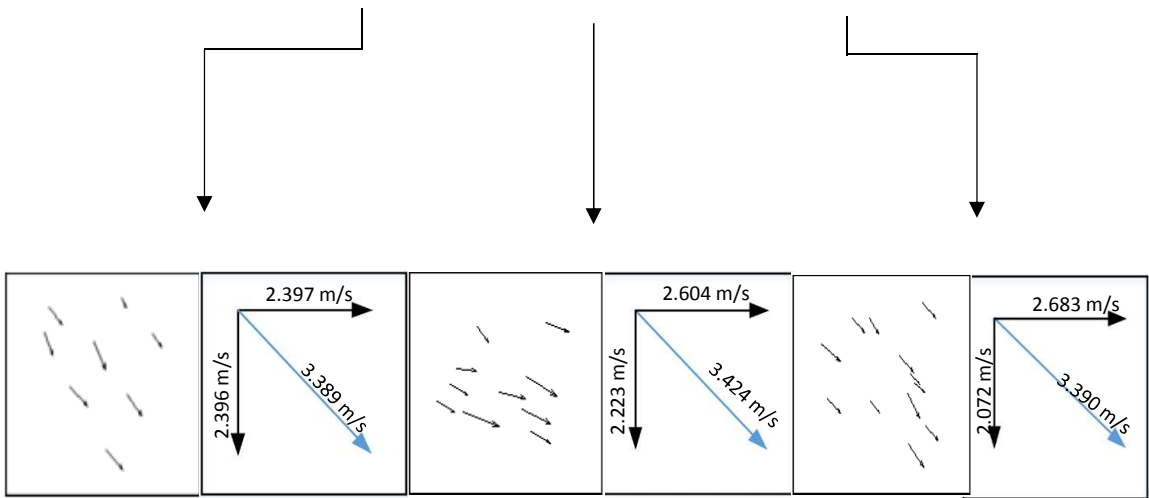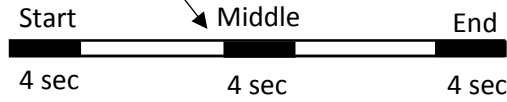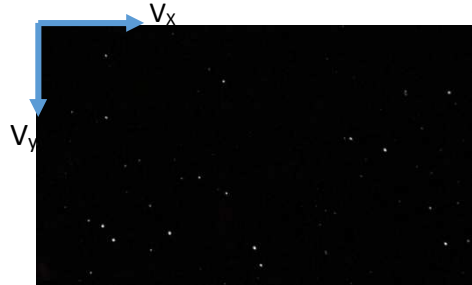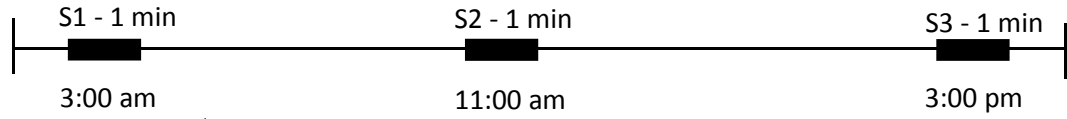
E5_S1_Start: 221 images, 155 snowflakes

E5_S1_Middle: 241 images, 159 snowflakes

E5_S1_End: 240 images, 133 snowflakes

Event 5					
	V_x (m/s)	V_y (m/s)	Total Velocity (m/s)	Avg. Particle Snow Flake (pix)	Concentration (%)
E5_S1_Start	2.397	2.396	3.389	30.76	0.35
E5_S1_Middle	2.604	2.223	3.424	26.01	0.222
E5_S1_End	2.683	2.072	3.390	24.96	0.190
E5_S1_Average	**2.561**	**2.230**	**3.401**	**27.24**	**0.254**

27.24 pixels snow flake size = 3.20 mm in snow flake Diameter

Event 5	Angle from North is 318°		
	V_{x1} (m/s)	V_{x2} (m/s)	Total Wind Velocity (m/s)
E5_S1_Wind	2.824	2.543	3.8

134

Event 5 – S2: 02/08/2016 – 8 hours

S1 - 1 min | S2 - 1 min | S3 - 1 min

3:00 am | 11:00 am | 3:00 pm

V_X

V_Y

Start | Middle | End

4 sec | 4 sec | 4 sec

0.945 m/s — 0.875 m/s — 1.288 m/s
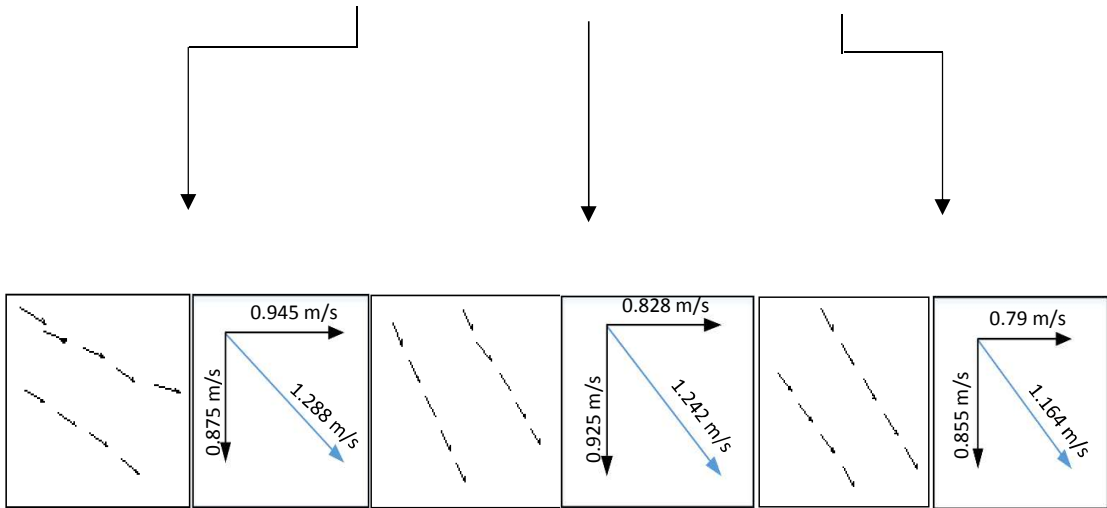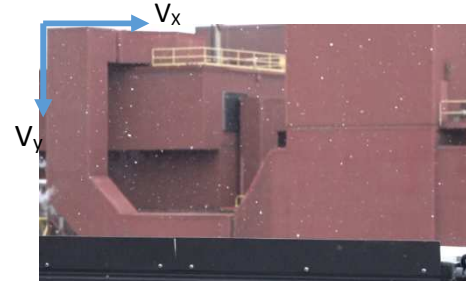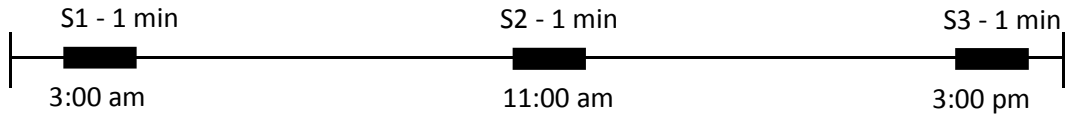
E5_S2_Start: 337 images,
145 snowflakes

0.828 m/s — 0.925 m/s — 1.242 m/s

E5_S2_Middle: 290 images,
79 snowflakes

0.79 m/s — 0.855 m/s — 1.164 m/s

E5_S2_End: 297 images,
66 snowflakes

Event 5	V_X (m/s)	V_Y (m/s)	Total Velocity (m/s)	Avg. Particle Snow Flake (pix)	Concentration (%)
E5_S2_Start	0.945	0.875	1.288	24.05	0.13
E5_S2_Middle	0.828	0.925	1.242	20.83	0.075
E5_S2_End	0.790	0.855	1.164	18.65	0.067
E5_S2_Average	**0.854**	**0.885**	**1.231**	**21.18**	**0.091**

21.18 pixels snow flake size = 2.49 mm in snow flake Diameter

Event 5	Angle from North is 346°		
	V_{x1} (m/s)	V_{x2} (m/s)	Total Wind Velocity (m/s)
E5_S2_Wind	0.970	2.419	2.6

Event 5 – S3: 02/08/2016 – 8 hours

S1 - 1 min 3:00 am
S2 - 1 min 11:00 am
S3 - 1 min 3:00 pm

V_x
V_y

Start 4 sec — Middle 4 sec — End 4 sec

E5_S3_Start: 244 images, 146 snowflakes
0.693 m/s
1.787 m/s
1.917 m/s

E5_S3_Middle: 234 images, 69 snowflakes
0.584 m/s
1.636 m/s
1.737 m/s

E5_S3_End: 205 images, 90 snowflakes
0.532 m/s
1.793 m/s
1.871 m/s
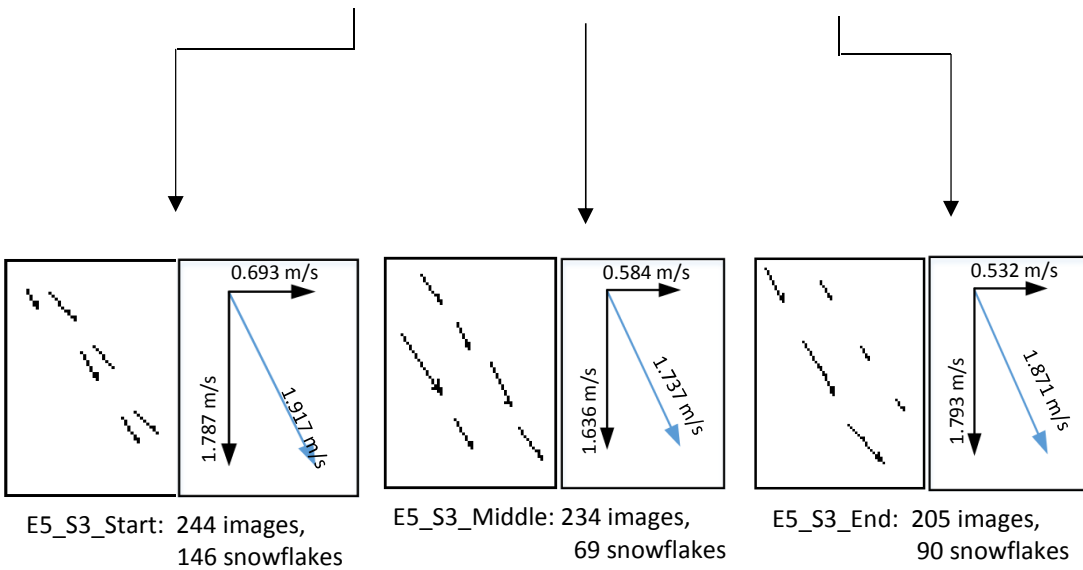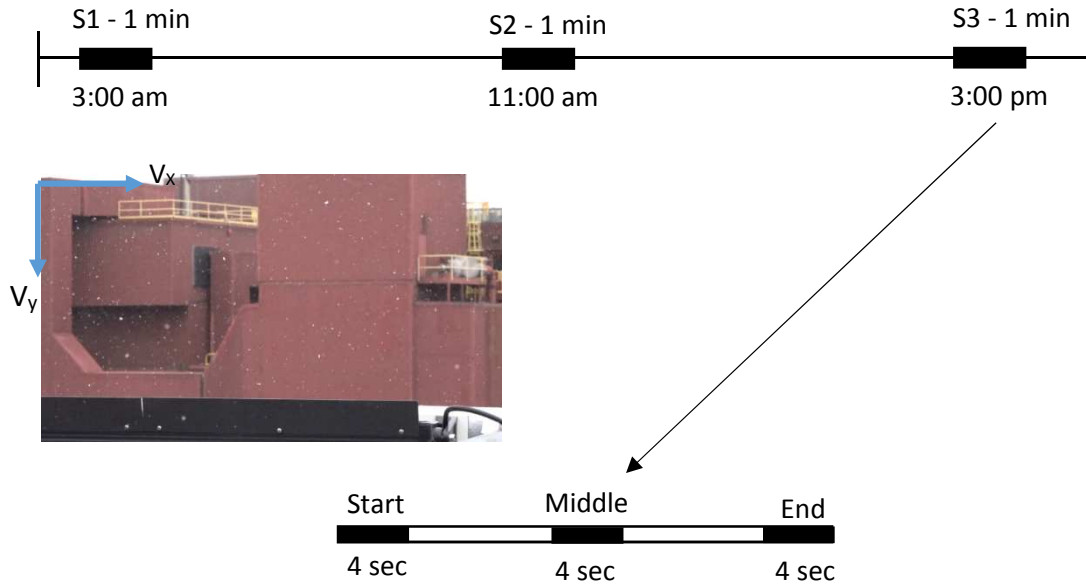
Event 5	V_x (m/s)	V_y (m/s)	Total Velocity (m/s)	Avg. Particle Snow Flake (pix)	Concentration (%)
E5_S3_Start	0.693	1.787	1.917	19.09	0.082
E5_S3_Middle	0.584	1.636	1.737	14.80	0.043
E5_S3_End	0.532	1.793	1.871	20.92	0.086
E5_S3_Average	**0.603**	**1.739**	**1.842**	**18.27**	**0.070**

18.27 pixels snow flake size = 2.61 mm in snow flake Diameter

Event 5	Angle from North is 316°		
	V_{x1} (m/s)	V_{x2} (m/s)	Total Wind Velocity (m/s)
E5_S3_Wind	0.719	0.695	1.0

Event 6: 02/14/2016 – 4.5 hours

S1 - 30 sec

7:30 pm

12:00 am

V_x

V_y

Start   Middle   End

4 sec   4 sec   4 sec

1.444 m/s

1.599 m/s

2.155 m/s
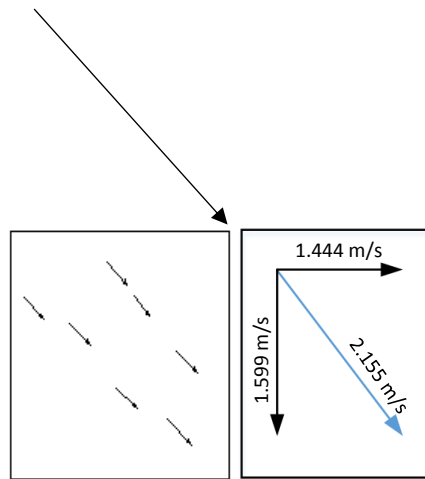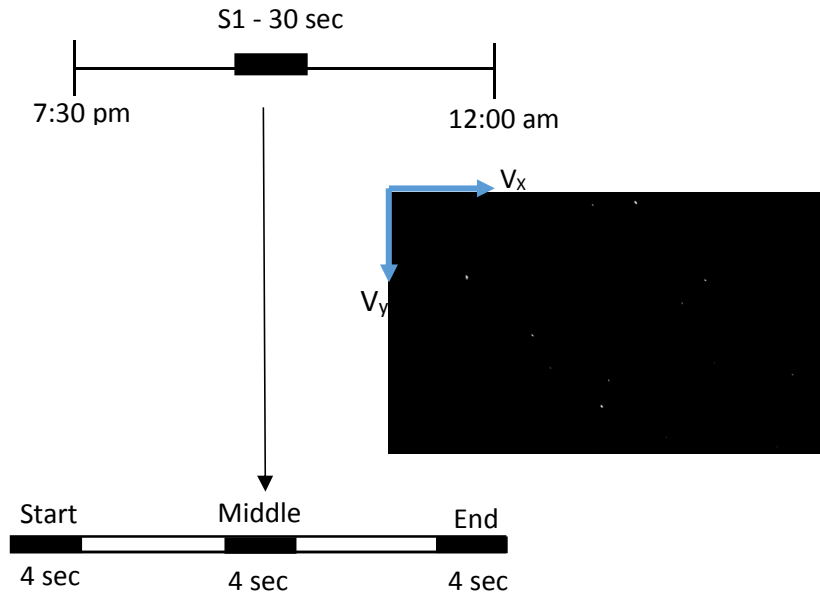
S1_Start: 302 images, 86 snowflakes

Event 6					
	Vx (m/s)	Vy (m/s)	Total Velocity (m/s)	Avg. Particle Snow Flake (pix)	Concentration (%)
E6_S1_Start	1.444	1.599	2.155	20.11	0.0107

20.11 pixels snow flake size = 2.84 mm in snow flake Diameter

Event 6	Angle from North is 115°		
	Vx1 (m/s)	Vx2 (m/s)	Total Wind Velocity (m/s)
E6_Wind	1.530	3.281	3.620

Snow Storm I: December 15-16, 2016 (no equipment as the approval to use the site)

WEST FENCE – Looking upwind (on the left of the school driveway)

EAST FENCE – Looking upwind (on the right of the school driveway)

WEST FENCE – Looking upwind (on the left of the school driveway)

Looking downwind

EAST FENCE – Looking upwind (on the right of the school driveway)

Looking downwind

SNOW STORM III: February 8, 2017 (from 2 am to 4 am)

WEST FENCE – Looking upwind (on the left of the school driveway)

Looking downwind

EAST FENCE – Looking upwind (on the right of the school driveway)

Looking downwind

147

SNOW STORM IV: March 12-13, 2017

WEST FENCE – Looking upwind (on the left of the school driveway)

Looking downwind

EAST FENCE – Looking upwind (on the right of the school driveway)

Looking downwind

REFERENCES

Adams, C. E., & Weatherly, G. L. (1981). Some effects of suspended sediment stratification on an oceanic bottom boundary layer. *Journal of Geophysical Research: Oceans*, *86*(C5), 4161-4172.

Admiraal, D. (2017). Large-scale Particle Tracking Velocimetry, in Experimental Hydraulics, Vol II (Eds. Aberle, J., Rennie, C., Admiraal, D. and Muste, M), Taylor & Francis, New York, NY.

Adrian, R. J. (1991). Particle-imaging techniques for experimental fluid mechanics. *Annual review of fluid mechanics*, *23*(1), 261-304.

Adrian, R. J. (2005). Twenty years of particle image velocimetry. *Experiments in fluids*, *39*(2), 159-169.

Andreescu, M. P., & Frost, D. B. (1998). Weather and traffic accidents in Montreal, Canada. *Climate Research*, 225-230.

Andrey, J., & Olley, R. (1990). The relationship between weather and road safety: past and future research directions. *Climatological Bulletin*, *24*(3), 123-137.

Baker, H. A., & Williams, C. J. (1990). *Guidelines for Controlling Snowdrifting on Canadian Highways. Final Report* (No. TP 9937).

Basnet, K., Muste, M., Constantinescu, G., Ho, H., & Xu, H. (2016). Close range photogrammetry for dynamically tracking drifted snow deposition. *Cold Regions Science and Technology*, *121*, 141-153.

Bintanja, R. (2001). Modification of the wind speed profile caused by snowdrift: results from observations. *Quarterly Journal of the Royal Meteorological Society*, *127*(577), 2417-2434.

Budd, W. F. (1966). The Drifting of Nonuniform Snow Particles1. *Studies in Antarctic Meteorology*, 59-70.

Constantinescu, G., Muste, M., & Basnet, K. (2015). TR-626: Optimization of Snow Drifting Mitigation and Control Methods for Iowa Conditions.

Cooper, M. A. R., & Robson, S. (1996). Theory of close range photogrammetry.

Dyer, K. (1986). Coastal and estuarine sediment dynamics. *John Wiley and Sons, Chichester, Sussex (UK), 1986, 358*.

Elghobashi, S. E., & Abou-Arab, T. W. (1983). A two-equation turbulence model for two-phase flows. *The Physics of Fluids*, *26*(4), 931-938.

Fincham, A. M., & Spedding, G. R. (1997). Low cost, high resolution DPIV for measurement of turbulent fluid flow. *Experiments in Fluids*, *23*(6), 449-462.

Fujita, I., Muste, M., & Kruger, A. (1998). Large-scale particle image velocimetry for flow analysis in hydraulic engineering applications. *Journal of hydraulic Research*, *36*(3), 397-414.

Fujita, I., Muste, M., & Kruger, A. (1998). Large-scale particle image velocimetry for flow analysis in hydraulic engineering applications. *Journal of hydraulic Research*, *36*(3), 397-414.

Garrett, T. J., Fallgatter, C., Shkurko, K., & Howlett, D. (2012). Fall speed measurement and high-resolution multi-angle photography of hydrometeors in free fall. *Atmospheric Measurement Techniques*, *5*(11), 2625.

IDOT (2005). Iowa's Cooperative Snow Fence Program (2005). http://www.iowadot.gov/maintenance/pdf/snowfencebooklet.pdf

Kaneko, M., Watanabe, T., Matsuzawa, M., & Ito, Y. (2012). *Revision of" Highway Snowstorm Countermeasure Manual": Focus on Snowbreak Woods* (No. WM-STW12-131).

Kathlein, C. (2009) Physics of snow drift, Report presented for the graduate course AT-301 "Infrastructure in a changing climate" Univ. Centre in Svalbard, Norway.

Kersten, T. (2006). Combination and Comparison of Digital Photogrammetry and Terrestrial Laser Scanning for the Generation of Virtual Models in Cultural Heritage Applications. In *The 7th International Symposium on Virtual Reality, Archaeology and Cultural Heritage, VAST* (pp. 207-214).

Kobayashi, S. I. (1978). Snow transport by katabatic winds in Mizuho Camp area, East Antarctica. *Journal of the Meteorological Society of Japan. Ser. II*, *56*(2), 130-139.

Kobayashi, S. I. (1980). Studies on interaction between wind and dry snow surface. *Contributions from the Institute of Low Temperature Science*, *29*, 1-64.

Kraus, K. (1992). Photogrammetry Fundamentals and Processes.

Lee, S. J. (2001). PIV/PTV velocity field measurement technique-theory and practice. *PIV'2001 Lecture Note*.

Kunapo, J. (2005). Spatial data integration for classification of 3D point clouds from digital photogrammetry. *Applied GIS*, *1*(3), 26-1.

Liang, S., Ma, X., & Zhang, H. (2010). Numerical Simulation of Snow Drifting Disaster on Embankment Project. *JCP*, *5*(1), 139-143.

Lloyd, P. M., Stansby, P. K., & Ball, D. J. (1995). Unsteady surface-velocity field measurement using particle tracking velocimetry. *Journal of Hydraulic Research*, *33*(4), 519-534.

Lourenco, L. M., Gogineni, S. P., & LaSalle, R. T. (1994). On-line particle-image velocimeter: an integrated approach. *Applied optics*, *33*(13), 2465-2470.

Maiwald, F., Vietze, T., Schneider, D., Henze, F., Münster, S., Niebling, F., & Cottbus-Senftenberg, G. F. (2017). Photogrammetric Analysis of Historical Image Repositories for Virtual Reconstruction in the Field of Digital Humanities. *ISPRS-International Archives of the Photogrammetry, Remote Sensing and Spatial Information Sciences*, 447-452.

Matsuzawa, M., Harada, Y., Ueda, M., Matsushita, H., & Ito, Y. (2012). Recent Trends in Changes in Snowfall and Snow Depth in Japan and Their Impact on Snow Control Measures. *and Surface Transportation Weather*, 292.

Matthews, N. A. (2008). *Aerial and close-range photogrammetric technology: providing resource documentation, interpretation, and preservation*. US Department of the Interior, Bureau of Land Management.

McClung, D. and Schaerer, P. 1993. *The Avalanche Handbook*, The Mountaineers, Seattle, WA, 271 pp.

Mellor, M., & Fellers, G. (1986). *Concentration and flux of wind-blown snow* (No. CRREL-SR-86-11). Cold Regions Research and Engineering Lab Hanover NH.

Muramoto, K. I., Matsuura, K., & Shiina, T. (1995). Measuring the density of snow particles and snowfall rate. *Electronics and Communications in Japan (Part III: Fundamental Electronic Science)*, *78*(11), 71-79.

Muste, M., Z. Xiong, J., Schöne, Z. Li. (2004). "Flow Diagnostic in Hydraulic Modeling Using Image Velocimetry," J. Hydraulic Engineering, 130(3), 175–185

Muste, M., Fujita, I., & Hauet, A. (2008). Large-scale particle image velocimetry for measurements in riverine environments. *Water Resources Research*, *44*(4).

Muste, M., Hauet, A., Fujita, I., Legout, C., & Ho, H. C. (2014). Capabilities of Large-scale Particle Image Velocimetry to characterize shallow free-surface flows. *Advances in Water Resources*, *70*, 160-171.

Muste, M., Baranya, S., Tsubaki, R., Kim, D., Ho, H., Tsai, H., & Law, D. (2016). Acoustic mapping velocimetry. *Water Resources Research*, *52*(5), 4132-4150.

Naaim, M., Naaim-Bouvet, F., & Martinez, H. (1998). Numerical simulation of drifting snow: erosion and deposition models. *Annals of glaciology*, *26*, 191-196.

Nemoto, M., Sato, T., Kosugi, K., & Mochizuki, S. (2014). Effects of Snowfall on Drifting Snow and Wind Structure Near a Surface. *Boundary-layer meteorology*, *152*(3), 395-410.

Nixon, W. A., Davison, M., & Kochumman, G. (2003). Living snow fences: Iowa Highway Research Board Project TR 460. *IIHR Technical Rep*, *460*.

NOAA (2013). "Snow Measurement Guidelines for National Weather Service Surface Observing Programs," NOAA, National Weather Service, Office of Climate, Water and Weather Services, Silver Spring, MD.

Osborne Jr, L. F., Hershey, B. W., & Mewes, J. J. (2012). Operational Blowing Snow Modeling: Benefits for the End User. *Transportation Research E-Circular*, (E-C162).

Peel, T., Ahmed, M., & Ohara, N. (2017). Investigating the Safety Effectiveness of Wyoming Snow Fence Implementations along a Rural Mountainous Freeway. In *Transportation Research Board 96th Annual Meeting* (No. 17-02223).

Perchanok, M., & Bacchus, A. (1993). Cost Analysis of Snow Control Structures in Ontario. In *Proceedings of the Annual Meeting-Eastern Snow Conference* (Vol. 50, p. 365). Eastern Snow Conference.

Perchanok, M. S. (1998). *Design and maintenance procedures to minimize impacts from drifting snow on highways-provisional guidelines*. Report MAT-98-01. Ontario Ministry of Transportation, Research and Development Branch, Downsview, Ontario.

Pomeroy, J.W. (1989) A process-based model of snow drifting, *Ann. Glaciol*. 13, 237-240.

Pomeroy, J. W., & Gray, D. M. (1990). Saltation of snow. *Water resources research*, *26*(7), 1583-1594.

Pomeroy, J. W., & Gray, D. M. (1995). Snowcover accumulation, relocation and management. *Bulletin of the International Society of Soil Science no*, *88*(2).

Raffel, M., Willert, C. E., Wereley, S., & Kompenhans, J. (1998). *Particle image velocimetry: a practical guide*. Springer.

RTK surveying training guide, (2003), http://www.gisresources.com/wp-content/uploads/2014/08/Real-Time-Kinematic.pdf

Sañudo-Fontaneda, L. A., Castro-Fresno, D., del Coz-Díaz, J. J., & Rodriguez-Hernandez, J. (2011). Classification and comparison of snow fences for the protection of transport infrastructures. *Journal of Cold Regions Engineering*, *25*(4), 162-181.

Schaerer, P. A. (1972). Control of snow drifting about buildings.

Schmidt, R. A. (1986). Transport rate of drifting snow and the mean wind speed profile. *Boundary-Layer Meteorology*, *34*(3), 213-241.

Skarlatos, D., & Kiparissi, S. (2012). Comparison of laser scanning, photogrammetry and SFM-MVS pipeline applied in structures and artificial surfaces. *ISPRS annals of the photogrammetry, remote sensing and spatial information sciences*, *3*, 299-304.

Tabler, R. D. (1986). *Snow fence handbook*. Tabler & Associates, Laramie, Wyoming. 169 pp.

Tabler, R. D., N. H. Berg, D. Trabant, H. Santeford, and P. A. Rechard. (1990). Measurement and evaluation of winter precipitation. *Cold Regions Hydrology and Hydraulics, ASCE Technical Council on Cold Regions Engineering Monograph*. pp. 9-38.

Tabler, R. D. (1991). *Snow fence guide* (No. SHRP-H-320). Washington: Strategic Highway Research Program, National Research Council.

Tabler, R. D. (1994). *Design guidelines for the control of blowing and drifting snow* (No. SHRP-H-381). Strategic Highway Research Program, National Research Council.

Tabler, R. D. (2003). Controlling blowing and drifting snow with snow fences and road design. *National Cooperative Highway Research Program Project*, (20-7), 147.

Takeuchi, M. (1980). Vertical profile and horizontal increase of drift-snow transport. *Journal of Glaciology*, *26*(94), 481-492.

Tang, Z. Z., Liang, J., Guo, C., & Wang, Y. X. (2012). Photogrammetry-based two-dimensional digital image correlation with nonperpendicular camera alignment. *Optical Engineering*, *51*(2), 023602-1.

Trimble Correction Services. http://www.trimble.com/agriculture/CorrectionServices/CenterPointRTK.aspx.

Weather Online. (n.d.). Blowing snow. Retrieved May 25, 2017, from http://www.weatheronline.co.uk/reports/wxfacts/Drifting-snow.htm

Weather underground. Weather History for KIOW - March, 2016. (n.d.). Retrieved April 29, 2017, from https://www.wunderground.com/history/airport/KIOW/2016/3/12/DailyHistory.html?req_city=&req_state=&req_statename=&reqdb.zip=&reqdb.magic=&reqdb.wmo=

Westerweel, J., Elsinga, G. E., & Adrian, R. J. (2013). Particle image velocimetry for complex and turbulent flows. *Annual Review of Fluid Mechanics*, *45*, 409-436.

Westoby, M. J., Brasington, J., Glasser, N. F., Hambrey, M. J., & Reynolds, J. M. (2012). 'Structure-from-Motion'photogrammetry: A low-cost, effective tool for geoscience applications. *Geomorphology*, *179*, 300-314.

Wolf, P. R., & Dewitt, B. A. (2000). *Elements of Photogrammetry: with applications in GIS* (Vol. 3). New York: McGraw-Hill.